


Università degli Studi di Cagliari

Molecular and Translational Medicine

Cycle XXXII

Development of a Liver-specific immune 3D microenvironment for the study of primary and metastatic liver tumour

Scientific Disciplinary Sector: Med/04

PhD Student: Maria Giovanna Vilia

Coordinator of the PhD Program: Prof. Sebastiano Banni

Supervisors: Prof. Amedeo Columbano

Final exam. Academic Year 2018 – 2019
Thesis defence: January-February 2020 Session

Maria Giovanna Vilia gratefully acknowledges Sardinian Regional Government for the financial support of her/his PhD scholarship (P.O.R. Sardegna F.S.E.-Operational Programme of the Autonomous Region of Sardinia, European Social Fund 2014-2020- Axis III Education and training, Thematic goal 10, Investment Priority 10ii), Specific goal 10.5.

Acknowledgements

I am grateful to Prof. Amedeo Columbano for his support during my PhD and for giving me the opportunity to join his Lab. I would also like to take the chance to say thank you to everyone who has been a part of the lab over the time I have been there.

I would like to thank Dr. Giuseppe Mazza who supported me during the last two years; you had a huge impact on my scientific growth, enhancing my passion for research and my professional development. Thank you!

I am deeply grateful to Prof. Krista Rombouts for her availability, priceless advice and infinite patience. Thank you for all your help and time spent helping me during the last months writing this thesis.

My sincere thanks to Prof. Massimo Pinzani who provided me the opportunity to join his great team at the Department of HLDH of London and helped me with his knowledge and experience.

I also deeply thank Walid Al-Akkad, a huge thank you for your friendship, all the help and suggestions during the last years.

Elisabetta Caon and Martina Marrali for being the best friends and colleagues I would have hoped for, thank you for all your help!!

Since I joined the Pinzani's Lab two years ago I felt as part of a big family, so I take the chance to thanks everyone who have been part of the team during the time I spent there; among all a special thanks to Luca Frenguelli!

Special thanks to Elisabetta Puliga, Sandra Mattu, Claudia Orrù and Simona Onali for being amazing colleagues and friends.

Major thanks to my family, Mom and Dad, that gave me all the support during all the years I spent studying abroad. It is because of your sacrifices and support that I have been able to go this far. Thank you! A special thanks to my brother Pietro and Jessica, all my Aunties and Uncles, and all my lovely cousins, thank you for being always there for me, giving me love and support.

I would also like to show my gratitude to my family in law, thank you for the constant caring and encouraging.

To all my friends for their friendship and support through all these last years, I cannot thank you enough for everything that you have done for me!

Lastly, I deeply appreciate and thank Angelo for all the love, patience and all the support he gave me when I needed the most and pushing me to go forward in this adventure. Thank you!

Table of Contents:

1. **ABBREVIATIONS** **8**

2. **LIST OF PUBLICATIONS AND ABSTRACTS** **11**

3. **ABSTRACT** **13**

4. **TABLE OF FIGURES:** **15**

5. **INTRODUCTION** **18**

5.1 HCC 18
5.1.1 Cirrhosis *20*
5.1.2 Non-cirrhotic hepatocellular carcinoma *21*
5.1.3 Hallmarks of cancer in HCC *22*
5.2 ECM AND LIVER CANCER 23
5.3 LIVER IMMUNOLOGY 26
5.3.1 The liver microenvironment: liver-resident immune cells *29*
5.3.1.1 Phagocytes: Macrophages and Monocytes 29
5.3.1.2 Lymphoid & myeloid cells of the liver 30
5.4 THE IMPORTANCE OF THE IMMUNE SYSTEM IN HCC 32
5.4.1 Immune cells reaching and infiltrating the tumour site *34*
5.4.2 Immune escape and immunosuppression in HCC *36*
5.4.3 EMT: epithelial to mesenchymal transition *39*
5.5 LIVER METASTASIS 42

6. **ANTI-TUMOUR TREATMENTS AND IMMUNOTHERAPY** **45**

6.1 OVERVIEW OF CANONICAL TREATMENTS FOR LIVER CANCER 45
6.1.1 Sorafenib treatment *48*
6.1.2 Immunotherapy *49*
6.1.2.1 T cell-targeting immunotherapies 50
6.1.2.2 Immune Checkpoint Inhibitors: Reactivation of Tumour Infiltrating T-Cells 51
6.1.2.3 T cell engaging Bispecific antibodies for cancer therapy 53
6.1.3 Limitations of immunotherapy in solid tumours *56*
6.2 3D MODELS 58
6.2.1 Immune cells: 2D vs. 3D *59*

7. **MATERIALS & METHODS** **62**

7.1 GROWTH CONDITIONS OF CELLS 62
7.2 THAWING CELLS 62
7.3 PREPARATION OF PERIPHERAL BLOOD MONONUCLEAR CELLS (PBMC) 63
7.4 FREEZE/THAWING OF PBMC 63
7.5 ORIGIN OF DECELLULARIZED LIVER TISSUE CUBES. 64
7.6 SCAFFOLDS PREPARATION: 64
7.6.1 Sterilization of 3D scaffolds *65*
7.6.2 Seeding of cell lines and immune cells 3D scaffolds. *65*
7.6.2.1 Human cancer cell lines 65
7.6.2.2 Immune cells 66
7.7 RNA EXTRACTION AND GENE EXPRESSION ANALYSIS 66

7.7.1 RNA extraction 66
7.7.2 Reverse-Transcription for complementary DNA (cDNA) synthesis 66
7.8 Quantitative Real-Time PCR (RT- qPCR) analysis 67
7.9 Histology and Immunohistochemistry 68
7.9.1 Samples processing 68
7.9.2 Immunohistochemistry 69
7.9.3 Immunofluorescence: 69
7.10 3D extraction: Preparation of infiltrating cell suspensions. 70
7.10.1 Mechanical Disruption 70
7.11 Flow cytometry 71
7.11.1 Surface staining of PBMC and cancer cells for phenotype 71
7.11.2 Intracellular staining of PBMC and cancer cells lines. 71
7.12 Cell viability assay 73
7.12.1 Viability on cells on 2D cultures (Metabolic assay) 73
7.12.1.1 Presto blue 73
7.12.2 Viability on cells on 2D/3D scaffolds 73
7.12.2.1 Annexin/PI/sytox staining 73
7.13 Data acquisition Flow cytometry 74
7.14 Western blot 74
7.15 Treatments 75
8. THESIS AIM 76
9. **RESULTS** 77
9.1 Recreating the immune microenvironment using three-dimensional human liver extracellular matrix scaffolds. 77
9.1.1 Introduction 77
9.1.2 Decellularization of human 3D liver scaffolds 78
9.1.3 Re-population of decellularized human 3D liver scaffolds with human PBMCs 79
9.1.4 T cell population in 3D liver scaffolds 85
9.1.5 Natural killer cells on 3D liver scaffolds 92
9.1.6 Monocyte macrophages population in 3D liver scaffolds. 93
9.1.7 Gene expression of remodelling genes and Integrins in immune cells in 3D scaffolds 96
9.2 The extracellular matrix derived from human cirrhotic liver strongly reduces the anti-cancer immune response in a 3D model of hepatocellular carcinoma 100
9.2.1 Introduction 100
9.2.2 HCC cell line in healthy and cirrhotic environment 101
9.2.3 Sorafenib treatment of human hepatocellular carcinoma cells line SNU-449. 104
9.3 Co-culture: human HCC cell line SNU-449 with PBMCs in 3D scaffolds 108
9.3.1 Co-culture: HCC cell lines and PBMCs in 3D liver scaffolds 108
9.3.2 Modulation of PD-1 and PDL-1 expression in 3D co-cultures treated with Sorafenib 120
9.3.3 Conclusions 124
9.4 Modelling the liver metastasis immune microenvironment using three-dimensional human liver extracellular matrix scaffolds. 125
9.4.1 Introduction 125
9.4.2 Recreating a metastatic microenvironment 126
9.4.3 T-cell-based cancer immunotherapy: BiTe treatment in 3D scaffolds. 131
9.4.4 Conclusion: 152
10. **DISCUSSION** 154

11. **REFERENCES:** **163**

1. Abbreviations

2D Two-dimensional

3D Three-dimensional

BiTe Bispecific T cell engager

CD cluster of differentiation

CK cytokeratin

CTLA-4 cytotoxic T-lymphocyte-associated protein

CXCR chemokine receptor

DC dendritic cell

DMSO dimethyl sulfoxide

ECM extracellular matrix

EDTA ethylenediamine tetra acetic acid

FBS foetal bovine serum

FcR blocking reagent

FOXP3 forkhead box P3

gMDSC granulocytic myeloid-derived suppressor cells

HBV Hepatitis B virus

HCC hepatocellular carcinoma

HCV Hepatitis C virus

HLA human leukocyte antigen

HSC hepatic stellate cell

ICAM1 (CD54) intercellular adhesion molecule 1

IFN interferon

IHC: immunohistochemical

IL- interleukin

KC Kupffer cells

LSEC liver sinusoidal epithelial cell

mAb monoclonal antibody

MDSC myeloid-derived suppressor cells

MHC major histocompatibility class

NHS National Health Service

NK natural killer cell

NKT natural killer T cell

OS overall survival

PBMC peripheral blood mononuclear cells

PBS phosphate buffered sulphate

PCR polymerase chain reaction

PD-1 programmed death 1

PDAC pancreatic ductal adenocarcinoma

PD-L1 programmed death ligand 1

PMN premetastatic niche

PLC Primary Liver Cancer

PRR pattern recognition receptor

R.T. room temperature

Rpm revolutions per minute

TAA Tumour-Associated Antigens

TCR T cell receptor

TGFβ transforming growth factor beta

TIL tumour-infiltrating T lymphocyte

TLR toll-like receptor

TME tumour microenvironment

TNF tumour necrosis factor

Treg regulatory T cells

2. List of Publications and Abstracts

Publications

- IRAK4 inhibitor interrupts Toll-like receptors signalling and sensitizes chronic lymphocytic leukaemia cells to apoptosis.
  Vincenza Simona Delvecchio, Ilenia Sana, Maria Elena Mantione, **Maria Giovanna Vilia**, Pamela Ranghetti, Alessandra Rovida, Piera Angelillo, Lydia Scarfò, Paolo Ghia, and Marta Muzio
  British Journal of Haematology, October 2019.

- Dichotomous Toll-like receptor responses in chronic lymphocytic leukaemia patients under ibrutinib treatment.
  Gounari M, Ntoufa S, Gerousi M, **Vilia MG**, Moysiadis T, Kotta K, Papakonstantinou N, Scarfò L, Agathangelidis A, Fonte E, Ranghetti P, Nenou A, Xochelli A, Coscia M, Tedeschi A, Stavroyianni N, Muzio M, Stamatopoulos K, Ghia P.
  Leukemia. 2019 Apr;33(4):1030-1051. doi: 10.1038/s41375-018-0335-2. Epub 2019 Jan 3.

- Toll-like receptor 9 stimulation can induce IκBζ expression and IgM secretion in chronic lymphocytic leukaemia cells.
  Fonte E, **Vilia MG**, Reverberi D, Sana I, Scarfò L, Ranghetti P, Orfanelli U, Cenci S, Cutrona G, Ghia P, Muzio M.
  Haematologica. 2017 Nov;102(11):1901-1912. doi: 10.3324/haematol.2017.165878. Epub 2017 Aug 3

- Characterization of a long isoform of IL-1R8 (TIR8/SIGIRR).
  Vilia MG, Tocchetti M, Fonte E, Sana I, Muzio M.
  Eur Cytokine Netw. 2017 Jun 1;28(2):63-69. doi: 10.1684/ecn.2017.0395

- The inhibitory receptor toll interleukin-1R 8 (TIR8/IL-1R8/SIGIRR) is downregulated in chronic lymphocytic leukaemia.
  Vilia MG, Fonte E, Veliz Rodriguez T, Tocchetti M, Ranghetti P, Scarfò L, Papakonstantinou N, Ntoufa S, Stamatopoulos K, Ghia P, Muzio M.
  Leuk Lymphoma. 2017 Oct;58(10):2419-2425. doi: 10.1080/10428194.2017.1295142. Epub 2017 Feb 28

Abstracts

- Abstract #1687"The extracellular matrix derived from human cirrhotic liver strongly reduces the anti-cancer immune response in a 3d model of hepatocellular carcinoma

Mrs. Maria Giovanna Vilia, Mr. Walid Al-Akkad, Ms. Elisabetta Caon, Mr. Andrew R Hall, Dr. Tuvinh Luong, Prof. Krista Rombouts, Prof. Massimo Pinzani and Mr. Giuseppe Mazza.
AASLD, The Liver Meeting, Boston, 8-12 Nov 2019, Abstract and poster presentation.

- Dissecting and targeting toll---like receptors signalling pathways in chronic lymphocytic leukaemia
  Simona Delvecchio, Ilenia Sana, Maria Giovanna Vilia, Maria Elena Mantione, Pamela Ranghetti, Alessandra Rovida, Piera Angelillo, Lydia Scarfò, Paolo Ghia, Marta Muzio.
  Cambridge Lymphoma Biology International Symposium, 17---18 July 2018, Abstract

- PS-209-Whole Human liver decellularisation-recellularisation for future liver transplantation and extracorporeal device application
  Walid Al-Akkad, Eric Felli, Bettina M Buchholz, Joerg-Matthias Pollok, Tariq Al-Akkad, Toby Proctor, Luca Frenguelli, Simone Canestrari, Domenico Bagordo, Gabriele Spoletini, Domenico Tamburrino, Maria Giovanna Vilia, Krista Rombouts, Massimo Malago, Paolo De Coppi, Etienne Sokal, Massimo Pinzani, Giuseppe Mazza.
  EASL, he International Liver Congress 2019 10-14 April 2019, Vienna, Austria. Abstract

- SAT-397-HIC-5 and GARP expression is upregulated by hydrogen peroxide and TGF beta in primary human hepatic stellate cells cultured on decellularized human liver 3D ECM scaffolds
  Simona Onali, Elisabetta Caon, Kessarin Thanapirom, Martina Marrali, Maria Giovanna Vilia, Luca Frenguelli, Walid Al-Akkad, Giuseppe Mazza, Massimo Pinzani, Krista Rombouts
  EASL, he International Liver Congress 2019 10-14 April 2019, Vienna, Austria. Abstract

- The Interleukin-1 receptor/Toll-like receptor family member TIR8 is downregulated in chronic lymphocytic leukemia.
  Vilia MG, Fonte E, Veliz Rodriguez T, Tocchetti M, Ranghetti P, Scarfò L, Papakonstantinou N, Ntoufa S, Stamatopoulos K, Ghia P, Muzio M.
  EACR-AACR-SIC 2017, Special Conference, 24-27 June 2017, Florence. Abstract and Poster presentation.

3. Abstract

Two dimensional (2D) in vitro models have been insufficient in replicating the complex interplay that occurs in the in vivo microenvironment between cancer and immune cells. The main reason for this discrepancy is due to the lack of cell-cell interactions and the cell-tumour microenvironment in conventional 2D plastic models. Indeed, cancer is a product of the complex interaction between cancer cells and tumour microenvironment, which comprises a three-dimensional (3D) extracellular matrix (ECM) together with tissue-resident cells as well as immune cells.

The aim of this project was to evaluate immune and cancer cells interaction, cell infiltration and the ability of immune cells to target cancer cells, within tissue-specific and disease-specific human ECM scaffolds. Additionally, we aimed to test a 3D liver model of primary and metastatic liver cancer for therapy and immunotherapy.

The results revealed that 3D cultures induced a mesenchymal-like phenotypes depending on disease-specific biochemical and biomechanical composition of the scaffold (Healthy or Cirrhotic). In fact, 3D, unlike 2D cultures of hepatocellular carcinoma (HCC) cell line, induced E-cadherin downregulation in healthy and cirrhotic scaffolds, suggesting the activation of the epithelial to mesenchymal transition (EMT).

Current models for testing new immunotherapeutic drugs in solid tumours are not satisfactory. One of the potential limitations affecting the translation of therapies towards effective treatments for solid tumours is due to the lack of reliable in vitro and in vivo models.

Therefore, another aim of my thesis is to investigate the impact of tissue-specific and disease-specific ECM scaffolds in modulating tumour and immune cells behaviours as well as response to immunotherapy. Our results demonstrated that the disease-specific 3D environment promoted a protective microenvironment for cancer cells as well as an immune cells exclusion phenotype, accounting for the low therapeutic efficacy found in clinical practice. Based on the finding that 3D healthy and cirrhotic scaffolds recreate molecular features of immunological “hot” and “cold” tumour, respectively, we propose 3D ECM cultures as a novel and powerful platform for drug screening. Finally, the observation that the efficacy of sorafenib and immunotherapy (anti-PD1 and anti-PDL1)

is strongly reduced in 3D (especially cirrhotic ECM) compared to 2D models suggests that 3D scaffolds can represent also a useful tool for the study of the mechanisms underlying cancer cell resistance.

4. Table of figures:

Fig. 1 Global map presenting age-standardized incidence rates of liver cancer by world countries for males and females for all ages in 2018 [1]..... 18
Fig. 2 Evolution of Primary Liver Cancer (PLC)..... 19
Fig. 3 Causes of non-cirrhotic hepatocellular carcinoma (HCC) 21
Fig. 4 The next generation of hallmarks of cancer...... 22
Fig. 5 ECM production in human disease. 25
Fig. 6 Anatomical organization of the liver...... 26
Fig. 7 Liver microanatomy. 28
Fig. 8 Schematic view of the micro-architecture of the hepatic sinusoid. 30
Fig. 9 The Cancer-Immunity Cycle. 33
Fig. 10 Hot and cold tumour immune phenotype and biological phenotype..... 35
Fig. 11 Stages of cancer immunoediting. 37
Fig. 12 The counteracting forces regulate the balance between tumour progression and tumour elimination. 38
Fig. 13 Schematic representation of the EMT programme. 40
Fig. 14 The tumour metastatic process. 43
Fig. 15 Representation of EASL recommendations for treatment 45
Fig. 16 Molecularly targeted therapies for HCC and their target signalling pathways. ... 47
Fig. 17 Targeting cancer cells with immunotherapy..... 50
Fig. 18 Mechanism of action of PD-1–blockade therapy..... 52
Fig. 19 structure and mechanism of a BiTe. 53
Fig. 20 Decellularization of human 3D liver scaffolds. 60
Fig. 21 SEM imaging of decellularized 3D healthy and cirrhotic scaffolds. 78
Fig. 22 Histological observation of PBMCs engrafted in the two different 3D liver scaffolds. 79
Fig. 23 Immunohistochemistry staining of Ki-67 in sections of healthy and 3D liver scaffolds repopulated with PBMCs..... 80
Fig. 24 Histological sections of 3D Healthy and cirrhotic ECM repopulated with PBMCS after 5 days..... 81
Fig. 25 schematic representation of the experimental protocol..... 82
Fig. 26 Total cell number after enzymatic digestion and mechanical dissociation using five different extraction protocols. 82
Fig. 27 Viability staining of PBMCs extracted from healthy and cirrhotic 3D liver scaffolds. 83
Fig. 28 Flow cytometry analysis of lymphocyte populations from whole blood w/o infiltration in healthy and cirrhotic 3D liver scaffolds 84
Fig. 29 Distinct phenotypic subset infiltrating the 3D liver scaffolds. 86

Fig. 30 percentage of T cell populations in 2D system compared to 3D ECM scaffolds. .. 88
Fig. 31 Percentage of T cell populations in culture medium and conditioned "3D ECM scaffold" medium. 89
Fig. 32 Western blot of decellularized 3D healthy and cirrhotic ECM. 91
Fig. 33 phenotypical changes in circulating NK and infiltrating NKs. 93
Fig. 34. Phenotypical changes during the culture of the monocytic lineage in 3D liver scaffolds. 95
Fig. 35 Graphs showing mRNA levels assessed by real time PCR in infiltrating and non-infiltrating cells in both types of 3D liver scaffolds. 99
Fig. 36 Representative pictures of haematoxylin and eosin (H&E) of SNU-449 cells in healthy and cirrhotic 3D scaffolds. 102
Fig. 37 KI-67 IHC staining of 3D healthy and cirrhotic 3D liver scaffolds repopulated with the SNU-449 cell line. 103
Fig. 38 EMT status of SNU-449 growing in 2D and 3D healthy and cirrhotic 3D liver scaffolds. 104
Fig. 39 Effect of Sorafenib on SNU-449 cell viability on 2D. 105
Fig. 40 Effect of Sorafenib on SNU-449 cell viability on 3D scaffolds. 106
Fig. 41 Sorafenib-induced apoptotic effect on SNU-449 cells after 48 hours of exposure. 107
Fig. 42 schematic representation of the experimental protocol for the co-culture..... 108
Fig. 43 Morphological changes of SNU-449 cells in single culture and in co-culture with PBMCs growing in healthy and cirrotic 3D liver scaffolds. 109
Fig. 44 Immunofluorescence image for PBMCs infiltrating Healthy and Cirrhotic 3D liver scaffolds. 111
Fig. 45 Flow cytometry of CD3 T cell population of SNU-449 cells co-cultured with PBMCs. 112
Fig. 46 immunophenotypic analysis of T cell in 3D cancer models. 113
Fig. 47 Immunophenotypic analysis of T cell infiltrating 3D cancer models..... 114
Fig. 48 Distinct phenotypic subset infiltrating the 3D liver scaffolds. 115
Fig. 49 Morphological changes of SNU-449 cells in co-culture with PBMCs growing in healthy and cirrotic 3D liver scaffolds. 117
Fig. 50 PD-L1 expression on SNU-449 cancer cells repopulating 3D liver scaffolds. 118
Fig. 51. PD-1 expression on CD8+ cells infiltrating the 3D liver scaffolds. 119
Fig. 52. PD-L1 expression on SNU-449 cells positively correlates with infiltrating CD8⁺ T cells frequencies in healthy ad cirrhotic 3D liver scaffolds. 120
Fig. 54 Differential expression of PD-L1 in HCC cancer cell line SNU-449 engrafted in healthy and cirrhotic 3D scaffolds, in single culture and co-culture with PBMCs before and after Sorafenib treatment. 121
Fig. 55 Differential expression of PD-1 in CD8+ infiltrating the 3D scaffolds, in single culture and co-cultured with cancer cells before and after Sorafenib treatment. 122

Fig. 56. Section of healthy 3D liver scaffolds repopulated with the metastatic cell line PK-1. 126
Fig. 57 Immune cells are detectable within the healthy 3D liver scaffolds repopulated with metastatic cell line. 127
Fig. 58 . Immunofluorescent analysis was performed on 3D liver scaffolds repopulated with PK-1 (12 days) and cultured with PBMCs for additional 5 days. 128
Fig. 59. Confocal Z-stack of Healthy 3D liver scaffolds repopulated with PK-1 cells and PBMCs. 129
Fig. 60. Percentage of T cell subpopulations in 2D compared to 3D metastatic cancer model. 130
Fig. 61. CD4/CD8 comparison of human cancer and 3D metastatic cancer model. 131
Fig. 62. Measurement of the amount of ROR-1 antigen by flow cytometry. 132
Fig. 63. Outline of 3D experiment. 133
Fig. 64 T cell subpopulations in 3D liver scaffolds repopulated with PK-1 human metastatic cell line before and after treatment (ROR-1 BiTe) 134
Fig. 65. Morphologic appearance of PK-1 and T cells in co-culture following repeated treatment with ROR-1 BiTe (1µm) or control. 136
Fig. 66. PK1 repopulation with T cells treated and untreated with ROR1-BiTe in healthy 3D scaffolds. 137
Fig. 67 Differential viability of PK-1 cells co-cultured with T cells in 2D and 3D after 3 cycles of ROR1 BiTe treatment. 138
Fig. 68. Changes in cell surface expression of PD-1 and PK-1 cells after ROR1 BiTe treatments in 2D and 3D scaffolds. 140
Fig. 69. Viability of PK-1 cells and T cells cultured in two-dimensional (2D) conditions. 142
Fig. 70. Phase contrast of PK-1 cells and T cells cultured in two-dimensional (2D) conditions. 143
Fig. 71. Viability of PK1 cells and T cells cultured in 3D scaffolds. 144
Fig. 72. Anti-tumour capacities of ROR1 Bite and PD-1 inhibitors in 3D scaffolds. 145
Fig. 73. Percentage of immune cells infiltrating the scaffolds after treatments. 146
Fig. 74. Cell surface CD107a on T cells 72h after treatments. 147
Fig. 75 C*hanges in cell surface expression of PD-1 and PD-L1 after treatments.* 149
Fig. 76. Flow cytometry staining for Cytokeratin^{+} cells in the supernatants. 151
Fig. 77 Schematic representation of 3D scaffolds-based model for Hot and Cold tumour. 157

5. Introduction

5.1 HCC

Primary liver cancer or hepatocellular carcinoma (HCC) is the 6th most prevalent cancer worldwide and the second leading cause of death from cancer estimated to be responsible for 780,000 deaths per year globally with 840,000 new cases in 2018[1] (Fig.1).

HCC comprises for 75%-85% of primary liver cancer, while the rest is mostly intrahepatic cholangiocarcinoma (comprising 10%-15% of cases) as well as other rare types. To note, among liver cancer in the United States and Europe, secondary liver cancer is much more common than primary liver cancer.

The main risk factors for HCC are chronic infection with hepatitis B virus (HBV) or hepatitis C virus (HCV), aflatoxin-contaminated food, heavy alcohol intake, obesity, smoking, and type 2 diabetes and the major risk factors vary from region to region[2].

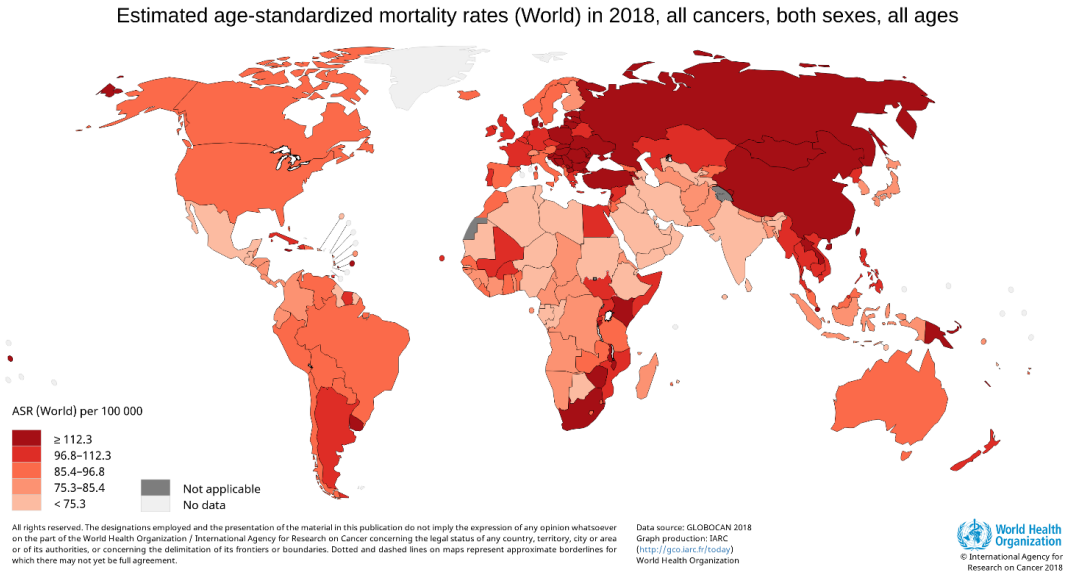

Fig. 1 Global map presenting age-standardized incidence rates of liver cancer by world countries for males and females for all ages in 2018 [1].

In most of the cases, HCC is associated with advanced fibrosis or with cirrhosis[3], which makes the situation for the patient even more difficult. The precise mechanisms responsible for the development of HCC in cirrhotic liver and more in general in advanced

chronic liver diseases are poorly understood; hence, intensive research is currently ongoing.

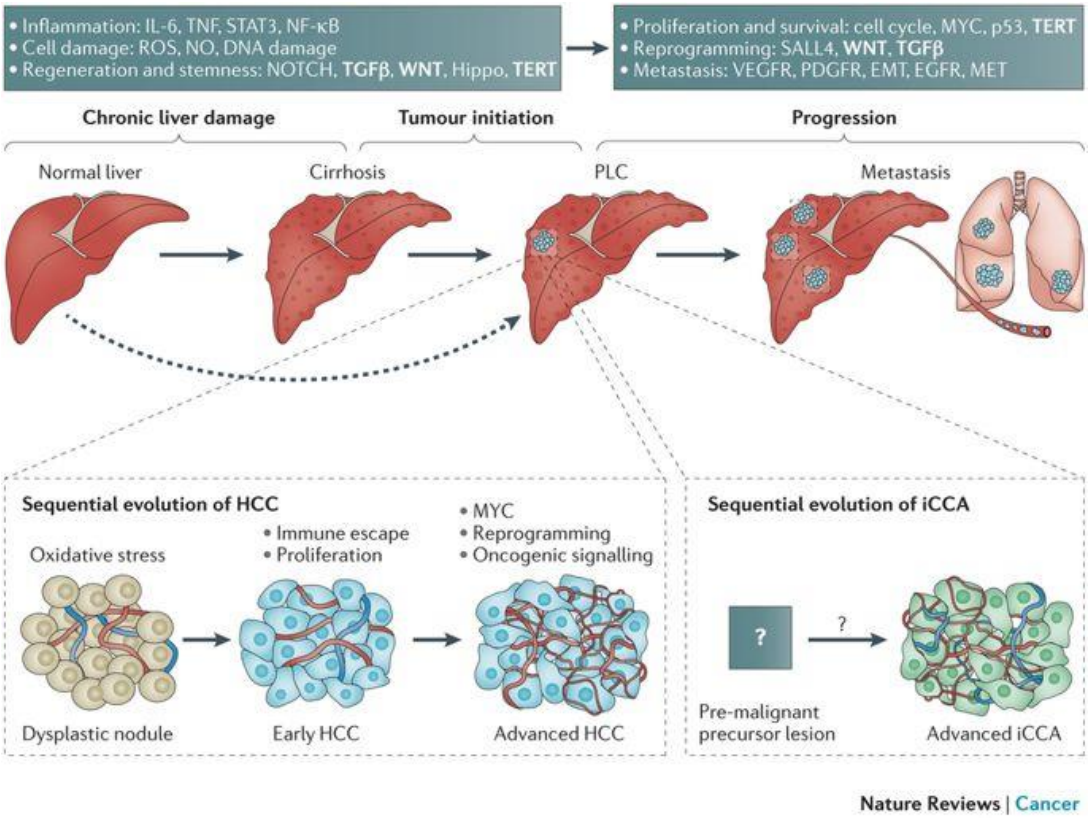

Fig. 2 Evolution of Primary Liver Cancer (PLC).

The common end stage of the majority of chronic liver diseases is the development of liver cirrhosis. Therefore, the chronically altered liver microenvironment, induced by cirrhosis, can be considered a necessary predisposing factor for cancer development in the vast majority of primary liver cancers. The dashed arrow indicates that a minority of tumours arise from a normal liver and develop into PLC without cirrhosis. In hepatocellular carcinoma (HCC), a multistep process is characterized by the occurrence of morphologically distinct stages: dysplastic nodules, early HCC and advanced HCC. For intrahepatic cholangiocarcinoma (iCCA), the sequential evolution and underlying phenotypic features are not well known*[3]*.

5.1.1 Cirrhosis

Among all the risk factors for HCC, cirrhosis of the liver is the most important as not only it is present in approximately 80% of HCC patients but it is a link between also other factors important for the pathogenesis[4]. Cirrhosis is characterised by distortion of the liver parenchyma associated with fibrous septae and formation of regenerative nodules, extensive neo-angiogenesis and progressive increase of portal pressure due to an increase in intrahepatic vascular resistance (portal hypertension)[5].

Although the aetiology of cirrhosis is multifactorial, all cases of liver cirrhosis share some pathological features that include necrosis of hepatocytes, and replacement of liver parenchyma by fibrotic tissues and regenerative nodules, and loss of liver function[6]

Multiple cell types contribute to the pathogenesis of liver cirrhosis, both hepatic parenchymal (hepatocytes) and non-parenchymal cells are involved. The walls of hepatic sinusoids are lined by three different non-parenchymal cells: liver sinusoidal endothelial cells (LSECs), Kupffer cells (KCs), and hepatic stellate cells (HSCs).

5.1.2 Non-cirrhotic hepatocellular carcinoma

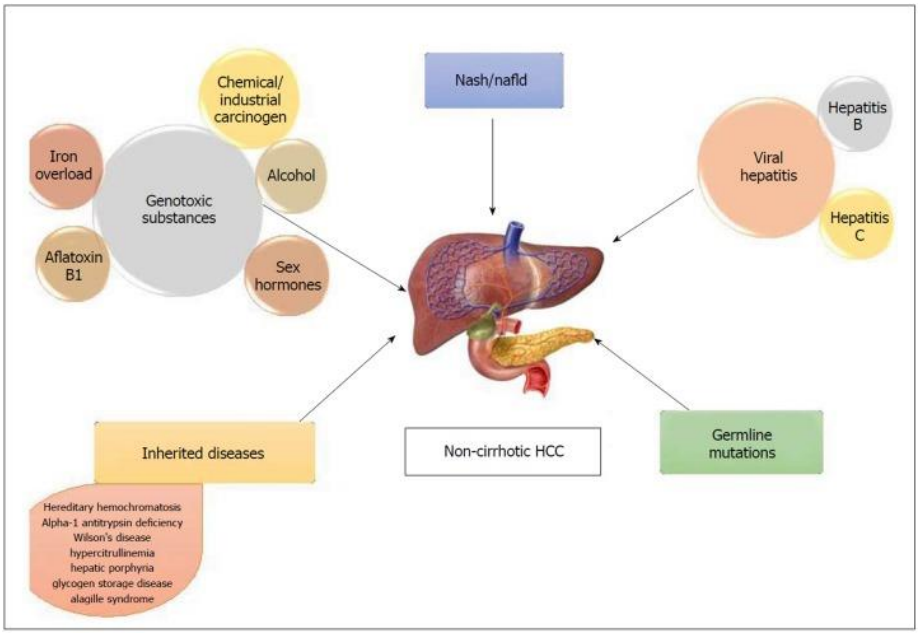

Fig. 3 Causes of non-cirrhotic hepatocellular carcinoma (HCC)

Illustration shows causes involved in carcinogenesis of hepatocellular carcinoma (HCC) in non-cirrhotic liver. HCC can also be associated with other liver diseases, such as non-alcoholic fatty liver disease (NAFLD), non-alcoholic steatohepatitis (NASH), Viral hepatitis, exposure to genotoxic substances and sex hormones, inherited diseases, genetic mutations[7].

The percentage of cases of HCC in the absence of cirrhosis varies widely between various geographical areas. However, on average, HCC arises in a non-cirrhotic liver in 20% of patients [2].

This may be the consequence of different patterns of underlying risk factors, such as viral hepatitis, alcohol abuse and non-alcoholic fatty liver disease (NAFLD). Indeed, this is more commonly associated with patients who have as background viral hepatitis and non-cirrhotic HCC occurs more commonly in less developed regions of the world than in the Western countries[8].

NAFLD is a leading cause of chronic liver disease in Western countries. It has recently been demonstrated that also in non-cirrhotic livers, the presence of NAFLD, and especially non-alcoholic steatohepatitis (NASH), is strongly associated with HCC[9]. Furthermore, steatosis is often present as co-factor in patients with other risk factors that underlie liver disease [10, 11].

5.1.3 Hallmarks of cancer in HCC

For the development of HCC, a tumour cell or the whole tumour respectively, needs to acquire several modifications, which were classified by Hanahan and Weinberg as the hallmarks of cancer [12, 13] as depicted in Fig. 4. They include sustained proliferative signalling, evasion from growth suppressors, resistance to apoptosis, and induction of angiogenesis, tissue invasion and metastasis. Moreover, recently the hallmarks were extended with two enabling hallmarks, which are genome instability and tumour-promoting inflammation, and the ability to avoid immune destruction.

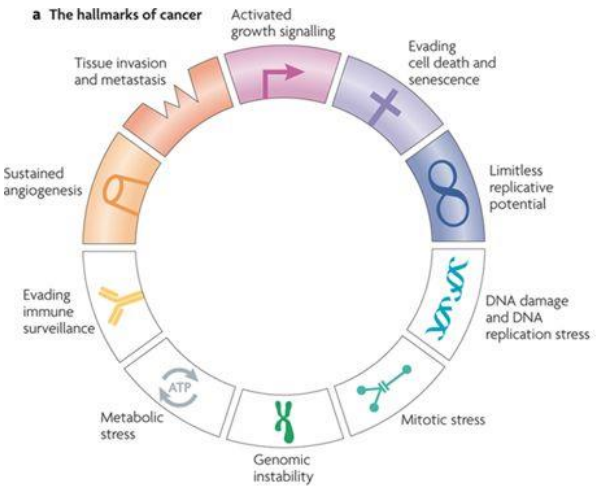

Fig. 4 The next generation of hallmarks of cancer.

Schematic representation of key features of tumour cells together with the underlying mechanisms allowing for a rapid progression of cancer cells[12].

Inflammation is a key hallmark of a chronic injured liver. The inflammatory response leads to production of pro inflammatory cytokines such as IL6, TNF-α, IL1 and IL18 through inflammasome dependent or independent pathways and aid to the further development of an environment favouring tumour development. Furthermore, tumour cells are altered in such a way that they can escape the immune system[14].

The development of a tumour like HCC occurs in several steps with frequent mutations and is not only driven by genetic alterations in the cancer cells alone but also by tumour microenvironment[15]. Researcher focused on the identification of factors that could contribute to the disruption of the liver microenvironment and promote the generation of a pre-malignant niches that leads to liver cancer development [16].

Thus, it is mandatory to consider that a specific tumour microenvironment characterizes the pathogenesis of liver cancer. The tumour microenvironment is a complex system, largely orchestrated by inflammatory cells, that includes cancer cells, stromal elements, such as immune cells, fibroblasts, myofibroblasts, as well as the surrounding extracellular matrix (ECM). The role and the functionality of the ECM and immune cells in HCC will be discussed in detailed in the subsequent chapters of this thesis.

5.2 ECM and Liver cancer

The ECM can regulate many of the same cellular responses that characterize the cancer hallmarks describe above. ECM includes the interstitial matrix and the basement membrane and it is composed of structural collagens as well as many different glycoproteins, proteoglycans and hyaluronan. In particular, proteoglycans have the function of storing growth factors within the ECM.

Important, every organ has a specific ECM composition to serve a particular tissue-specific function. In the organs, resident cells can change and produce ECM components in accordance with the needs of the tissue [17].

In chronically inflamed tissues, aberrant ECM expression and fragments of the ECM that are derived from tissue-remodelling processes can influence immune cell activation and survival, thereby actively contributing to immune responses at these sites[18] (Fig.5). Indeed, the development of the pre-neoplastic niche almost always occurs in a cirrhotic liver, and in this chronic setting immune cells are sensing the tissue injury, thus creating a “proinflammatory cytokine storm” that results in hepatocyte cell death. This sequence

of events leads to the phenomenon called necroinflammation. Moreover, the response of the resident cells to necroinflammation and cellular death culminates in the deposition of extracellular matrix (ECM) by activation of hepatic stellate cells (HSCs) and activation of mature hepatocytes to proliferate and regenerate[19].

This process is associated with distortion of the parenchyma and vascular architecture characterized by progressive capillarization, with reduction of endothelial cell fenestrae size, and deposition of basement membrane components including collagen type IV and laminin within the space of Disse[20].

As mentioned before, the preneoplastic setting of the cirrhotic background provides a favourable environment for cellular transformation. This promotes the development of dysplastic nodules and their malignant transformation to early HCC supporting the accumulation of mutations and epigenetic aberrations in preneoplastic hepatocytes or liver stem cells[21].

Several findings have revealed that the deposition of cancer-associated ECM changes its physical and biochemical composition[22]. Increased stiffness has also been observed in HCC tumours, promoted by LOX-mediated collagen crosslinking that could stiffen ECM [23, 24]. HCC ECM overexpress-enzymes such as MMPs that allows cells to overcome the physical barrier of basement membrane and acquire invasiveness capacity. For example, *MMP-9* is probably involved in HCC invasion, and its overexpression in HCC patients correlates with different pathological clinical parameters (i.e. tumour stage and size) [25, 26]. Therefore, the role of the microenvironment in tumour initiation and progression in HCC is critical and alterations within the microenvironment may favour tumour progression and play an important role in chemoresistence[21].

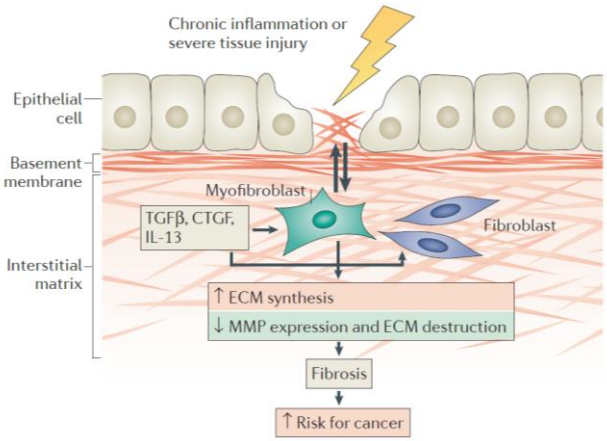

Fig. 5 ECM production in human disease.

Chronic inflammation a tissue injury cells (myofibroblasts and fibroblast) are stimulated to produce more ECM resulting in pathological fibrosis[18].

5.3 Liver immunology

The liver is considered the largest internal organ of the body. It functions as the primary site for the metabolism as nutrient storage and detoxification activities. Furthermore, the liver is involved in the clearance of bacterial products and toxins from the blood.

Even if the liver is classically perceived as a non-immunological organ, it is now recognised as a secondary lymphoid organ[27].

The liver is a site marked by a complex immunological activity, responsible for the production of acute phase proteins, cytokines and chemokines all mediated by immune cells as well as non-hematopoietic cell populations[28].

The liver has an unusual hemodynamic scheme. It receives blood from the pancreas, spleen, and gastrointestinal (GI) tract that reaches the liver via the portal vein but the liver receives blood from the systemic circulation (Fig. 6).

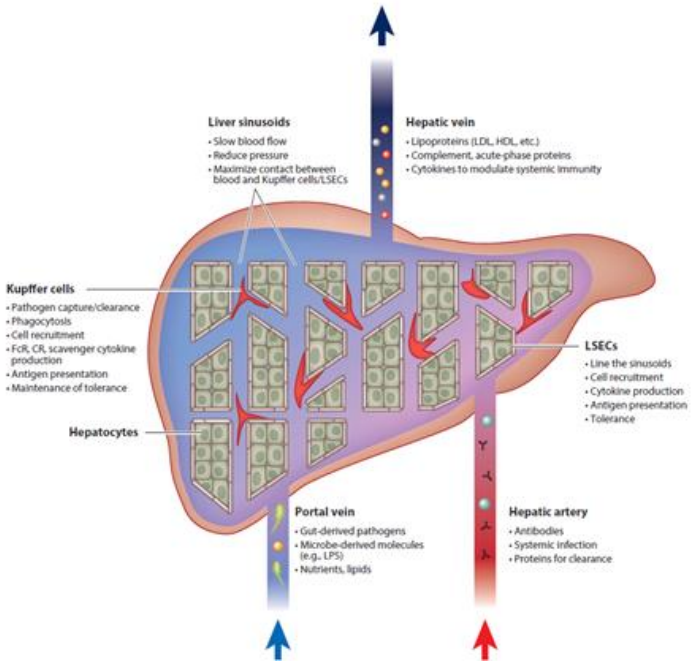

Fig. 6 Anatomical organization of the liver.

The liver is supplied with blood by both the hepatic artery and the portal vein (bottom). As the blood enters the liver, it is forced into the honeycomb of the sinusoids. The low flow rate increases the exposure of the blood to the Kupffer cells (KC) and liver sinusoidal endothelial cells (LSECs). Both Kupffer cells and LSECs filter the blood, removing pathogens and molecules. Under appropriate conditions, these cells can activate and

initiate the immune response through the production of cytokines and the recruitment of additional immune cells[29].

The internal structure of the liver is made of several liver lobules. Each lobule consists of a central vein surrounded by six hepatic portal veins and six hepatic arteries. Blood will then slowly flow within the sinusoids. The vascular architecture together with a slow blood flow allows a close interaction between the systemic circulation and liver cells[30]. The sinusoids are lined by liver sinusoidal endothelial cells (LSECs) that are perforated by fenestrations allowing the extension of membrane protrusions from both hepatocytes and infiltrating lymphocytes. Hepatic stellate cells (HSCs) and dendritic cells (DCs) are present in the space of Disse between the endothelial cells and the hepatocytes.

Kupffer cells (KC), which are liver-resident macrophages, are adhered to the endothelium and emit extensions into the space of Disse acting as a bridge between the blood and components of the liver parenchyma [31].

T cells constitute nearly 50% of the liver-resident lymphocytes, including conventional αβ T cells, innate-like MAIT cells (almost 50% of all T cells in the human liver), iNKT cells (1% of human liver-resident T cells) and γδ T cells (comprising about 15% of human liver-resident T cells)[32, 33]. The remaining liver-resident lymphocytes comprise NK cells (nearly 50% of the liver-resident lymphocytes) and B cells[34].

The low flow rate result in stasis, which extends the contact between lymphocytes and antigen-presenting cells (APC) and promotes lymphocyte extravasation and gain access to the space of Disse via cytoplasmic extensions (Fig. 7).

LSEC are important liver-resident antigen-presenting cells (APCs) that can take up antigens from the blood stream or from the liver tissue and present these to lymphocytes, primarily CD8+ and CD4+ T cells[30] .

In the liver, hepatocytes, APCs and effector cells of the innate (NK and NKT cells) and the adaptive (T and B cells) immune system are able, when necessary, to induce an immune response[35].

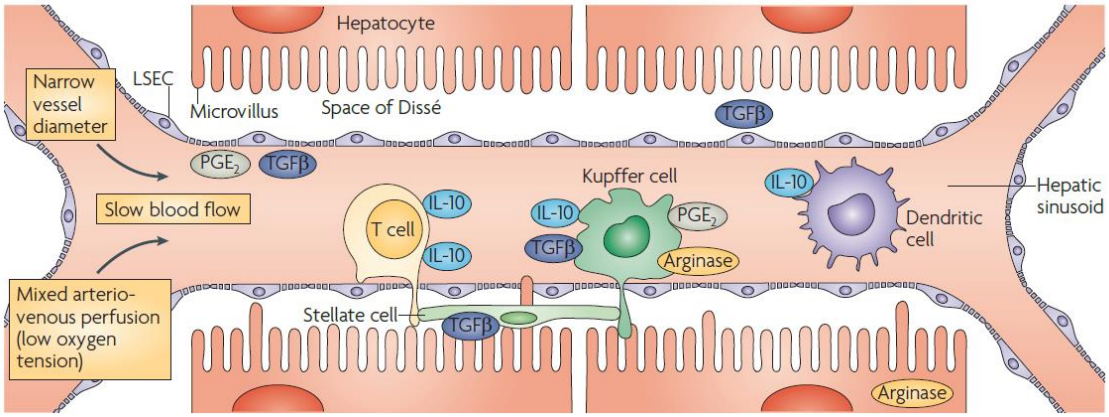

Fig. 7 Liver microanatomy.

Schematic view of the microanatomy of the hepatic sinusoid. Hepatocytes are separated from the blood rich in antigen-specific and non-antigen specific CD8+ T cells, NK cells and myeloid cells, passing through the sinusoids of the liver lined by non-parenchymal LSEC. The space between the sinusoid and parenchyma, within which lie HSC, is referred to as the Space of Disse[36] .

A peculiar hepatic regulatory mechanism prevents the induction of immunity against innocuous antigens, such as gut-derived nutrients, antigens from aged or damaged cells that are cleared from the circulation in the liver and neo-antigens that arise by adduct formation of metabolic products during detoxification of, for example, alcohol.

One plausible model for liver tolerance is that, when CD8+ T cells are primed in the liver, appropriate CD4+ T-cell help may not always be available. The consequence is dysfunctional, exhausted CD8+ T cells and thus failure to eliminate the pathogen. The immune response's impairment is amplified by other factors, including the prevalence of liver antigen-presenting cells (APCs) expressing co-inhibitory ligands, such as programmed death ligand 1 (PD-L1), which stimulate regulatory T (Treg) cells. All these factors may contribute to immune failure through parallel mechanisms.

Naive T cells do not typically enter non-lymphoid tissues without having been activated previously upon recognition of their corresponding antigen presented by APCs[37]. The liver, however, represents an exception to this, as it has the ability to retain prime naive T cells that are activated within this non-lymphoid organ following antigen-presentation by various liver-resident cells[38].

5.3.1 The liver microenvironment: liver-resident immune cells

5.3.1.1 Phagocytes: Macrophages and Monocytes

The largest population of macrophages reside in the liver as resident Kupffer cells (KCs). Indeed, this population represents almost 80–90% of total tissue macrophages and represent ∼35% of the liver non-parenchymal cells. These cells are located inside the sinusoids in direct contact with the blood circulation. Moreover, KCs and endothelial cells form a network by cytoplasmic extensions called the reticuloendothelial system (RES), which represents the first line of defence against immunoreactive material reaching the liver from the GI tract via the portal circulation. Accordingly, this system may be regarded as the final component of a functional gut barrier [39, 40]. In this context, KCs are able to discriminate between immune cells, red blood cells and platelets and possible pathogens that may have entered the bloodstream[41].

The immunophenotype of hepatic macrophages is quite heterogeneous. Although the lack of a specific marker to identify hepatic Kupffer cells, these cells are identified by their expression of CD14, CD16, CD68 (subset with phagocytic activity) and CD11b (a subset with cytokine producing capacity) [42]. KC express numerous pattern recognition receptors, such as Toll-like receptors (TLRs), complement receptors, and antibody receptors, all of which are molecules that are necessary for the detection, binding and internalization of pathogen-associated molecules. Furthermore, through these receptors, KC function as an immune sentinel, activating downstream signalling pathways resulting in the production of cytokines and interferons, and alerting other components of the immune system to the presence of pathogens[43].

KC play an important role as antigen presenting cells (APCs), expressing MHC-I, MHC-II and co-stimulatory molecules that are necessary for T cell activation[44]. Kupffer cells are modulated by innate immune signals, pathogen-associated molecules (TLR ligands, in particularly LPS) or inflammatory cytokines. This induces a switch in their immunological

role from tolerance-inducing APC to immunogenic APC capable of robust activation of T cells[44].

Immune regulation in the liver may also be controlled by another myeloid lineage populations beyond that of the resident KC. Local aggregations of myeloid monocytes expressing CD11b, which have been termed iMATES (intrahepatic myeloid cell aggregates for T cell clonal expansion), promote proliferation of $CD8^+$ T cells in the apparent absence of local antigen. iMATE myeloid population could be considered advantageous to an anti-viral or anti-tumour immune response. Moreover, other populations of immature myeloid cells have also been described in the liver[45]. One such subset is the granulocytic Myeloid-Derived Suppressor Cells (MDSC). MDSC exhibit a wide-range of immunosuppressive functions, that affect both the innate and adaptive immune systems [46].

5.3.1.2 Lymphoid & myeloid cells of the liver

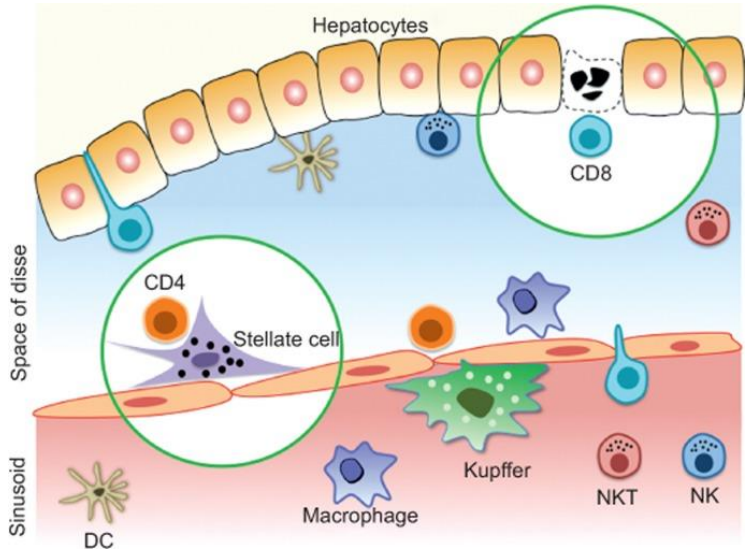

Fig. 8 Schematic view of the micro-architecture of the hepatic sinusoid.

Hepatocytes are separated from the blood, rich in antigen-specific and non-antigen specific CD8+ T cells, NK cells and myeloid cells, passing through the sinusoids of the liver lined by non-parenchymal LSEC. To interact directly with hepatocytes, CD8+ T cells must cross the endothelial barrier and enter the space of Disse. CD4+ T cells also enter this space but cannot directly interact with hepatocytes. However, they find other interacting partners such as DCs and hepatic stellate cells that reside in the Space of Disse[47].

As already mention, the composition of the total lymphocyte population of the liver is uncommon. Between 40-60% of the intrahepatic lymphocytes are NK cells, which is three times more than the ones present in the periphery. NK cells are lymphocytes belonging to the innate immune system and are able to kill virus-infected or malignant cells. Moreover, in contrast to T cells, NK cells can be classified also as innate immune effector cells because they do not need priming for activation and their receptors are not generated via the process of somatic recombination[48].

NK cells are defined by the cell surface expression of CD56, the 140-kDa isoform of neural cell adhesion molecule (NCAM), found on NK cells and a minority of T cells and by the absence of CD3 (called NKT)[49]. $CD56^{+}$ cells can be further classified into two subsets, depending on their immunophenotype and function: $CD56^{dim}$ and $CD56^{bright}$. $CD56^{dim}$ constitutes 90% of the total NK cell population in peripheral blood. In contrast, $CD56^{bright}$ NK cells represent 50% of the NK cells resident in the liver[50].

NK cells kill target cells via the formation of an immune synapse and by releasing cytotoxic granules (containing perforin and granzyme). However, NK cells can also produce and release pro-inflammatory cytokines, such as IFNγ and TNFα [49, 51, 52].

Not only NKs cells but also T cells are more abundant in the liver compared to the periphery. In fact, the ratio between CD4+ and CD8+ T cells is different in the liver. The T cells population, which express the CD3 surface marker, are classified in $CD4^{+}$ helper (Th) or $CD8^{+}$ cytotoxic (CTL) populations. $CD4^{+}$ helper T cells are further classified based on the cytokine profile of the cells as Th1 and Th2. The most common markers used to identify Th1 cells are IFN-gamma producer and expression of the T-bet transcription factor, while IL-4 is the most commonly used marker for Th2 cell identification. In normal conditions, the peripheral blood percentage of $CD4^{+}$ T cells is higher than $CD8^{+}$ T cell. In the liver, this ratio is inverted, with $CD8^{+}$ T cells more present than their $CD4^{+}$ counterparts (1:3.5 for liver versus 2:1 for blood lymphocytes). Resident hepatic T cells are phenotypically different from T cells in the peripheral blood. The CD8α chain with no CD8β chain was present in 15.4% of hepatic $CD3^{+}$ T cells, while that phenotype was not observed in blood $CD3^{+}$ cells. The liver also contains a large number of γδ T cells, which

again have altered frequencies in the intrahepatic environment. Moreover, a population of T cell absent in the PB, have been found and characterized as intra hepatic (T-bet^{lo}Eomes^{lo}Blimp-1^{hi}Hobit^{lo}). These observations suggest local control of function and/or differentiation of hepatic lymphocyte populations compared to peripheral blood [53].

5.4 The importance of the immune system in HCC

Different inflammatory conditions can lead to neoplastic transformation. However, whether or not the inflammation is present in the beginning of carcinogenesis, most tumours progress from a state of chronic inflammation that fuels different aspects of tumour progression, including genomic and epigenomic instability, immune evasion, stromal organisation, angiogenesis, and metastatic dissemination.

Nowadays it is well known that chronic inflammation is an important hallmark of cancer, often associated with microbial infections, autoimmunity, and immune deregulation.

T cells are the main component involved in the anti-tumour immune response. The anti-tumour T-cell response in particular has been proven to be effective at targeting and eliminating cancer cells[54]. The density of $CD8^+$ T cell in the tumour microenvironment is associated with positive prognosis for the majority of cancers [48]. Although HCC is not generally considered an immunogenic tumour, high levels of tumour infiltrating lymphocytes (TILs) in HCC patients have been correlated with a lower risk of recurrence and a better prognosis. This suggests that an immunomodulation to elicit potent antitumor responses should be explored for the treatment of HCC [55].

The balance between effector and tolerogenic immune response could dictate tumour fate. Indeed, during the early stages of tumour development, effector immune cells eliminate immunogenic cancer cells[56]. In the first step of cancer immunity (Fig. 9), the death of cells caused by the growing tumour results in the release of danger immunogenic signals and the expression of cytokines[57]. All these signals cause

dendritic cell (DC) activation and consequently DCs mobilization towards the lymph node and to secondary or tertiary-lymphoid structures for processing and for the presentation of antigens[58]. During antigen presentation, naïve T cells carrying a TCR specific for the tumour-associated antigens (TAAs) are primed and activated. This is a critical stage in the immune response, as at this point the balance between a T effector or T regulatory response is determined. Activated effector T cells (Teff) exit the lymphoid organs, after which they migrate through the bloodstream[57].

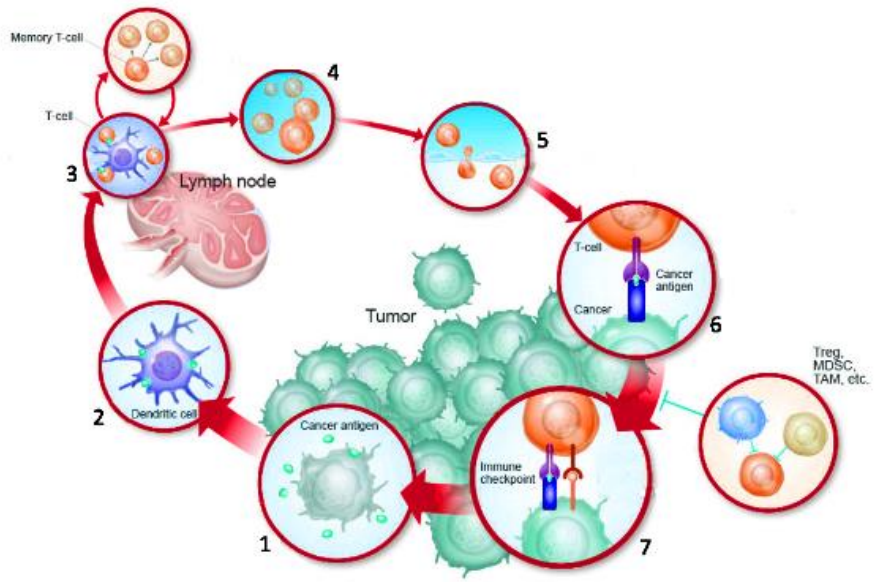

Fig. 9 The Cancer-Immunity Cycle.

In the first step, neoantigens are released by cancer cells (1) captured by dendritic cells (DCs) for processing (2). Next, DCs present the captured antigens on MHCI and MHCII molecules to T cells (3), resulting in the priming and activation of effector T cell responses against the cancer-specific antigens that are now viewed as foreign, or antigens against which central tolerance has been incomplete. Finally, the activated effector T cells migrate (4) and infiltrate the tumour bed (5), specifically recognizing and binding to the cancer cells through the interaction between its T cell receptor (TCR) and its cognate antigen bound to MHCI (6), and kill their target cancer cell (7). Immunity can be promoted or inhibited by engagement of immune checkpoints that can reduce immune activity and/or prevent autoimmunity (adapted from[59]).

At the tumour site, activated T cells transmigrate across the endothelial layer. Once in the tumour microenvironment, T cells recognize TAAs presented on MHC-I by the tumour

cells through their TCR and are able to exert their cytotoxic activity. The killing of tumour cells results in more release of TAAs and the start of a new cycle from step 1 of the cancer-immunity cycle (Fig. 9)[59].

However, cancer cells adopt different strategies to avoid the immune response, for example by inducing peripheral immune tolerance and by the recruitment of immunosuppressive immune cells.

5.4.1 Immune cells reaching and infiltrating the tumour site

It is now clear that the presence of TIL may affect the clinical evolution of the disease and even on patients' survival. Early evidence indicated that HCC, with marked T cell infiltrate, were associated with a lower recurrence rate and higher 5-year survival rate compared to tumours without T cell infiltration [60, 61]. Thus, one of the goals of immunotherapy is to enhance immunogenicity and immune cells infiltration, increase TILs density, and induce a systemic tumour-specific T cell response in the tumour bed.

Infiltration of T cells into the tumour microenvironment is an important factor of cancer progression. In HCC tissues, $CD4^+CD25^+$ Tregs impair proliferation and activation of $CD8^+$ as well as their cytotoxicity (degranulation, production of granzymes and perforin)[62]. In this condition, chemokines play a pivotal role in orchestrating T cell trafficking and consequently the immune response. Tumours with high presence of TILs also express high amounts of chemokines that can attract them to the tumour bed. Among those chemokines are for example CCL2, CCL3, CCL4, CCL5, CXCL9 and CXCL10 that can promote the gathering of lymphocytes in HCC [63, 64].

The characterisation and quantification of immune cells accumulated within the tumour may be an important prognostic factor. Since 2009, a new definition has been proposed for an immune-based classification of the tumour, introducing the concept of "hot", "altered" and "cold" tumour[65]. Indeed, this classification of tumours is based on the density of lymphocytic infiltrate in tumour microenvironment and defined as such: 1)

inflamed tumours (hot tumours) are those with lymphocytic infiltrate; 2) immune-excluded (or cold tumours), tumours with lymphocytes only at tumour edges, and 3) immune-deserts (altered), those with few lymphocytes near tumour tissue (Fig. 10) [66].

Among the cold tumours, the immune desert phenotype is characterized by a microenvironment that lacks immune-effector T cells. In this context the lack of immunogenicity functions are the results of an ineffective T cell priming or activation. Although in the immune-excluded phenotype T cells are present near the tumour, T cells seem to be unable to infiltrate the stroma and the tumour parenchyma. Therefore, T cells cannot penetrate the tumour site to recognize and kill cancer cells. Both immune-desert and immune-excluded cold phenotype tumours are associated with low responsiveness to treatments[66].

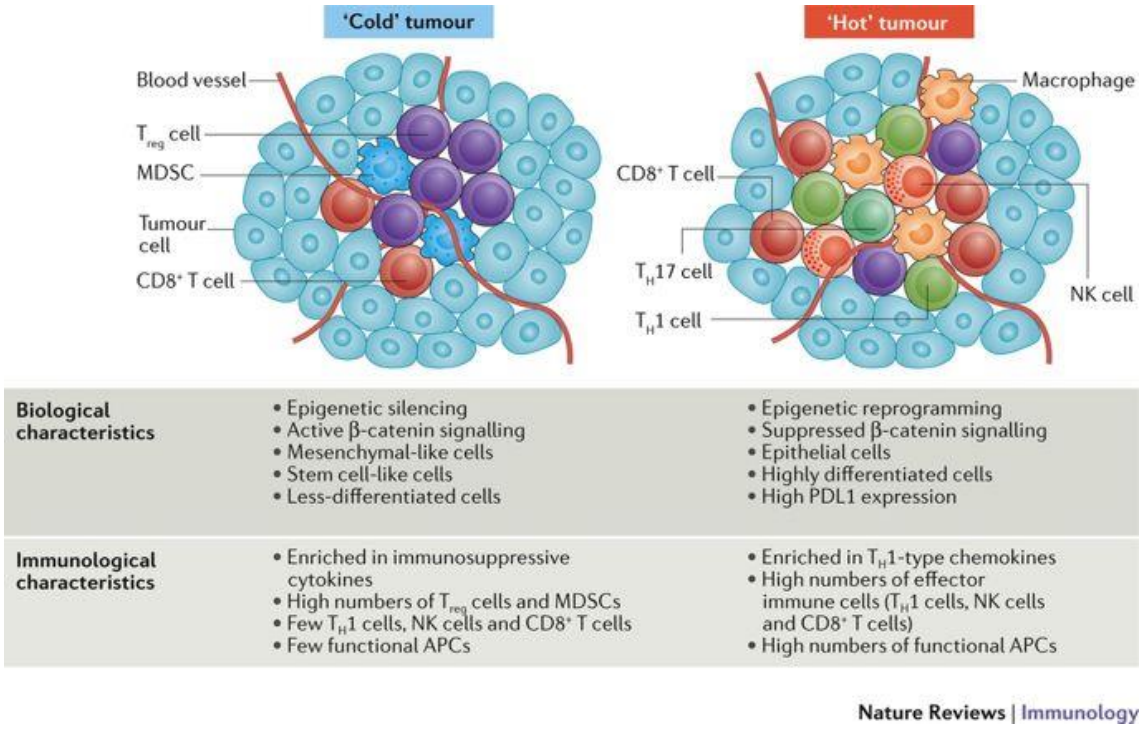

Fig. 10 Hot and cold tumour immune phenotype and biological phenotype.

The biological and immunological phenotypes of the tumour regulate those mechanisms such as chemokine expression and control of immune cell infiltration into tumours. This affect the presence of high or low immune cell infiltration, allowing the immunological classification of tumours into 'hot' (inflamed) or 'cold' (non-inflamed) phenotypes (right and left, respectively)[67].

Hot tumours on the contrary are characterized by the presence of efficient T cells and the local production of pro-inflammatory cytokines which makes cancer cells more sensitive and responsive to immunotherapy treatments[66, 68]. The density and distribution of immune cell infiltration might also help to stratify patients into responders and non-responders to anticancer therapies [69].

The response to therapies in the different phenotypes will be discussed in detailed in the subsequent chapters of this thesis.

5.4.2 Immune escape and immunosuppression in HCC

One of the most important challenges in the immune oncology field is understanding how cancer cells avoid destruction by the immune system.

Tumours have developed a number of unique ways to suppress the recruitment of T cells to the tumour site. The exact mechanisms have not been fully elucidated, but the disruption of chemokine production is believed to be a contributing factor.

The immunoediting to avoid immune detection by cancer cells can be summarized into three main mechanisms, illustrated in figure 11, which are the so-called “3E”: (1) elimination, (2) equilibrium, and (3) escape.

In the elimination phase, the immune system is activated by danger signals from the tumour cells and recognizes TAAs, initiating to mount an adaptive immune response.

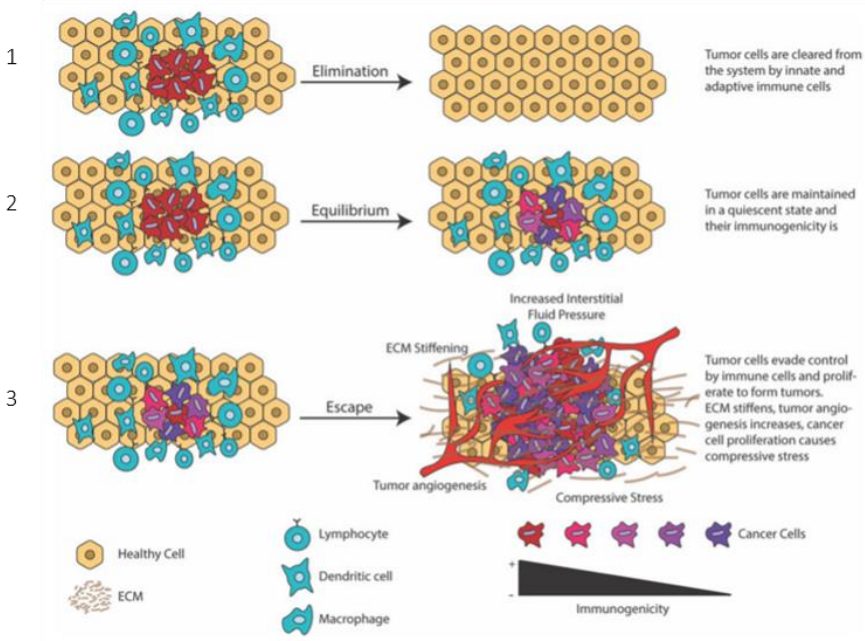

Fig. 11 Stages of cancer immunoediting.

Elimination: cancer cells are controlled and removed from the body by the innate (e.g., macrophages and dendritic cells) and adaptive (e.g., B- and T-lymphocytes) immune system. Equilibrium: cancer cells are kept at a dormancy state and tumour size is constant. Escape: cancer cells breach the immune system and grow uncontrollably. In addition, the ECM stiffens, tumour angiogenesis and interstitial fluid pressure increases, and cancer cell proliferation causes compressive stress in the interior of the tumour. In later stages, cancer cells collectively migrate and invade neighbouring tissues and finally enter the vascular system to form metastasis in distant organs[70].

In the equilibrium phase, tumours avoid immune destruction resulting in co-existence of adaptive immune response and the tumour. This phase includes the downregulation of MHC I expression, thereby reducing self-antigen presentation, the upregulation of immune checkpoint molecules such as PD-L1 to induce T cell exhaustion [71, 72].

Immune checkpoints are co-inhibitory molecules that control the duration and the strength of the immune response to prevent hyper-activation of T cells. This class of molecules includes CTLA-4, PD-1, TIM-3, lymphocyte activation gene 3 protein (LAG-3) and B and T lymphocyte attenuator (BTLA)[73].

Not only cancer cells but also components of the immune system may promote, rather than suppress, the development of tumours that are able to evade the immune

surveillance. The immunoediting process lead to a continuous selection by the immune system on tumour cells. Cells that “escape” from this immunosurveillance could result in progressively immunoresistant cancer variants[74].

Immunosurveillance can play an active role in suppressing the growth of early tumours. However, when tumours progress and grow, indicates that they may have “escaped” from this immunosurveillance. Another hypothesis is that tumours function as immunologically normal tissue and are not recognized by immune cells. In fact, tumour cells appear immunologically as healthy cells that do not send out danger signals to activate the immune system (cancer immunity cycle), because they do not express signals that can alarm the innate immune cells[75].

Under physiological conditions, the liver has the capacity to induce tolerance against antigens delivered from the intestine and as consequence can inhibit immune responses (Fig.12) [45].

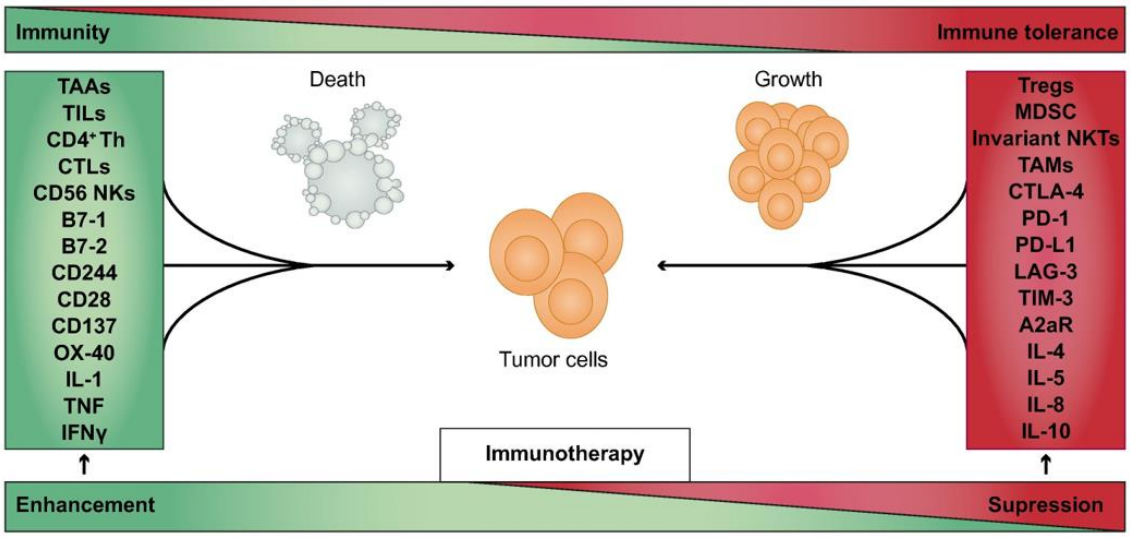

Fig. 12 The counteracting forces regulate the balance between tumour progression and tumour elimination.

Immune status of an HCC-bearing host is characterized by different immune responses leading to immunity or immune tolerance and thereby promoting tumour cell death or growth, respectively. Unfortunately, multiple immune alterations associated with carcinogenesis and disease progression shift the immune response towards tumour immune tolerance and disease progression. Treatment approaches such as immune checkpoint blockers can bring the balance back towards immunity and cancer cell death.

In fact, factors significantly contributing to the development of HCC are those that can induce tumour antigen tolerance, alterations in the function of immune components and decrease recognition of malignant cells [76].

The expression of immune checkpoints by tumours is a well-established mechanism of immune evasion (escape phase). CTLA-4 is expressed by activated T cells and by Tregs cells. It competes with the activating molecule CD28 for binding CD80 and CD86 and activates Tregs [60, 77].

Activated T and B lymphocytes, NK cells, monocytes and DCs express PD-1[78]. The interaction between PD-1 and PD-L1 inhibits T cell effector function and leads to T cell exhaustion. The immune infiltrate of HCC is enriched in $PD1^+$ $CD8^+$ cells and their density are associated with disease prognosis [79]. The expression of PD-L1 in HCC has also been reported as an adverse prognostic factor [80, 81].

Cytokines are also involved in the regulation of immune cell function as their role include pro- and anti-inflammatory functions. In HCC patients, high levels of IL-10 and TGF-β, and reduced levels of IFN-γ have been detected[14]. IL-10 has a tolerogenic effect in the liver that leads to inhibition of CD4+ T cell activation and, as a consequence, of cytotoxic CD8+ T-cell function[82]. In addition, TGF-β, produced by parenchymal and non-parenchymal liver cells, is implicated in the maintenance of liver immune homeostasis. TGF-β can induce the differentiation of naive CD4+ T-cells into Tregs, that could inhibit the differentiation of naive CD8+ T cells to effector cells[83] and this leads to a reduced expression of perforin and IFN-γ that further prejudice the CD8+ T-cell cytotoxic activity[84].

5.4.3 EMT: epithelial to mesenchymal transition

EMT is the process by which an epithelial cell switches to a more mesenchymal-like phenotype (Fig. 13). This shifting in phenotype consists of a diverse range of cellular

events including an increased resistance to apoptosis, loss of apical-basal polarity, dissociation of cellular adhesion junctions (cell-cell and cell-basement membrane attachments), and major architectural reorganization of the cytoskeleton. These events are associated with simultaneous up-regulation of mesenchymal markers and downregulation of epithelial markers[85]. The acquisition of mesenchymal properties increases motility of the cells together with increased enzymatic activity, which causes remodelling of the basement membrane. This facilitates migration of transitioned cells to gather/accumulate in the interstitium of the tissue[86].

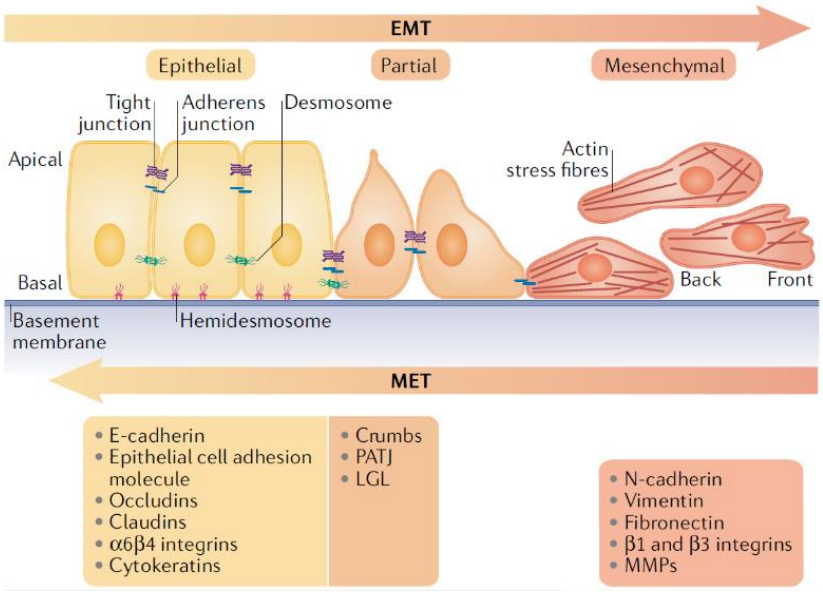

Fig. 13 Schematic representation of the EMT programme.

Epithelial cells showing apical–basal polarity is held together by tight junctions, adherens junctions and desmosomes and are tethered to the underlying basement membrane by hemidesmosomes. Induction of epithelial– mesenchymal transition (EMT) leads to progressive loss of epithelial features (listed in the yellow box) together with the acquisition of a partial or complete set of mesenchymal features; mesenchymal features acquired (listed in the orange box), and cells display front-to-back polarity and a reorganized cytoskeleton. During EMT, cells become motile and acquire invasive capacities. EMT is a reversible process, and mesenchymal cells can revert to the epithelial state by undergoing mesenchymal–epithelial transition (MET)[87].

EMT is a process, which is responsible for a degree of epithelial-phenotype destabilization and acquisition of mesenchymal-like cellular features that alters the migratory abilities of

cells. These events can be due to changes in the cell-cell junctions, the cytoskeleton and cell-ECM adhesion as well as the migration of invasive cells[88].

With the loss of cellular adhesive junctions, cytoskeletal reorganization and loss of apical-basal polarity, cells acquire invasive properties. Furthermore, this can increase resistance to apoptosis and anoikis, which is programmed cell death initiated following loss of cell attachment to the surrounding ECM [89, 90].

Different regulatory pathways modulate EMT; TGF-β is a potent inducer of EMT both during development and in cancer. It was shown to promote single-cell migration of mammary tumour cells[91].

Furthermore, EMT is associated with loss and reorganization of other epithelial markers, such as loss of keratin expression is considered as an important EMT indicator. Beside E-cadherin, the expression of other tight junction associated proteins, such as occluding and claudin are downregulated during EMT [92]. Vimentin is another protein that has been shown to participate in the cytoskeletal reorganization that occurs during EMT[93].

In a fibrotic context, epithelial cells are likely to undergo EMT as a response to injury. Recently, the association of EMT to the ‘‘redox-based escape mechanism from death’’ of the hepatocytes has been proposed. In fact, cells develop an adaptive response and “escape” from a hostile microenvironment characterized by an altered ECM composition, inflammation, increased production of reactive oxygen species and hypoxia [5, 94, 95].
Such motility prospects two possible outcomes: the motile epithelial cell migrate in metastatic areas by reversing their mesenchymal phenotype (MET), or in the presence of a sustained hostile milieu, the newly acquired ‘‘escaping’’ phenotype becomes again sensitive to anoikis with the consequent induction of apoptosis[95].

5.5 Liver metastasis

One of the biggest obstacles to finding a cure for most solid cancers is not the removal of the primary tumour, but the elimination of metastases. Metastasis remains the cause of over 90 % of deaths from solid tumours[96]. Among all the organs, the liver is the most common site for colonization of cancer cells, resulting in a high incidence of liver metastasis and a high risk of cancer-related death. In addition, the liver is a favourite site of metastasis of other cancers for colorectal cancer (CRC)[97], oesophageal cancer[98] and pancreatic cancer[99]. This is mainly due to its anatomy and function as “portal” organ receiving the whole splanchnic circulation through the portal system. In addition, the liver microenvironment, which is populated by different stromal cells and characterised by a complexity of extracellular matrix components, is favourable for the growth and invasion of cancer cells [12].

The development of tumour metastasis consists of different steps that allow cancer cells to move from the primary neoplasm to a distant location (Fig. 14). Cancer cells need to detach from the primary tumour to migrate and invade the surrounding tissue. Once in the circulation, they must extravasate into a tissue and grow in the metastatic site. Some cells remain dormant for a long time before they start the formation of metastatic foci[100].

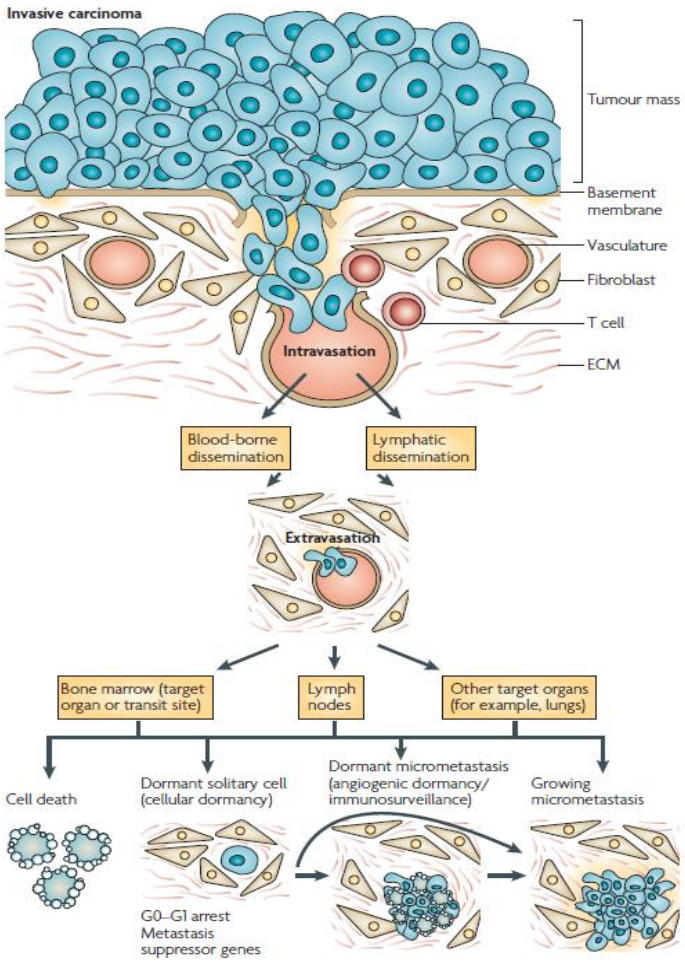

Fig. 14 The tumour metastatic process.

At the primary tumour site, tumour cells invade into the lymphatics or directly into the circulation. Once in the bloodstream, tumour cells must survive and avoid the immune attack to extravasate. Tumour cell arrest/immobilization happens most often by size restriction in capillary beds but can involve specific adhesive interactions. The definition of metastatic colonization is the process by which tumour cells form micro metastases followed by progressive grow, and forming vascularized macro metastases in a distant organ. Metastatic colonization involves reciprocal interactions between tumour cells and cells in the microenvironment of the distant organ, and can pause for periods of dormancy (G0-G1 arrest)[100].

Metastatic spread of cancer cells remains a major cause of cancer mortality, particularly in the case of pancreatic ductal adenocarcinoma (PDAC). PDAC have a characteristic tendency to metastasize preferentially to the liver, and only 8% of patients survive more than 5 years following diagnosis[96, 99].

New discoveries, reveal that primary tumours induce the formation of supportive microenvironments in secondary organs to form so-called pre-metastatic niches (PMNs) that support the engraftment, survival of cancer cells even before their arrival at these site[101]. The metastatic niche model is based on Paget's seed and soil hypothesis that suggested a temporal evolution for the development also of the soil (host organ)[102].

This means that the premetastatic niche must evolve for tumour cells to be able to engraft (metastatic niche) and proliferate at secondary sites (micro- to macro- metastatic transition). This hypothesis suggests the key involvement of cellular and molecular components within the metastatic microenvironment[103]. The development of PMNs is governed by a complex series of reciprocal interactions between tumour cells and various components of the tumour microenvironment, as well as the exploitation of resident and recruited cells in secondary target organs[104].

Tumour cell survival and proliferation may be influenced by cell-cell and cell-matrix interactions at the metastatic site. Indeed, metastatic cancer cells must evade many cell deaths signals, which are induced by the disruption of attachment to other cell types (anoikis), and the extracellular matrix (amorphosis)[105].

6. Anti-tumour Treatments and immunotherapy

6.1 Overview of canonical treatments for liver cancer

Progress in treatment and early detection has led to a significant improvement of cancer management. Considering the heterogeneity of HCC, the stratification of patients is very important in designing personalized therapies. Although several HCC staging systems have been proposed, the Barcelona Clinic Liver Cancer (BCLC) staging classification is the most used for patient stratification and consequently for choosing the treatment.

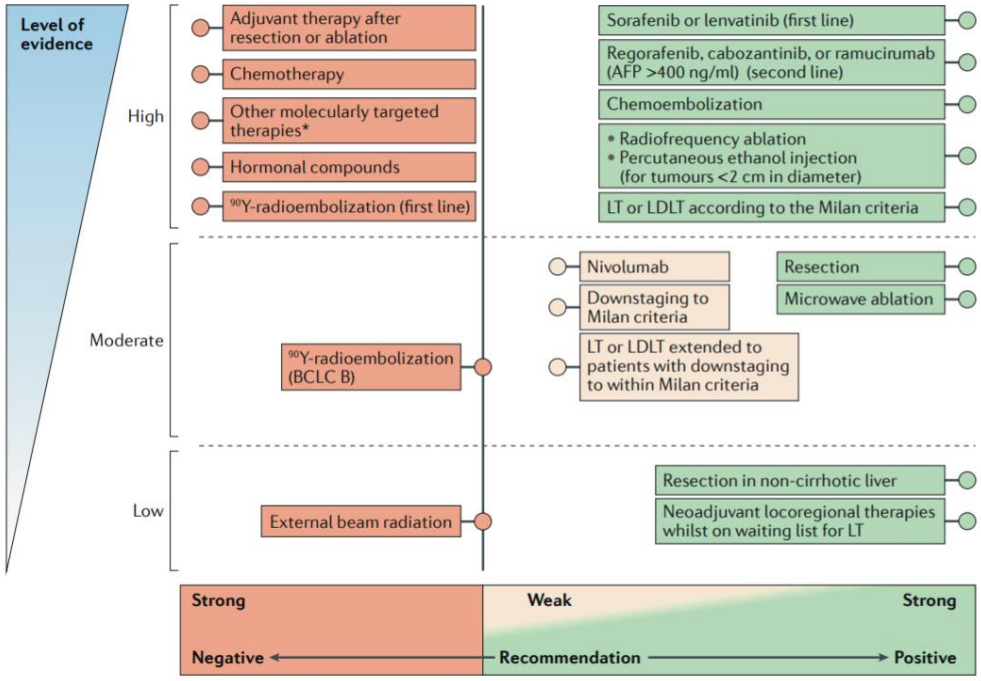

Fig. 15 Representation of EASL recommendations for treatment

*Treatment recommendations from the European Association for the Study of the Liver (EASL) international guidelines are illustrated according to levels of evidence and strength of recommendation. Treatments endorsed in the international guidelines (strong positive recommendation) are shown in green. Treatments for which more evidence is needed (weak positive recommendations) are shown in orange, whereas those not endorsed (strong negative recommendation) are shown in red. AFP, α-fetoprotein; BCLC, Barcelona Clinic Liver Cancer; LDLT, living donor liver transplantation; LT, orthotopic liver transplantation. *Other molecularly targeted therapies include sunitinib, linifanib, tivantinib, erlotinib, and enviroximes. MW, microwave; PEI, percutaneous ethanol injection; RF, radiofrequency ablation[106].*

Current HCC treatment can be divided in two main classes, surgical or intraoperative and systemic. For patients with HCC at early stages (BCLC stage 0–A), potentially curative for early-stage disease is recommended the following treatments: surgical resection, transplantation, or percutaneous ablation [107].

Those treatments offer a high rate of complete responses and thus, potential to cure. Surgical resection is still currently considered the definitive treatment for HCC and the only treatment that offers the prospect to cure, or at least long-term survival.

Where conventional surgical resection is contraindicated, orthotopic liver transplantation is an option, particularly for those who have early tumours[108] but this option remains a possibility due to shortage of donor organs.

Patients diagnosed in an advanced stage of HCC are ineligible for these curative approaches, the few non-curative treatments that improve survival are Trans-arterial chemoembolization (TACE) and systemic treatments through chemotherapeutic agents.

In particular, patients diagnosed with advanced-stage HCC (BCLC stage C) can benefit from Sorafenib. More recently, first-line Levatinib [109] and second-line Regorafenib and cabozantinib[110] have also been demonstrated to provide survival benefits for patients with advanced stage disease.

In clinical trials, the median overall survival durations achieved with these therapies are around 1 year. Nivolumab is another new option in the second line setting on the basis of the promising response rates and durations observed in the phase I–II trial of this agent[111] (further discuss in the followings chapters).

Nevertheless, attempts are being made at investigating different approaches in patients with primary liver cancer (Fig. 16)

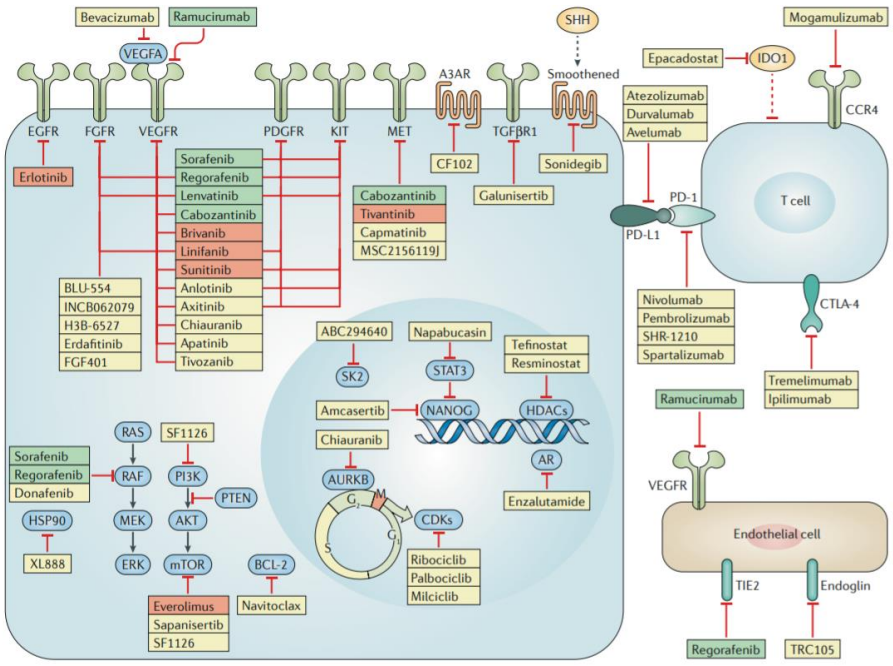

Fig. 16 Molecularly targeted therapies for HCC and their target signalling pathways.

Green boxes indicate drugs with positive results from phase III trials (Sorafenib, regorafenib, lenvatinib, cabozantinib, and ramucirumab). Red boxes indicate drugs with negative results from phase III trials (everolimus, sunitinib, linifanib, erlotinib, brivanib, and tivantinib). Drugs in yellow boxes are currently in development for hepatocellular carcinoma (HCC) in either phase I, phase II, or phase III clinical trials (Table 2). The dashed lines indicate indirect activities [112].

The current HCC treatment options remain unsatisfactory. Although advances have been made to dissect molecular mechanisms in HCC, this knowledge have not yet given a positive impact on the clinical side. The last few years have seen the failure of several first- and second-line phase III clinical trials of novel molecular targeted therapies, indicating the need for a change in the way how new therapies are investigated in HCC[112]. Potential reasons for these failures include clinical and molecular heterogeneity of the cancer, lack of specific biomarkers and appropriate models for molecular testing[113].

6.1.1 Sorafenib treatment

Sorafenib is a small molecule that inhibits tumour-cell proliferation and tumour angiogenesis and increases the rate of apoptosis. Sorafenib is a multikinase inhibitor that blocks the autophosphorylation of multiple cell surface tyrosine kinases such as VEGFR and PDGFR-β, which are important during the angiogenic process during tumour development. Additionally, it has been shown that Sorafenib controls downstream intracellular serine/threonine kinases in the MAPK cascade [114]. These kinases are involved in tumour cell signalling, proliferation, angiogenesis and apoptosis. Indeed, recent research has demonstrated that in vitro, Sorafenib inhibited HCC cell proliferation of HCC cells, induced apoptosis, reduced tumour angiogenesis and was shown to induce tumour cell apoptosis in animal models of HCC.

However, in HCC patients the overall efficacy of Sorafenib has demonstrated to be low. Sorafenib treatment in HCC patients resulted in a median overall survival of 10.7 months and a median time to progression of 5.3 months [115, 116].

Moreover, it is associated with serious adverse side effects, and drug resistance often develops, furthermore Some HCC patients resistant to Sorafenib since the first attempt to treatment. Several mechanisms have been found to be involved in the acquired resistance to Sorafenib, such as crosstalk involving the PI3K/Akt pathways, the activation of hypoxia-inducible pathways, as well as others[117].

In addition, different studies have demonstrated that Sorafenib resistance mechanisms may involve EMT. After long-term exposure to Sorafenib in HCC cell lines, changed in appearance, lost E-cadherin and high expression of Vimentin, indicating epithelial to-mesenchymal transition was assessed. The resistant cells showed reduced adherent growth, became more invasive and lost liver-specific gene expression [118].

Although the exact mechanism between EMT and Sorafenib resistance is still unknown.

Sorafenib, as a multi-target kinase inhibitor, is could also affect the function of immune cells, especially NK cells, that are important cytotoxic cells in liver[117]. Therefore, to find

ways to improve efficiency, it is necessary to explore the effect of Sorafenib on immune cells.

The fact that Sorafenib treatment can elicit a malignant phenotype has important implications for treatment protocols and clinical trial development with Sorafenib in patients with HCC. Combination treatment with a second drug that may circumvent the development of resistance and maybe not affecting the immune microenvironment that is essential player for the regression of HCC.

6.1.2 Immunotherapy

With advances in the understanding of the steps leading to hepatocarcinogenesis, multiple novel treatment strategies have emerged.

Nevertheless, first-line conventional therapies currently available have offered limited benefit and indeed treatments are still not effective enough and the toxic effect on healthy representing a major cause of morbidity. Consequently, there is an urgent need for more effective therapeutic options.

One of the newly emerging therapy is immunotherapy. In the last years, the pivotal role of the immune system in controlling tumorigenesis and tumour progression have been confirmed. Accumulating evidence showed the correlation between TILs in cancer tissue and favourable prognosis in various malignancies. In particular, the presence of $CD8^+$ cytotoxic T cells and the ratio of $CD8^+$ effector T cells/$CD4^+$ regulatory T cells (Tregs) seemed to correlate with improved prognosis and long-term survival in many solid tumours[119].

When a T cell encounters a tumour antigen, this results in activation, clonal proliferation/expansion and a cytolytic response. Both the innate and adaptive immune systems interact to mediate the anticancer immune surveillance and immune editing [71, 120]. Dysfunctional tumour immune interactions leading to immune evasion are key events in tumorigenesis and metastasis[12].

Thus, drugs targeting various mechanisms of immune tolerance and combinations thereof are being actively investigated. Cancer immunotherapies consisting of a variety of treatment approaches can be divided into four major categories: (1) cytokines/immunomodulation agents, (2) monoclonal antibodies, (3) cell-based therapies (TCR Engineering approaches), and (4) oncolytic viruses (Fig.17).

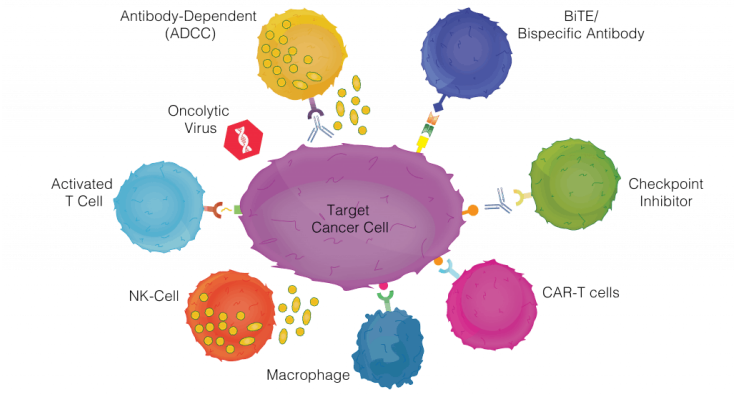

Fig. 17 Targeting cancer cells with immunotherapy.

Immune cell-mediated tumour cell killing can involve the components of both the innate and adaptive immune systems including: (1) natural killer (NK) cells, (2) cytotoxic T cells (MHC-dependent), (3) antibodies secreted by B lymphocytes, (4) engineered antibodies such as Bispecific antibodies and Bispecific T cell engagers (Bites), (5) checkpoints inhibitors (6) genetically engineered T cells targeting specific tumour antigens (e.g., CAR-T; MHC-independent), and (7) macrophage-mediated phagocytosis.

6.1.2.1 T cell-targeting immunotherapies

Therapeutic Antibodies (Abs) are created to work on three basic mechanisms: blocking the ligand receptor interaction, by triggering intracellular signals or recruiting immune cells and triggering upon binding their effector function [121].

Targeted antibodies can affect tumour cells when targeted Abs disrupt growth signalling pathways through the activation or inhibition of receptors or cytokines critical for cancer growth and proliferation[122].

6.1.2.2 Immune Checkpoint Inhibitors: Reactivation of Tumour Infiltrating T-Cells

Mounting a proper immune response requires to overcome several immunological checkpoints. Monoclonal antibodies that target immune checkpoints reinvigorate antitumor immune responses by interrupting co-inhibitory signalling pathways and by promoting immune-mediated elimination of tumour cells[123].

Among other newly emerged negative regulatory receptors that mediate these inhibitory feedbacks, is the programmed cell death protein 1 (PD-1) which is one of the most intensively investigated regulators due to its indispensable role in fine-tuning T cell's function and maintaining the immune system homeostasis. PD-1 is commonly associated with tolerance, but is also capable of eliciting the immune checkpoint response of T cells[124]. Indeed, a balance of positive and negative signals is extremely important for the immune system's ability to defend the host while maintaining immunologic tolerance and preventing autoimmunity[125]. Indeed, PD-1 expression is induced on T cells when they become activated. Its ligands are PD-L1 (B7-H1) and PD-L2 (B7-DC) and these are members of the B7 family of costimulatory molecules. Further, upon binding of PD-L1 or PD-L2 to PD-1 this can inhibit T cell function or cause anergy. Many tumours express PD-L1 and it can be also expressed by APCs. Tumour cells take advantage of this checkpoint negative regulation to suppress immunity and evade immune surveillance (Fig. 18) [126, 127].

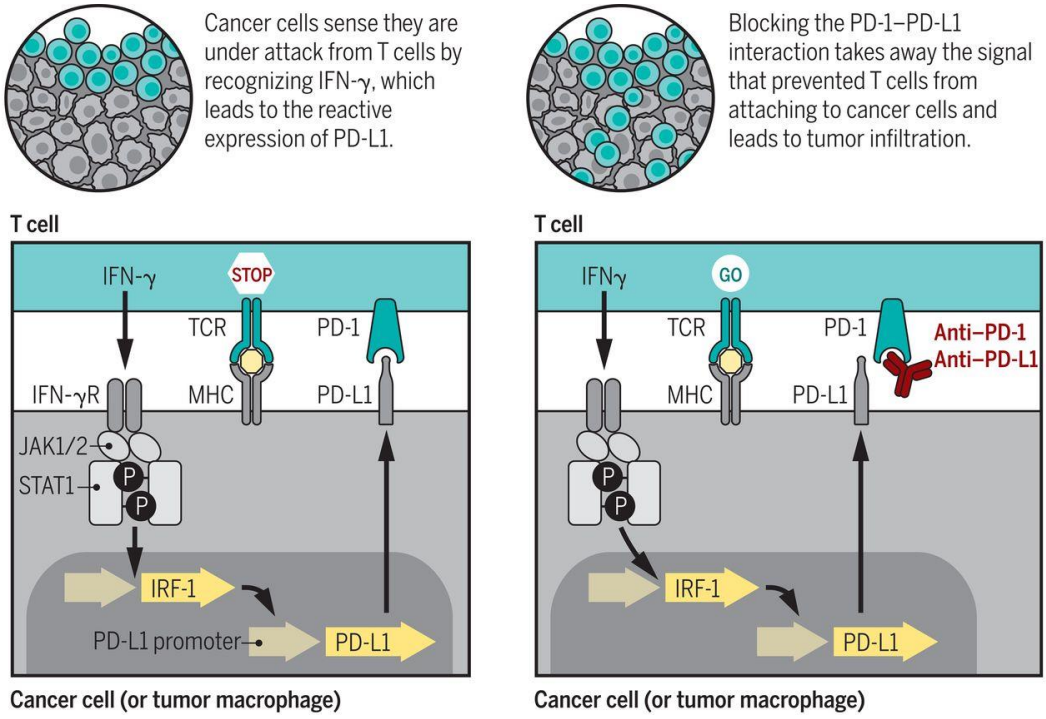

Fig. 18 Mechanism of action of PD-1–blockade therapy.

(Left) TCR recognition of the cognate antigen presented by MHC molecules on the surface of cancer cells results in T cell activation. T cells then produce IFN-γ and other cytokines. Cancer cells and other cells in the tumour microenvironment have IFN-γ receptors (IFN-γR) activating the cascade, leading to PD-L1 surface expression. The expression of PD-L1 turns off the T cells that are trying to attack the tumour, and these T cells remain in the margin of the cancer. (Right) Blockade of the PD-1–PD-L1 interaction with therapeutic antibodies results in T cell proliferation and infiltration into the tumour, inducing a cytotoxic T cell response that leads to an objective tumour response[128].

Important results have been achieved by using checkpoint inhibitors by employing antibodies which neutralize PD-1 or its ligand PD-L1, or CTLA-4[128].

Nevertheless, high number of patients (up to 60–70%) are refractory to the therapy or acquire resistance [129, 130] with different responses across different tumour types. As mentioned before, the response to these therapies depend on multiple factors such as the density and the site of T cells in the tumour microenvironment.

The presence of TILs also correlates with the clinical response to checkpoints targeting both PD-1 and CTLA-4 receptors[131]. It is the case of tumour microenvironments which

lack T-cell infiltration (immunologically cold), which fail to attract these cells to the tumour site[66].

6.1.2.3 T cell engaging Bispecific antibodies for cancer therapy

Advances in protein engineering have provided platforms for the development of novel antibody constructs such as the Bispecific T cell engager (BiTe) molecules.

The Bispecific T cell engager (BiTe) have two single chain antibody variable fragments (scFv), that are joined by a linker, and simultaneously bind to two targets, on one side the anti-CD3, as well as tumour surface antigen[101]. BiTe are relatively small fusion proteins; their molecules consist of a single non-glycosylated polypeptide chain of 50 to 60-kDa molecular weight.

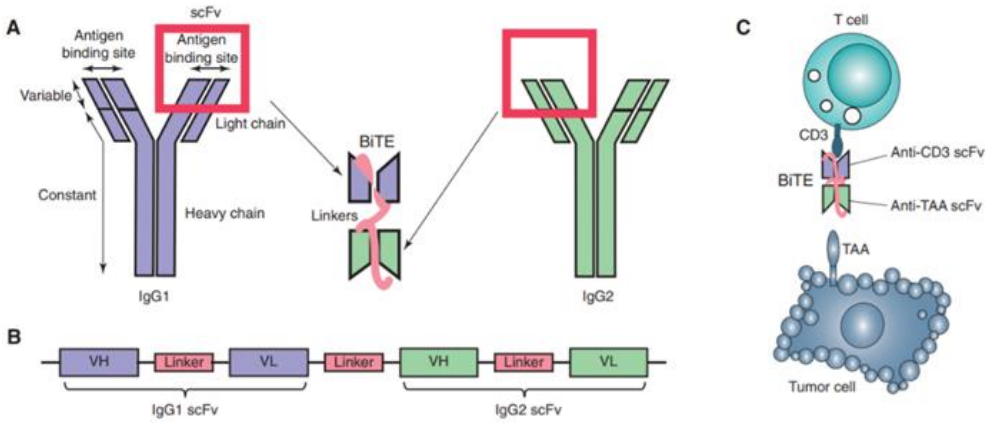

Fig. 19 structure and mechanism of a BiTe.

A, Schematic representation of the derivation and structure of a BiTe generated from two antibodies, with specificity for a T-cell activation molecule and a tumour-associated antigen (TAA). B, Schema of a BiTe gene used to produce the recombinant BiTe protein. Linkers were constructed between VH and VL domains of the scFv and between the two scFv. C, A BiTe creates an immunologic synapse by binding simultaneously to a tumour cell via TAA, and a T cell via CD3[132].

Bispecific antibodies can be divided on the basis of three types of targeting strategies, that could be direct or indirect: cytotoxic effector cell redirectors (including T-cell

and NK-cell redirectors), tumour-targeted immunomodulatory and dual immunomodulators[133].

Their small size allows them to bring together T cells and the tumour cells to force the formation of the immunologic synapse and lead to a polyclonal T cell response and cytotoxicity of the tumour cell. Forcing T cells and target cells into close proximity results in a T cell activation, proliferation an T cell-induced cancer cell lysis[134, 135].

Importantly, BiTe molecules recruit T cells regardless of their T cell receptor (TCR) specificity, meaning that this process is independent of MHC expression, thus bypassing one of the mechanisms of tumour immune evasion[136]. As already explained (chapter 4.4.2) one of the mechanisms by which cancer cells avoid the immune system include loss of MHC-I and blocking T cells activity by creating a suppressive environment.

Upon engagement of Bite with resting peripheral T cells, an upregulation of activation markers CD69 and CD25 occurs on the cell surface. In addition, expression of cell adhesion molecules such as CD2 increases and the transient release of inflammatory cytokines such as IFN-γ, TNFα, IL-2, IL-6 and IL-10. Moreover, this can be achieved at low nanomolar concentrations, without the need for co-stimulation [136].

Bite-mediated T cell activation is only observed in the presence of target cells expressing the antigen and showed that individual T cells were highly mobile and able to serially eliminate multiple target cells in 2D co-culture[136].

The number of Bispecific immunotherapeutic antibodies in development and used in clinic has grown considerably over the last years.

Examples of BiTe molecules currently used in early clinical or preclinical phases is summarized in table 1, updated 2018. T-cell redirecting therapy has more than 25 compounds in clinical development. Two such compounds, blinatumomab and catumaxomab, have been approved for haematological malignancies (B cell lymphoma) [137]. A potential disadvantage of such compounds may be the risk of toxicity related to the strong immune activation, even if such compounds are usually designed to lack activity in the absence of tumour antigen, the safety profile may be superior to most other immunotherapeutic compounds. However, new targets have been proposed and research is ongoing to identify new potential targets.

Class	Description	Targets	Examples	Stage*
T-cell redirectors	Redirects T cells to malignant cells by targeting a tumor antigen and CD3	CD19 × CD3	Blinatumomab	Market
		EpCAM × CD3	Catumaxomab	Marketed (withdrawn)
		CD20 × CD3	XmAb13676 BTCT4465A RO7082859	I
		CD123 × CD3	MGD006 JNJ-63709178 Xmab14045	I
		BCMA × CD3	JNJ-64007957 BI 836909	I
		B7H3 × CD3	MGD009	I
		CEA × CD3	RO6958688 MT111	I
		PSMA × CD3	Pasotuximab ES414/MOR209	I
NK-cell redirectors	Redirects NK cells to malignant cells by targeting a tumor antigen and CD16A	CD30 × CD16A	AFM13	II
		EGFR × CD16A	AFM24	PC
		BCMA × CD16A	AFM26	PC
Tumor-targeted immunomodulators	Directs potent costimulation to the tumor-infiltrating immune cells by targeting a tumor antigen and costimulatory molecules such as CD40 or 4-1BB	TA × CD40	ABBV-428	I
		HER2 × 4-1BB	PRS343	I
		FAP × 4-1BB	4-1BB agonist	PC
		5T4 × 4-1BB	ALG.APV-527	PC
Dual immunomodulators	Simultaneous targeting of two immunomodulating targets, resulting in blockade of inhibitory targets, depletion of suppressive cells or activation of effector cells	PD-L1 × TGF-β	M7824	I
		PD-1 × LAG-3	MGD013	I
			FS118	PC
		PD-1 × TIM-3	MCLA-134	PC
		PD-1 × CTLA-4	XmAb20717	PC
		CTLA-4 × OX40	ATOR-1015	PC

* I, clinical phase I; II, clinical phase II; PC, preclinical development; TA, tumor antigen.

Table 1 Summary of various classes of immunotherapeutic Bispecific antibodies.

BiTe list, divided by class: cytotoxic effector cell redirectors (including T-cell and NK-cell redirectors), tumour-targeted immunomodulators and dual immunomodulators. Examples of each class are listed with details on target and clinical stage[133].

As already mentioned, the main problem remains the treatment of solid tumours, as these therapies showed a low efficacy compared to haematological cancers. Moreover, the resolution of malignant disease requires large numbers of responding T cells and their sustained action over time. Bites administration, have been demonstrated an increase of the order of 2- to 4-fold in numbers of circulating T cells, suggesting expansion of the pool of T cells[138].

6.1.3 Limitations of immunotherapy in solid tumours

The main challenges posed to T cell immunotherapy are: finding, entering and surviving within the tumour, this indicates that new strategies are needed to understand and find proper TAA as well as increase T cell trafficking ,extravasation and tumour infiltration [139].

The major difference between solid tumours and haematological malignancies is difficulty to find an ideal target Ag, and even more difficult is to improve the infiltration of the T cells into the tumour tissue.

The lack of a sufficient TAA load could impair the mounting of an appropriate immune response. Whereas in haematological malignancies such as B-cell malignancies the CD19 represents the ideal target, no single antigen with equivalent characteristics has yet been identified for solid tumours[140].

An ideal solid tumour Ag target would be overexpressed in all cancer cells, absent or with very low expression in non-vital normal tissue and found in many patients. However, for most solid tumours it is more common to find a TAA overexpressed in the tumour as well as expressed at low levels in normal tissues[138]. The risk in lacking this specificity is the increased risk of an on-target off-tumour toxicity due to the high sensitivity of T cells for low-level antigen expression[139].

Even when a TAA is identified, T cells need to be in contact with cancer cells, but there are multiple, physical barriers that must be overcome in order to reach the tumour.

Specific infiltration capacity of the patient's immune system is one of the major goals for enhancing immunotherapy results. However, standard two-dimensional (2D) cell culture techniques lack the necessary complexity of a solid tissue in order to solve related questions. Recently, 3D in vitro models represent an important tool to study immune function (i.e. infiltration, immunomodulatory and regulatory capacity) and mechanisms for cells of the immune system.

Thus, compared to traditional 2D models, 3D cell culture models have demonstrated to provide insights that are better to translate into clinical effective readouts[139].

This difference will be discussed further, as the aim of this thesis is to establish a 3D human ECM model, which offers unique insights into T cell infiltration and antitumor mechanisms in the solid TME that could be used for testing the therapeutic capacity of new possible curative strategies.

6.2 3D models

Cell culture is an indispensable in vitro tool used to improve our perception and understanding of cell biology tissue morphology, mechanisms of diseases and drug action. Efficient cell culturing techniques in vitro and experiment in vivo allow researchers to design and develop new drugs in preclinical studies.

Up to date, two-dimensional (2D) cell cultures are still the main method in many biological studies, to identify molecular targets and to test therapies[138]. Traditionally, tumoricidal activity and immune evasion have been studied by utilizing 2D. However, 2D cell cultures poorly imitate the conditions in vivo. Recently, 3D cell cultures have received remarkable attention in studies such as drug discovery and development[141].

The 2D environment is not able to support the complex cell-cell interactions, meaning cells are unable to maintain their correct function. Although 2D cell cultures are used widely in drug discovery and in preclinical drug testing, data generated from their use not always translate the mechanism recurring in vivo. This is thought to be a significant contribution for drug failures, at Phase III clinical trials [142]. 2D systems do not represent in vivo responses, in fact, under physiological conditions, cells grow in a 3D environment and interacting with other cells and extracellular matrix (ECM). The ECM components of the microenvironment are necessary for the proper differentiation and function of cells, in order to mimic both physiological and pathological conditions [143, 144].

Nowadays, 3D cell cultures and co-cultures receive more attention as they exhibit protein expression patterns and intracellular junctions that are similar to the in vivo condition when compared to classic 2D monolayer cultures.

6.2.1 Immune cells: 2D vs. 3D

The most obvious difference between 2D culture and the 3D system is the tissue-specific biochemical and biomechanical composition. The context provided by a 3D environment affects the nature of cell–cell contacts and the formation of ECM surrounding the cells.

Several studies have been published that underline the 3D tumour models' superiority compared to 2D to better mimic the in vivo tumour microenvironment for different cell types[145].

In the last years, different 3D models were used to study the liver environment and to recreate the physiological and pathological milieu using cell spheroids, cell sheets or 3D scaffolds[146].

Among all the 3D systems, some have been used to develop 3D hepatic-and HCC models including: organoids, Organ on a chip, 3D bioprinting, precision-cut liver slices and acellular scaffolds. The differences among them are listed in table 2, considering advantages and disadvantages compared to 2D plastic system.

	2D plastic system	Organoids	Lab-on-a-chip	3D printing	Liver slices	Acellular scaffolds
Cell viability	+	+ +	+ +	+ +	+	+ +
Cell function	+	+ +	+ +	+ +	+	+ +
Length in culture	+	+ +	+ +	+ +	–	+ +
3D architecture	–	+	+	+ +	+ +	+ +
Tissue-specific architecture	–	–	–	+	+ +	+ +
Biomechanics	–	+	–	+	+ +	+ +
ECM protein	+	+	+	–	+ +	+ +

Table 2 Table comparing advantages and disadvantage of 2D and 3D systems.

Comparison of limitations and strengths of classical 2D cell culture techniques with recently developed 3D culture systems specific for modelling diseases in which tissue remodelling is a key factor in disease progression such as for example fibrosis and cancer[145].

For the purpose of this thesis, the canonical 2D system and 3D acellular scaffolds have been used and compared.

Biological scaffolds derived from ECM have been widely used in regenerative medicine purposes[147]. As explained in chapter 4.2 the ECM is an essential non-cellular component of the tissue microenvironment that provides structural support to cells, allowing cell migration, proliferation and differentiation. In order to have natural ECM, different organs and tissues have been successfully decellularized, using protocols that rely on chemical, enzymatic, or mechanical disruption in order to eliminate the cells. Human 3D liver scaffolds were obtained using liver tissue unsuitable for transplantation. Through the application of high shear stress, 3D liver cubes were decellularized while maintaining ECM protein composition, 3D-architecture, biochemical and biomechanical properties of the native tissue[148] (Fig. 20).

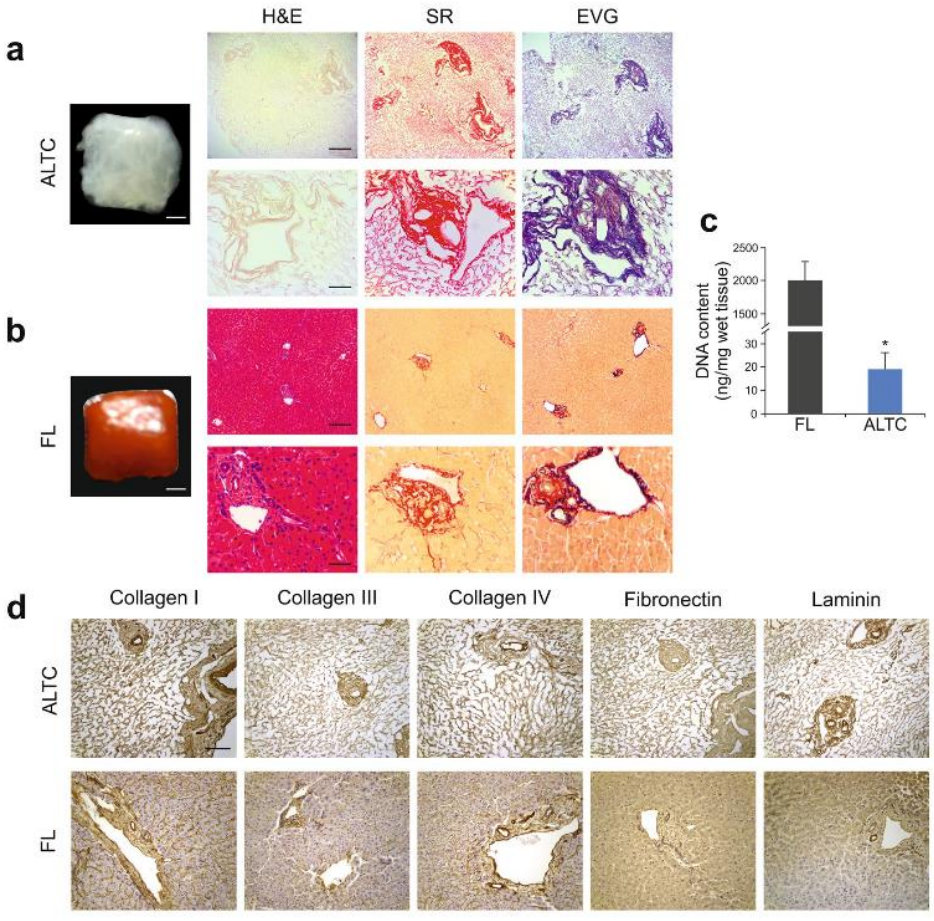

Fig. 20 Decellularization of human 3D liver scaffolds.

(a) Macroscopic appearance and histological analysis after decellularization (ALTC), confirming elimination of nuclear (blue; H&E) and cellular material (yellow; SR) and preservation of collagen (red; SR) and elastin (blue/black; EVG). (b) Macroscopic appearance and histological images of fresh human liver (FL). (c) DNA quantification showing significant elimination of DNA in the

*decellularized cubes. (d) Comparison of the expression and distribution of several ECM proteins, namely collagen I, collagen III, collagen IV, fibronectin and Laminin, evaluated by immunohistochemistry showing consistency between decellularized cubes (top panel) and fresh samples (bottom panel). Data are expressed as mean±s.d. ***p<0.0001. Scale bars, 1 mm macroscopic images (a, b) or 200µm top panel; a, b or 50µm bottom panel; a, b or 100µm (d). Biological replicates (n=16) are performed for all samples[148].*

The differences between the 2D and 3D system become even more important when applying in the immunology field. Immune cells need to infiltrate the 3D cell-matrix microenvironment in order to recognize and attack the target cell. In addition, tumour cells when cultured in 3D systems do more closely mimic the in vivo tumour immune biology in terms of signalling [149-151]. As a consequence, engineered 3D tumour cells display higher resistance to cytotoxicity in comparison to 2D cultures and therefore the efficacy of treatment is affected [152].

A possible explanation of the low response and different readouts in response to immunotherapy could be the lack of tissue architecture and unique biochemical and biomechanical disease-like microenvironment. Indeed, solid cancers display 3D geometry, whereas cytotoxicity of T cells efficacy is usually tested in standard in vitro assays using conventional 2D monolayer tumour cells[152].

The work presented in this thesis is concentrated on a 3D model to study cancer/immune cell interactions with the aim of creating a 3D immune oncology model to investigate immune cell homing, tumour cytotoxicity, and tumour immune evasion.

7. Materials & methods

7.1 Growth conditions of cells

HCC human cell line (SNU-449) and liver metastatic cell line (PK-1) were cultured in RPMI 1640 medium supplemented with 10 % FBS, 1 % penicillin/streptomycin and 1 % glutamine. Cells were incubated in humidified incubators at 37ºC with 5 % CO_2. Cells were passaged regularly, approximately 2-3 days apart, before reaching confluence each time. When passaging cells, medium was removed, cells were washed with HBSS once, and the trypsin-EDTA solution was added with a volume depending on the size of the culture flask, usually 1-2 ml for a T75 flask. After incubation, detached cells and trypsin/cell suspension was removed. Fresh culture medium, containing foetal bovine serum and inhibiting trypsin, was added and cells were collected by pipetting up and down with serological pipettes several times, and therefore mixed thoroughly. Cells were centrifuged at 1500 rpm for 5 minutes, supernatant was discarded. Afterwards, cells were re-seeded in the required dilutions. The medium, HBSS and trypsin-EDTA were stored at +4ºC refrigerator. FBS stock solutions were stored at -20ºC refrigerators. All solutions and media were warmed at 37ºC water bath prior to use.

7.2 Thawing cells

Cryovials stored in liquid nitrogen or at -80ºC were taken and immediately put on ice. Vials were placed in a 37 ºC water bath until thawed. The suspension was taken into 15 ml sterile centrifuge tube with approximately 10 ml growth medium and re-suspended. Cells were centrifuged at 1500 rpm for 3 minutes, supernatant was discarded, and the pellet was re-suspended in 10 ml fresh growth medium to be placed into 75 cm2 flasks. Flasks or dishes were rocked back and forth gently in order to allow the cell suspension to mix, and they were incubated overnight at a 37ºC humidified incubator with 5 % CO_2. The next day, cells were washed with 1x PBS, and culture media were replaced with fresh growth mediums.

7.3 Preparation of peripheral blood mononuclear cells (PBMC)

All venous blood samples were collected in sterile BD Vacutainers® containing EDTA and processed immediately. Peripheral blood mononuclear cells (PBMC) were isolated by Ficoll-Plaque Plus™ (GE Healthcare) density gradient centrifugation.

The whole blood (diluted 1:1 in PBS) was layered on Ficoll-plaque, followed by centrifugation at 2200rpm at 4℃ for 22 minutes with minimum acceleration and brake. PBMC were carefully extracted from the interface using 2ml Pasteur pipettes, then further diluted 1:1 with RPMI 1640 (complete culture medium?) and washed twice by centrifugation at 1600rpm for 15 minutes. Cell counts were determined using a c-chip counting chamber under light-microscopy.

7.4 Freeze/thawing of PBMC

Isolated blood cells not used for immediate experiments were re-suspended at $50x10^6$ cells/ml in heat-inactivated foetal bovine serum (FBS) (Invitrogen™) supplemented with 10% demethylated sulfoxide (DMSO) (Sigma-Aldrich®), transferred to cryovials (Corning) and stored in the freezing container MrFrosty (Fisher Scientific) at -80℃ for a minimum of 24 hours.

After 24 hours, cryovials were transferred for long-term storage in gas phase nitrogen tanks. When required, PBMC were thawed rapidly at 37℃ and washed by centrifugation in 30ml of RPMI 1640.

Once washed, cells were re-suspended for use in RPMI 1640 supplemented with:

- 10% heat-inactivated FBS (Invitrogen™),
- A/A (Invitrogen™),
- L-glutamine.

Co-culture: immune cells and human cancer cell lines

PBMC were co-cultured with SNU-449 or PK-1 cell line either in 2D plastic dishes or in healthy or cirrhotic 3D liver scaffolds. Cultured in a determined effector: target ratio (1:2, cancer cells: immune cells). In all the experiments, single cultures were also analysed in parallel. In all 3D co-culture experiments, human cancer cell lines were seeded and cultured for 12-15 days at 37℃. Every three days culture medium was changed.

After co-culture, cells were stained for flow cytometric analysis to assess T cell effector functionality as described above.

7.5 Origin of decellularized liver tissue cubes.

Livers unsuitable for transplant were prepared and processed in conformity with the UCL Royal Free Biobank Protocols under the research Tissue Bank Human Tissue Act licence and the National Health Service Blood and Transplant – Organ Donation and Transplantation (NHSBT-ODT), UCL Royal Free Biobank ethical committee and NHSBT Research Governance Committee, approved their use.

Four different livers were used to prepare Acellular Liver Tissue Cubes (ALTCs); three of them were defined as healthy due to the absence of fibrosis and fat by histological examination, while the fourth one was defined as cirrhotic.

Livers were first perfused with 1% Phosphate-buffered saline (PBS, Sigma-Aldrich, UK) to eliminate blood and then frozen at -80°C for a minimum of 24h. Afterwards, human livers were thawed at 4°C overnight, cut into 125 mm^3 cubes and stored again at -80°C for future use.

7.6 Scaffolds preparation:

The decellularization protocols to obtain 3D scaffolds ALTCs from human liver tissue cubes were established at the Institute for Liver and Digestive Health, Regenerative Medicine and Fibrosis (WO2015185912 A1 and WO2017017474).

Liver cubes were first placed in 2 mL Eppendorfs and thawed in a 37 °C water bath for 45 min followed by incubation for 15 min with the addition of 1.5 mL of phosphate-buffered saline 1X (PBS from Sigma-Aldrich). Afterwards, 1.5 mL of different decellularizing solutions was added to each Eppendorf and the cubes were agitated using a TissueLyser II (Qiagen)[148].

7.6.1 Sterilization of 3D scaffolds

After decellularization, scaffolds were sterilised using a solution containing 0.1% paracetic acid (PAA) (Sigma) and 4% absolute ethanol (x) for 30 minutes in an orbital shaker (Staurt). After the solution was changed with a fresh PAA for 15 minutes. This was followed by several washing steps with sterile 1X HBSS (Thermofisher Scientific) for a total of 25 minutes in an orbital shaker. The sterile scaffolds were then placed in a 48 well plate for 24 hours in the incubator with complete culture medium to check the sterilization prior to the addition of the cells.

7.6.2 Seeding of cell lines and immune cells 3D scaffolds.

Different protocols were used for the repopulation with different cell types:

7.6.2.1 Human cancer cell lines

Before cell seeding, the scaffolds were transferred into a 96 well plate. Cell lines were re-suspended at a concentration of $0.5x10^6$ cells per 20 µl for each scaffold. Cells were dropped on top of the decellularized scaffold. After that, 3D scaffolds were kept for 2 hours in the incubator at 37 °C with 5% CO2 in order to allow the cells to attach to the ECM. After 2h 180 µl of culture medium was added to each scaffold. After an overnight incubation, scaffolds were transferred into a 48 well plate and 1 ml of culture medium was added. The medium was changed every 3 days.

7.6.2.2 Immune cells

PBMCs or purified T cells were resuspended at a concentration of 1 million cells per scaffold. Experiment were performed using 3 scaffolds/well in a 48 well plate. Final concentration of immune cells was 3 million/mL in RPMI complete medium/48 well.

7.7 RNA extraction and gene expression analysis

7.7.1 RNA extraction

Total RNA was extracted from 2D and 3D cultures using Trizole reagent (Qiagen) and RNeasy Universal Mini Kit (Qiagen) as described by the manufacturer's instruction and as previously published (Mazza et al., 2017). Each frozen scaffold was placed in a 2 mL eppendorf with a 5 mm stainless steel bead (Qiagen) and 600 µL of RLT Buffer, and homogenised by shaking at 30 Hz for 2 to 4 minutes on TissueLyser II. The content of the tube (excluding the bead) was then transferred to a new 1.5 ml Eppendorf tube and RNA extracted following the manufacturer's protocol.

RNA was extracted from the 2D samples using RNeasy® Mini Kit (Qiagen) according to the manufacturers' protocol. For adherent cells, a cells scraper was used to detach the cells from the plastic well. For non-adherent cells, cells were collected and centrifuged, RNA extracted from pellet.

7.7.2 Reverse-Transcription for complementary DNA (cDNA) synthesis

Reverse transcription from mRNA to cDNA was performed using the High Capacity cDNA Reverse Transcription Kit (Applied Biosystems). One milligram of total RNA was reverse transcribed with random primers and MultiScribe RT enzymes (Applied Biosystems,) as described by the manufacturer's instructions. Briefly, the RNA samples were diluted in order to obtain a concentration not lower than 10 ng/µL, and 10 µL of each sample was added in a PCR microtube. Subsequently, 10 µL of the 2X RT mastermix (prepared as described in Table.3) was added to each tube to have a final volume of 20 µL.

RT MASTER MIX	Volume/Reaction (µl)
10✕ RT BUFFER	2
25✕ DNTP MIX (100 MM)	0.8
10✕ RT RANDOM PRIMERS	2
MULTISCRIBE REVERSE TRANSCRIPTASE	1
RNASE INHIBITOR	1
NUCLEASE-FREE H_2O	3.2

Table 3 composition of the reverse transcription master mix.

Afterwards, the reverse transcription was performed in a 2720 Thermal Cycler (Applied Biosystems®), with the program specified by the manufacturer (25 °C for 10 min, 37 °C for 120 min, 85°C for 5 min, and hold on 4 °C).

7.8 Quantitative Real-Time PCR (RT- qPCR) analysis

Gene expression was measured using TaqMan gene expression assays with the Applied Biosystems® 7500 Real-Time PCR system. The cDNA obtained with the Reverse transcription reaction was diluted in order to have a concentration of 1 ng/µL. A qPCR Master Mix was prepared following the set-up in table 3.

Specific TaqMan Probes for the different human target genes were used (Applied Biosystems, listed in table 4). cDNA dilution (5 µL) was added together with 15µl of the qPCR Mastermix in a Fast Optical 96-well TaqMan PCR plate (MicroAmp Applied Biosystems). The micro plate was then inserted in a 7500 Fast Real Time PCR System (Applied Biosystems®) and the reaction program was started for 40 RT-qPCR cycles Expression levels for each gene were calculated using the delta Ct method and normalized to the Ct of Glyceraldeyde-3-phospate dehydrogenase (GAPDH) as reference gene. Graphs represent averages ± SD of the relative gene expression data (n=3 per group).

Gene	Assay ID	Dye:	Company
GAPDH	Hs02786624_g1	FAM	Thermo Fisher
Vimentin	Hs00958111_m1	FAM	Thermo Fisher
E cadherin	Hs01023894_m1	FAM	Thermo Fisher
MMP-9	Hs00957562_m1	FAM	Thermo Fisher
ICAM-1	Hs00164932_m1	FAM	Thermo Fisher
TIMP-1	Hs01092512_g1	FAM	Thermo Fisher
CXCR7	Hs00664172_s1	FAM	Thermo Fisher
ITGB-1	Hs01127536_m1	FAM	Thermo Fisher

Table 4 List of TaqMan genes.

7.9 Histology and Immunohistochemistry

7.9.1 Samples processing

3D scaffolds samples, previously fixed in 4% formaldehyde, were processed using Leica TP1020; first step was dehydration in 70%, 80%, 95%, 100 % ethanol, followed by clearing xylene treatment and fixation in paraffin.

Afterwards, the samples were sliced into 4 µm sections using a Leica RM2035 microtome (Leica Biosystems). All sections were then were dewaxed using xylene, ethanol and water.

Different histological staining's were performed i.e. Haematoxylin and Eosin (H&E), immunohistochemical stainings (IHC) and Immunofluorescence (IF).

After hydration, sections were treated with haematoxylin Harris' formula (Leica Biosystems) for 10 minutes and then washed in tap water for 10 minutes. The sections were checked under the microscope and, when necessary, differentiated in 0.5% acid-

alcohol. Next, the sections were stained with eosin (Leica Biosystems) for 4 minutes, followed by washing with water. Subsequently, the sections were dehydrated with ethanol for few seconds and then soaked in xylene for 10 minutes before mounting.

7.9.2 Immunohistochemistry

Sections were deparaffinised and hydrated as previously described. After 5 minutes soaking in TBS, slides were microwaved in a pre-warmed retrieval solution (unmasking antigen agent) for 20 minutes, and cooled to retrieve the antigen binding sites. Slides were washed with TBS with 0.04% Tween-20 (Sigma-Aldrich) for 5 minutes. Peroxide blocking solution (3%) was used for 5 minutes. Blocking serum (normal horse serum 2.5%, ABC Kit Vector) was added for 5 minutes. Slide were then incubated for 1 hour in primary antibody Ki67 (Abcam ab21700, pre-diluted)

This was followed by a washing with TBST for 5 minutes, and incubated with Secondary biotinilated antibody (VECTASTAIN Elite ABC HRP Kit Peroxidase, Universal, and R.T.U.) for 30 minutes. The slides were washed again, and then placed for 30 minutes in ABC complex (VECTASTAIN Elite ABC HRP Kit Peroxidase, Universal, and R.T.U.), washed and incubated with DAB (Novolink 7230-K Leica) for 5 minutes. The slides were finally counterstained with Harris Haematoxylin (Sigma-Aldrich) for 1 minute.

All sections were washed with tap water, dehydrated through graded alcohols, cleared before mounting with OPX (Leica Biosystems) and cover slipped.

7.9.3 Immunofluorescence:

Sections were deparaffinised and hydrated as previously described. After washing twice with PBS 1X, samples were permeabilized with a solution of a 0.5% Triton X-100, 5% BSA in PBS 1X for 1 hour at room temperature. After washing three times with PBS 1X, samples were stained for F-actin using the antibodies listed in table X diluted in 5% BSA in PBS 1X for 1 hour at RT in the dark.

After washing for three times with PBS 1X, nuclei were counterstained with DAPI diluted 2 µg/mL in PBS 1X for 10 minutes. (Table 1) Mountant (ProLong™ Gold Antifade Mountant (Thermo fisher, P36930) was applied directly to fluorescently labelled cell on microscope slides.

Images were acquired with a Yokogawa CQ1 confocal microscope or Leica SP8 confocal.

Antibody	Dilution		Company
CD45	1:200	14-9457-82	Invitrogen
CD8	1:200	Sc-1177	Santa Cruz
Cytokeratin	1:200	04-586	Millipore
DAPI	2 µg/mL	10236276001	Sigma-Aldrich
Alexa Fluor 488	1:500	406404	Bio legend
Alexa Fluor 594	1:500	405326	Bio legend

Table 5 List of fluorescent dyes used for immunofluorescence staining

7.10 3D extraction: Preparation of infiltrating cell suspensions.

3D liver scaffolds were used for extraction of infiltrating cells. A prior mechanical disruption was necessary in order to analyse the 3D scaffolds condition.

7.10.1 Mechanical Disruption

Following culture, 3D scaffolds were washed three times with Hank's Balanced Salt Solution (HBSS) without Ca2- and Mg2- (Sigma). The cells in the 3D scaffolds were extracted using HBSS 1 mg/ml collagenase type IV (C5138-100MG) digested with shaking for 15 min at 37°C. The scaffolds were destroyed by pipetting with a P1000.

Upon mechanical disruption, the single cell suspension was then passed through a 35 µm cell strainer (BD Bioscience). The resulting cell suspension was centrifuged at 400 × g to pellet the cells. Followed by multiple washes with RPMI 1640 containing heat inactivated foetal calf serum (10%, Invitrogen) to inactivate the enzymatic activity of collagenase and to prevent clumping minimising cell loss.

7.11 Flow cytometry

Cells for flow cytometric analysis were harvested from culture models using collagenase and/or trypsin, and centrifuged at 400 × g for 10 min. Cells were resuspended in 1mL of Staining buffer (SB) (1x PBS 5% (v/v) FBS).

7.11.1 Surface staining of PBMC and cancer cells for phenotype

To determine cancer cells and immune cells subsets and phenotypes, cells were washed in staining buffer and centrifuged at 1600 rpm for 5 minutes. The supernatant was aspirated and cell pellets re-suspended by gentle vortexing.

Cells were initially subjected to a blocking step to prevent unwanted binding of antibody to Fc receptor-expressing cells (FcR blocking reagent: Hu Fc Block Pure – 564219) for 15 minutes at 4℃. Surface staining of cells then followed in the presence of the FcR blocking reagent by staining with relevant directly conjugated anti-human mAb for 30 minutes at 4℃ in the dark. Following a washing step with 1x PBS, cells were fixed with 300µl/tube with fixing buffer. An unstained control sample was used to set the voltage for each channel, and an isotype control sample (with cells) was also included.

Data were collected on a BD Fortessa and analysed using FlowJo v8.8.7.

Details of antibodies used are presented in Table 6

7.11.2 Intracellular staining of PBMC and cancer cells lines.

For detection of intracellular antigens, cells were blocked and surface stained as described above. Once surface stained, the cells were washed and resuspended in BD Cytox/Cytoperm (88-8824-00, eBioscience) for a further 20 minutes at 4℃ in the dark. After fixation and permeabilization, cells were washed and stained with relevant directly conjugated anti-human mAb for 30 minutes at 4℃ in the dark. After staining, the cells were washed and resuspended in 300µl/tube.

Data were collected on a BD LR Fortessa and analysed using FlowJo v8.8.7.

Details of antibodies used are presented in Table 6.

Markers	Catalog number	Fluorocrome	Company
Annexin V	11-8005	FITC	eBioscience™
CD107a	555800	FITC	BD
CD11b	562793	FITC	BD
CD25	557753	APC-CY7	BD
CD274 (PD-L1, B7-H1)	46-983-42	PerCP-eFluor 710,	eBioscience™
CD29	12-0299-47	PE	eBioscience™
CD3	563180	Bv421	BD
CD3	Mhcd0317	Pe-Texas red	Life technologies
CD4	564724	BUV395	BD
CD45RO	562299	PE-CF594	BD
CD56	560842	PerCP-Cy5.5	BD
CD68	25-0689-41	PE-Cyanine7	eBioscience™
CD8 Clone RPA-T8 (RUO)"	560347	V450	BD
Cytokeratin	AB174562	PE	Abcam
Ecadherin	ab99885	APC	Abcam
Mouse Anti-Human CD279	557860	FITC	BD
PI	00-6990	PI	eBioscience™
SYTOX	S34857	Pacific Blue	Life technologies
CD44	103027	APC/Cy7	biolegend
MCAM	318342	PercP	biolegend

Table 6 List of FACS antibodies

7.12 Cell viability assay

7.12.1 Viability on cells on 2D cultures (Metabolic assay)

7.12.1.1 Presto blue

For experiments performed on 2D plastic, culture media was discarded and the cells were washed three times with 200 µl 1X HBSS. Residual HBSS was discarded and 200 µl 10% Presto Blue (Thermofisher Scientific) in culture media was added to each well. The cells were allowed to incubate with the Presto blue in the dark for 2.5 hours in a humidified incubator at 37°C with 5% CO^2.

Fluorescence was read immediately after incubation on a Fluostar Omega fluorescence microplate reader (BMG Labtech) and fluorescence was quantified using excitation and emission wavelengths of 540 nm and 595 nm. The data measured in arbitrary units for the treated samples were normalised to the negative control (non-treated samples) and reduction in percent (%) survival was calculated.

7.12.2 Viability on cells on 2D/3D scaffolds

7.12.2.1 Annexin/PI/sytox staining

The percentage of apoptotic cells was determined by flow cytometric analysis with Annexin V and PI or sytox (eBioscience, 00-6990; Life technologies, S34857) staining. Annexin V binds with phosphatidylserine externalized from inner plasma membrane after cells undergo apoptosis. Thus, Annexin V signals indicated the apoptotic cells. Meanwhile, PI is able to stain the nucleotide fragments. Only in late stage of apoptosis, that nucleus membrane disappears or in necrosis that the nucleus membrane is broken, the PI signals can be detected.

In the pictures output from the flow cytometry, B1 quadrant represent Annexin V- /PI+ which usually means necrotic cells, B2 is Annexin V+ /PI+ as apoptotic cells in late 31

stage, B3 is Annexin V+ /PI- as apoptotic cells in early stage, and B4 is Annexin V- /PI- as vital cells. The percentage of apoptotic cells was defined as the sum of B2 and B3 quadrants.

7.13 Data acquisition Flow cytometry.

Data was acquired on a Fortessa LR BD flow cytometer. The cell suspensions were analysed for their fluorescence, size and granularity. The fluorophores coupled to the antibodies, which stain the cells, are excited by the lasers in the machine and emit fluorescence at specific wavelengths, which is measured by the cytometer. The combinations of fluorescence picked up by the channels allow to discover the possible identity of the cell type. The staining protocols were optimised to provide staining, high cell retrieval, and a high proportion of cell viability.

Voltages for FSC and SSC were kept the same for every experiment.

7.14 Western blot

Healthy and cirrhotic scaffolds were washed in PBS for 5 minutes, and then each sample lysed in a 2 ml Eppendorf with 200uL of RIPA buffer (Sigma Aldrich) completed with protease and phosphatase inhibitors (Roche) and 5 mm steal beads at 30htz for 10 minutes using the TissueLyser II (Qiagen). Samples were incubated on ice for 15 minutes and then centrifuged at 4 ° C for 15 minutes at 14000 rpm. The supernatant containing the protein lysate was recovered and transferred into another tube. Finally, the sample buffer (4X LDS, Invitrogen) and β-Mercaptoethanol (1:200) were added to lysates and incubated for 5 minutes at 95°C.

Protein lysates were run onto SDS-PAGE (sodium-dodecyl phosphate polyacrylamide gel electrophoresis) gel gradient (4-12%, Invitrogen). The run was carried out at 150V for one hour and a half, in the Running Buffer (MOPS, Invitrogen).

After the run, gels were assembled in a “sandwich”-like structure with the following order from top to bottom: cathode (-), fiber pad, filter paper, gel, nitrocellulose membrane, filter paper, fiber pad, anode (+). In this way, the negatively charged proteins were transferred into nitrocellulose membranes by using Transfer Buffer (Tris Glycine + Methanol at 10% or 20% respectively for one and two membranes transferred) at 75V for 1 hour. Ponceau S was used to stain the abundant protein bands on the membranes in order to check the transfer. Membranes were washed three times for 5 minutes with PBS-T (PBS + 0.1% Tween), and then incubated for one hour with 5% of BSA in PBS-T in order to avoid nonspecific binding sites.

To detect specific proteins, the membranes were incubated over-night at 4 ° C with the indicated primary antibody (IL-2, Santa Cruz, sc-398253). The immunoreactivity was detected by incubation for one hour at room temperature with secondary antibodies conjugated to HRP (Horseradish Peroxidase), followed by ECL (enhanced chemiluminescence, Thermo Scientific Pierce) reaction and exposure on the ChemiDoc Chemiluminescent Western Blot Scanner (LI-COR). Blots were stripped by incubation for 10 minutes at room temperature with a solution containing 0.2M NaOH, and incubated with a GAPDH antibody diluted in 1% BSA in PBS-T as an internal control.

7.15 Treatments

Cytotoxicity of the Sorafenib was tested in SNU-449 cells by presto blue and Annexin/Pi staining. 6, 12, 24, 48 and 96 µM concentrations of Sorafenib. Results were evaluated after 3 days as percentage of viable cells, and IC_{50} values are calculated according to these results with software PRISM. The IC_{50} was then used for treatment of single culture and co-culture with immune cells.

ROR-1 BiTe (provided by Prof.Natwani’s Lab, UCL, London, UK) PD1 (Ultra-LEAF™ Purified anti-human CD279 (PD-1) Antibody, Bio legend) were used for the liver metastatic model experiments. Both drugs were administered for 3 days and every day at a concentration of 1µg/mL.

8. Thesis aim

During the past few decades, research has provided breakthroughs that have enhanced our understanding of the mechanisms and pathways that regulate the immune system's response to cancer. However, despite these advances, obstacles still exist for the field of cancer immunotherapy in particular for solid tumours. A key challenge limiting the translation of effective therapies in this field is due to the lack of understanding of the tumour microenvironment's role in modulating both cancer and immune cells phenotypes.

The aim of this thesis was to establish a 3D cancer model employing human extracellular matrix (ECM) scaffolds to better recapitulate the complexity of solid tumour microenvironment. The ECM-based model might offers unique insights into T cell infiltration and antitumor mechanisms that could be used for identifying novel targets and testing the therapeutic efficiency of novel therapies currently under clinical development.

Thus, to investigate the role of ECM in modulating cancer and immune cells biology as well as response to therapies, we focused on the following aims:

- Recapitulate the in vivo 3D system to study cytotoxic human T cells and their infiltration into tumour tissue.

- The characterization of a novel 3D system that allows to perform a comprehensive phenotypical and functional analysis of tumour cell lines growing in a healthy and cirrhotic environment. Both approaches subsequently should be evaluated in a model of malignant cells and immune cells that we set up for these studies.

- to investigate the mechanisms of antibody-based immunotherapies and the role of the tumour microenvironment in mediating the anti-tumour immune response, in order to aid the development of improved immunotherapies for cancer patients.

9. Results

9.1 Recreating the immune microenvironment using three-dimensional human liver extracellular matrix scaffolds.

9.1.1 Introduction

Previous studies by Mazza et al. provided initial indications that the 3D microenvironment is essential for disease modelling underlining major differences in cell behaviour with the artefact results when working with 2D culture system [148].

Therefore, it was postulated that an even more complex cellular 3D human microenvironment would provide a better understanding of cancer biology and be an advanced tool for targets discovery and drug screening.

Considering the increased interest during last years in developing new therapeutics to modulate the immune cell phenotype within solid tumours, there is an unmet need in developing 3D models that recapitulate the complex tumour microenvironment.

Currently, only a limited number of in vivo and in vitro models are available to be used for such studies. Using *in vivo* models would be more appropriate to study and explore this complex system. However, considering the differences in the regulation of the immune system in mice compared to human[153], we propose a 3D human ECM model that could be the model of choice as it would allow to address pivotal questions such as the differential regulation of cellular phenotypes and translation for infiltrating T and NKs cells, their immune modulation in tumours, and response to chemotherapy and immunotherapy.

9.1.2 Decellularization of human 3D liver scaffolds

The decellularization of the 3D scaffolds derived from cirrhotic tissue was obtained by adapting the protocol described previously for the decellularization of the 3D healthy human liver scaffolds described in materials and methods (unpublished paper, Mazza et al.).

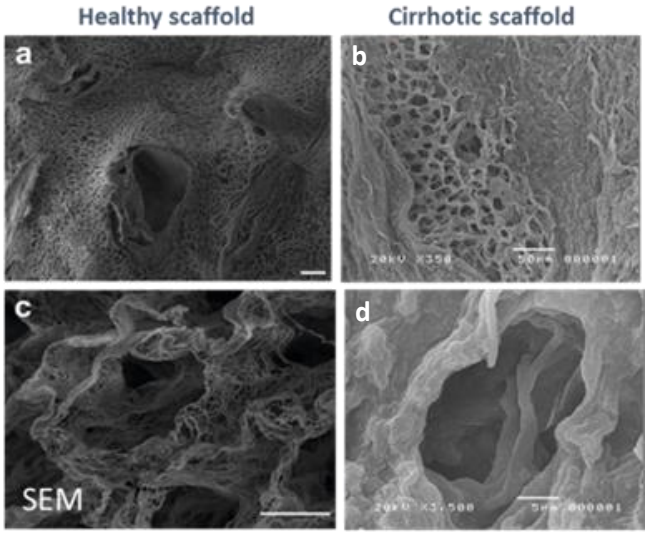

Fig. 21 SEM imaging of decellularized 3D healthy and cirrhotic scaffolds.

Pictures showing the preservation and conservation of the hepatocyte pockets of a decellularized 3D healthy (a, c) and cirrhotic scaffolds (b, d) (Scale bars 50 µm, 10 µm).

As internal control, the absence of cellular materials was confirmed by the reduction of DNA amount (Fig.20). The decellularization procedure did not affect the overall 3D architecture of both healthy and cirrhotic (Fig. 21). Indeed, the ultrastructure of healthy scaffolds was confirmed by SEM analysis showing preservation of hepatic lobule and lack of collagen boundaries as well as organised collagens structures (Fig. 21 left panel)). Preserved cirrhotic-like nodules as shown in Fig.21 (right panel) characterized the cirrhotic scaffolds.

9.1.3 Re-population of decellularized human 3D liver scaffolds with human PBMCs

A first set of experiments was performed by reseeding the decellularized healthy and 3D cirrhotic scaffold with $1^{\wedge}10^{6}$ PBMCs/scaffold in a 48 well plate. Engineered tissues were evaluated after 24h, 72h, and 5 days.

Histology was performed to detect and localize the PBMCs in 3D liver scaffolds. PBMCs, purified from blood of healthy donors (n>5), were able to infiltrate into both healthy and cirrhotic 3D ECM liver scaffolds with reserved cell integrity and morphology (Fig.22). H&E staining showed that PBMCs progressively engrafted into the acellular tissues over 5 days (Fig. 22).

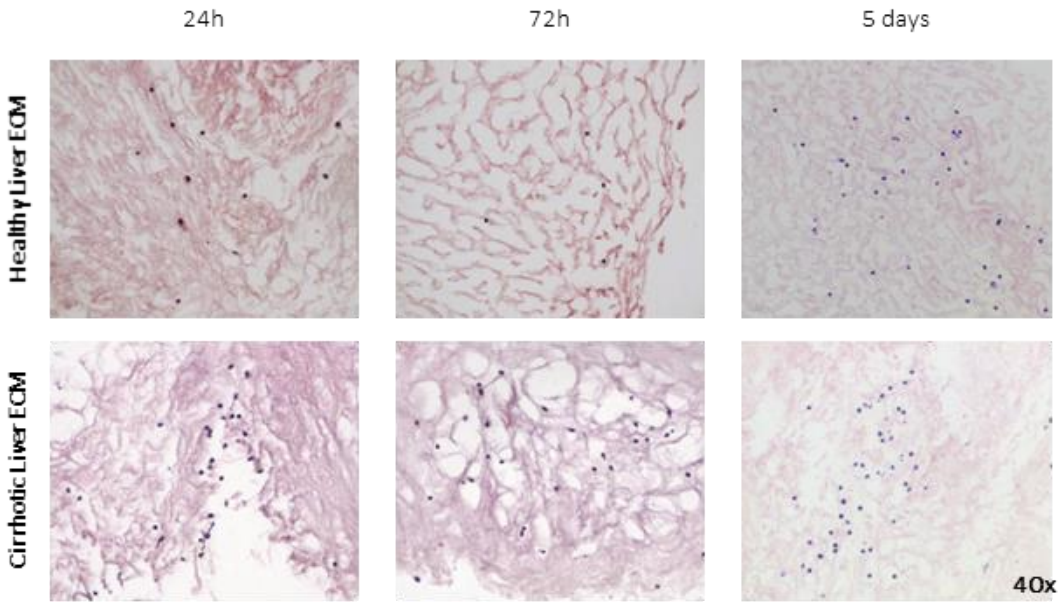

Fig. 22 Histological observation of PBMCs engrafted in the two different 3D liver scaffolds.

Haematoxylin and eosin staining showed the progressive engraftment of PBMCs in the decellularized 3D liver scaffolds. Upper panel: PBMCs cultured in a healthy 3D liver scaffold. Bottom panel: showing PBMCs in a cirrhotic 3D liver scaffold. Cell infiltration was analysed at different time points (1, 3 and 5, days). Magnification 40x.

Furthermore, the proliferation state of PBMCs was determined by performing immunohistochemistry staining against Ki67, a specific nuclear marker for cell proliferation. At all time points under investigation and within both types of scaffolds, proliferating cells were observed, and cells demonstrated to be viable up to day 5 (Fig. 23), further indicating the suitability of the system to develop long-term cultures without the addition of exogenous factors (i.e. cytokines).

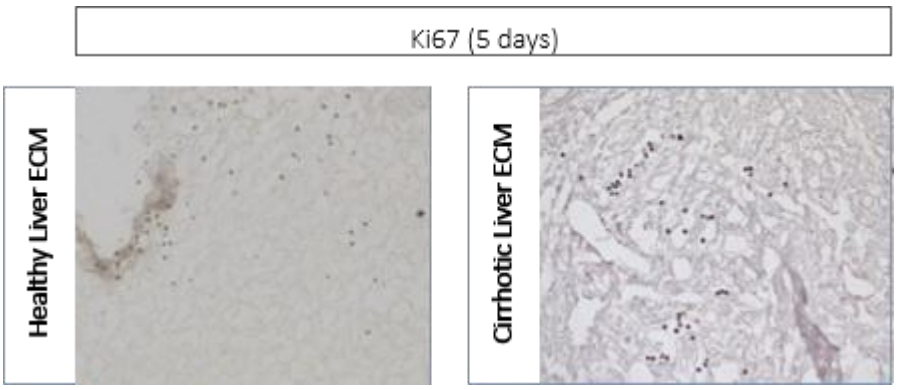

Fig. 23 Immunohistochemistry staining of Ki-67 in sections of healthy and 3D liver scaffolds repopulated with PBMCs.

Formalin-fixed, paraffin-embedded PBMCs in healthy (left) and cirrhotic (right) 3D liver scaffolds after 5 days in culture. Ki-67 immunohistochemistry showed a nuclear Ki-67 brown staining in cells (magnification 40x).

To further confirm these observations, the viability of cells was investigated after 5 days of culture by flow cytometry. The percentage of viable cells inside the scaffolds was assessed with Annexin V FITC+ and SYTOX- for identifying apoptotic cells, with Annexin V FITC+ and SYTOX+ for necrotic cells while viable cells were identified by negative staining for both markers (Annexin V- and Sytox blue-). Notably, no significant differences were observed in terms of cell viability between PBMCs cultured in healthy and cirrhotic scaffolds (Fig. 27)

Interestingly, the presence of different subpopulations was noticed (as indicated by the arrows in Fig. 24.) and those might include plasmablasts/plasmacytes, which were observed in both types of 3D liver scaffolds.

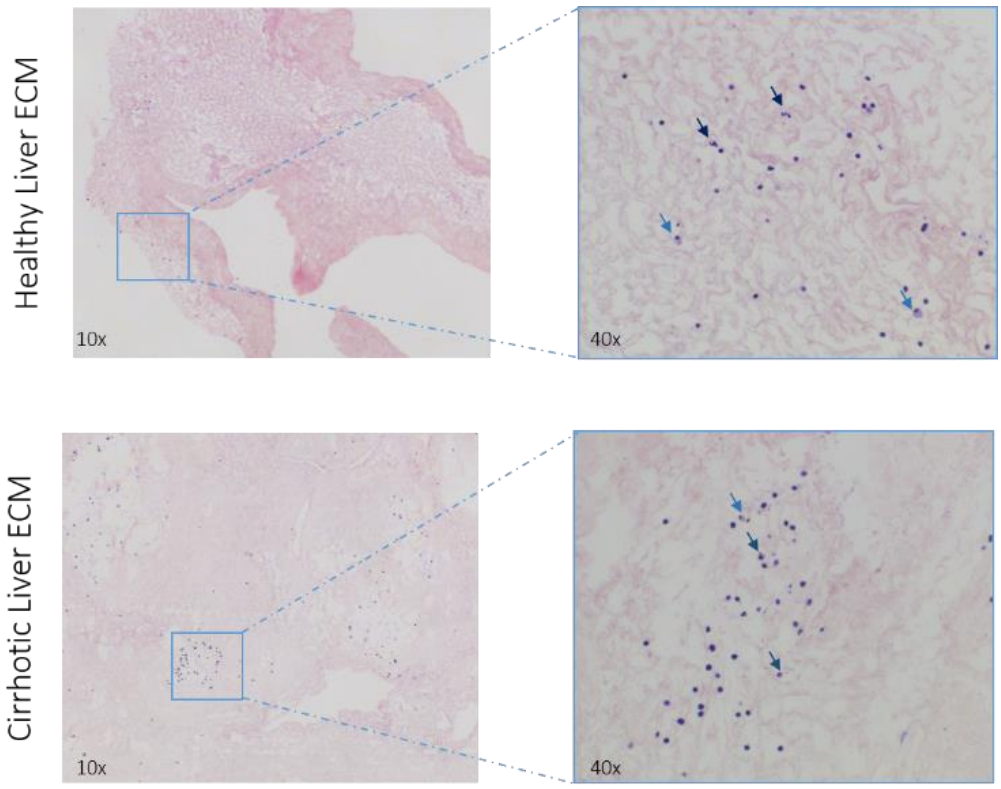

Fig. 24 Histological sections of 3D Healthy and cirrhotic ECM repopulated with PBMCS after 5 days.

Haematoxylin and eosin demonstrate infiltration of immune cells in both healthy (upper panel) and cirrhotic (bottom panel) 3D liver scaffolds after 5 days in culture. Already H&E distinguished few groups of hematopoietic cells. Lymphocytes and Plasma cells are marked by differences in nuclear morphology and size.

To assess whether different immune cell populations entered the 3D liver scaffolds, FACS analysis was performed to identify those cells engrafting the scaffolds (i.e. infiltrating cells) from those cell types, which remained in the culture media i.e. non-infiltrating cells (Fig.25). To assess this, different cell extraction protocols were assessed because enzymatic digestion of tissue can affect the viability of single cells derived from the starting tissue.

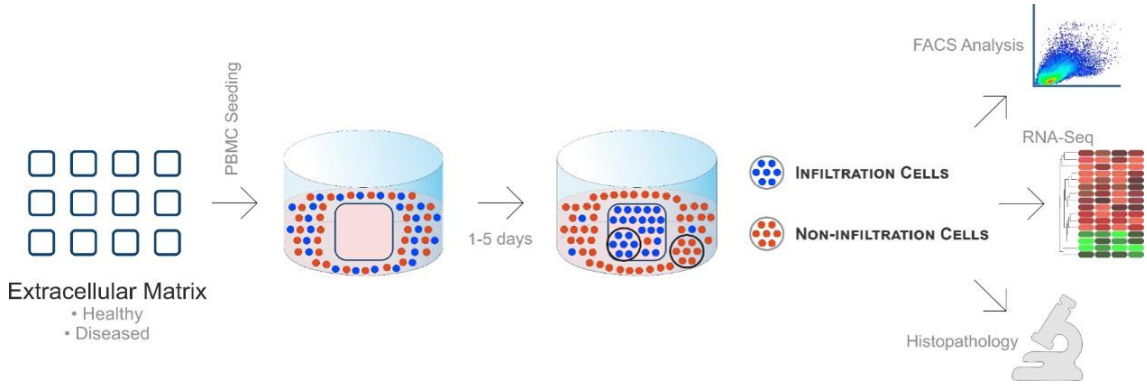

Fig. 25 schematic representation of the experimental protocol.

After decellularization of scaffolds derived from both healthy and cirrhotic ECM, PBMCs (previously purified from peripheral blood of healthy donors) were incubated up to 5 days. Then, we evaluate the presence of infiltrating cells and non-infiltrating cells present in the culture medium (cells still in suspension).

Therefore, different extraction protocols were explored to establish the most optimal protocol that resulted in the highest yield of cell number (Fig. 26). Figure 26 showed the cell count retrieved after each extraction protocol. From these results, it was decided to perform the next set of experiments by combining the protocol that uses collagenase and cell strainer due to the high yield of viable immune cells recovered after 15 minutes.

Fig. 26 Total cell number after enzymatic digestion and mechanical dissociation using five different extraction protocols.

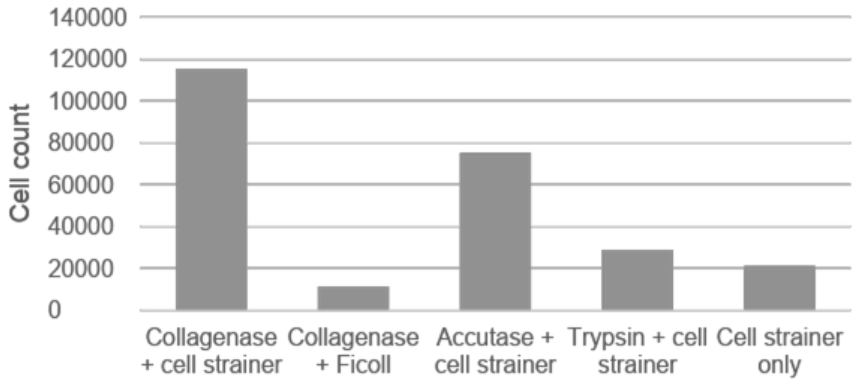

Representative graph showed the cell count after each extraction protocol. All protocols used for the cell extraction are based on mechanical and enzymatic dissociation.

After cell extraction, cell viability was analysed by Annexin/sytox staining (Fig. 27) of those cells extracted from the 3D liver scaffold by using the collagenase protocol. These data confirmed that by using this extraction protocol the viability of the sample was above 92%.

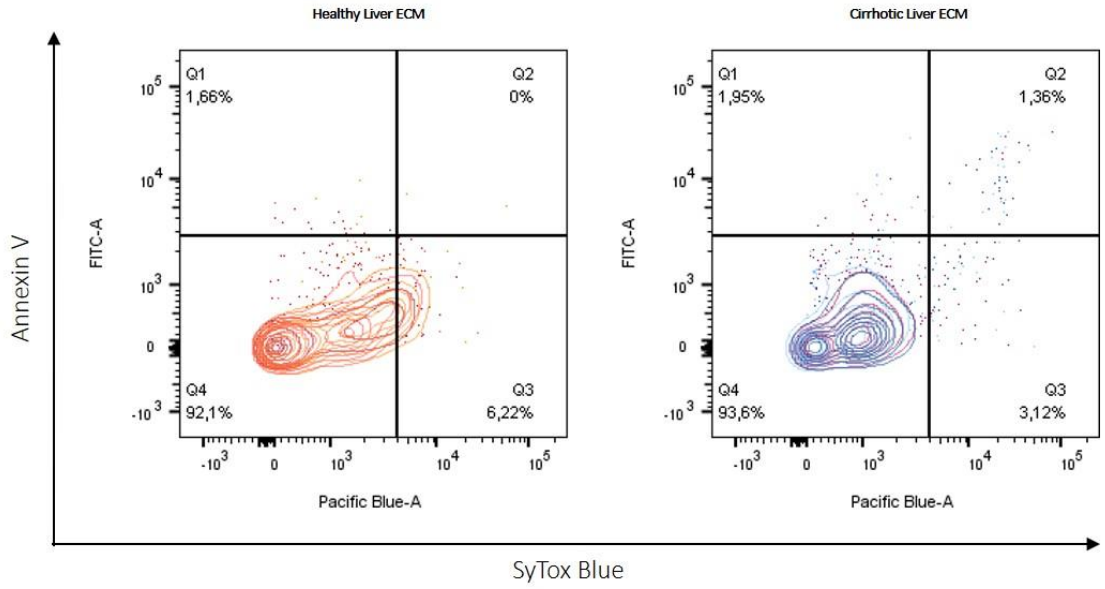

Fig. 27 Viability staining of PBMCs extracted from healthy and cirrhotic 3D liver scaffolds.

Apoptotic cells (Annexin V FITC+ and SYTOX-) and necrotic cells (Annexin V FITC+ and SYTOX+) were detected by flow cytometry analysis following the collagenase extraction protocol of PBMCs from healthy and cirrhotic 3D scaffolds. Results are displayed for PBMCs cells extracted from healthy (left) and cirrhotic (right) 3D liver scaffolds. Graph shows data from 3 biological technical repeats containing 3 samples each (n=9). Replicates each of it is a pool of 3 samples. Each condition is n=3 pooled samples.

To identify different lymphocyte populations, cells were gated for forward and side scatter (FSC and SSC, respectively) properties. Debris originated from the collagenase ECM digestion were excluded based on a FSC/SSC dot plot (Fig. 28).

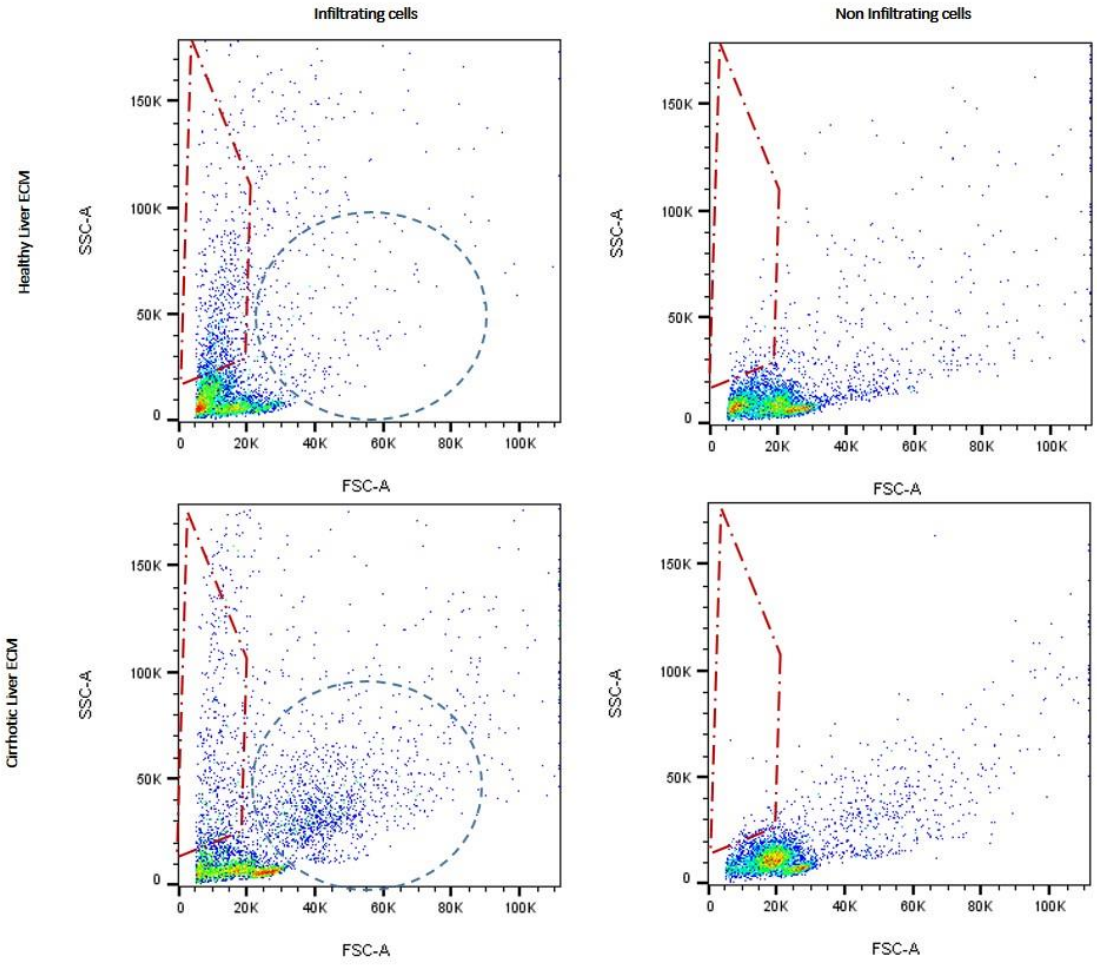

Fig. 28 Flow cytometry analysis of lymphocyte populations from whole blood w/o infiltration in healthy and cirrhotic 3D liver scaffolds

First, lymphocytes were gated based on FSC and SSC. This gating strategy can also be used to exclude debris (red gate, left corner of the plot) due to the collagenase enzymatic digestion of collagen ECM component. Inside the blue gate the monocyte population is detectable.

9.1.4 T cell population in 3D liver scaffolds

To analyse the different phenotypes of infiltrating and non-infiltrating immune cells, CD3 T lymphocytes were selected and further divided into CD4 and CD8 cells (Fig. 29). Healthy donor PBMCs populations were merged to create a single t-SNE (T-Distributed Stochastic Neighbour Embedding) map with the signal strength of key phenotypic markers defining specific cellular lineages expressed by different colours. Thus, t-SNE analysis was performed using the phenotypic markers for CD8 and CD4 and cell populations were projected onto t-SNE space and assigned specific colours.

When comparing the cellular proportions by IN (extracted, infiltrating cells) and OUT (in suspension, non-infiltrating cells) from both healthy and cirrhotic 3D scaffolds, the presence of different subpopulations of PBMCs was observed (Fig. 29,).

Clustering of T cell population was based on CD3, CD4 and CD8 expression that allowed to visualize the 3 different subsets: CD3 in blue, double positive for CD3 and CD4 in orange and double positive for CD3 and CD8 in green. These results show differences in frequencies of $CD3^{+}CD4^{+}$ (orange dashed circle) between infiltrating cells and the non-infiltrating cells. Same results can be noticed for the $CD8^{+}$ population (green dashed circle).

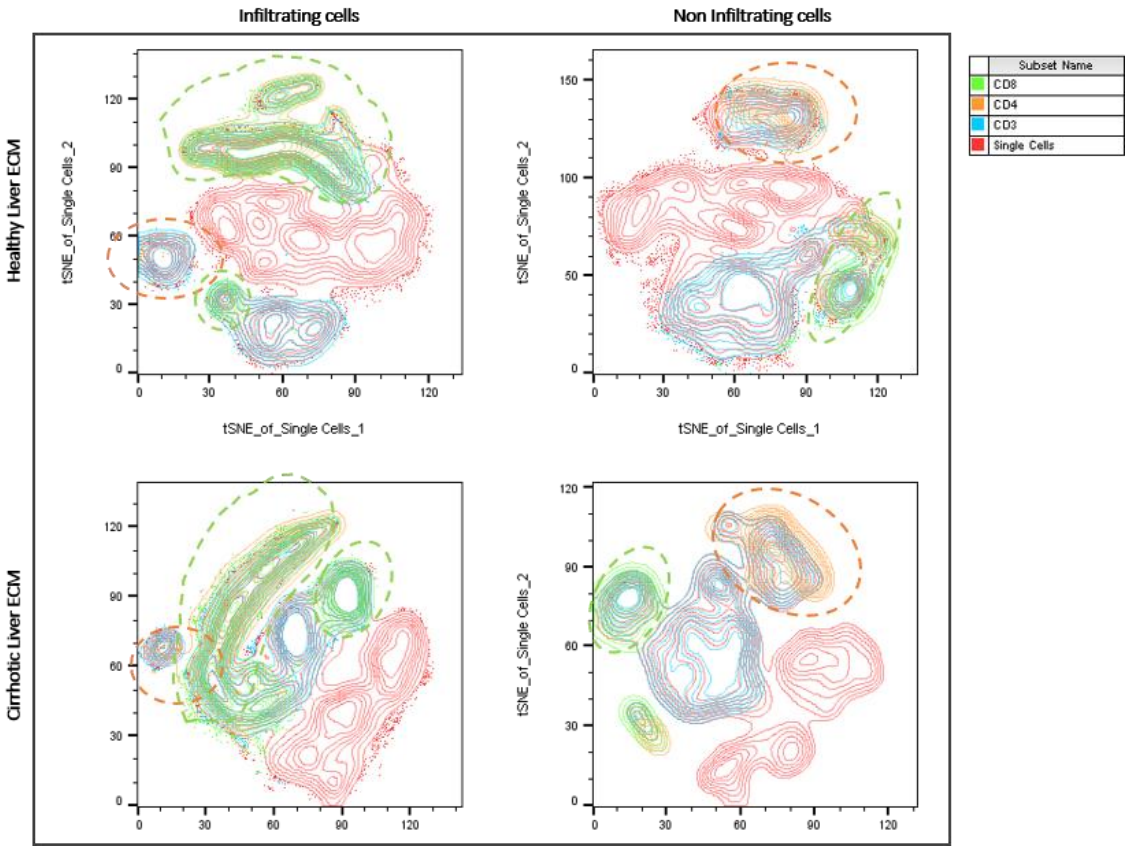

Fig. 29 Distinct phenotypic subset infiltrating the 3D liver scaffolds.

Example of a 3-color flow cytometry panel after tSNE was applied to reduce dimensionality into a 2-dimensional data space. t-SNE analysis was performed using 1,000 iterations, a perplexity of 40. Manually gated populations of known phenotypes were overlaid onto the tSNE space in the FlowJo Layout editor. This revealed how distinct phenotypic subsets of events cluster together and are enriched in distinct areas of the continent-like structure. Cell populations are indicated by different colours, in blue $CD3^+$ cells, in orange $CD4^+$ cells, in green $CD8^+$ population, in red cells negative for all 3 markers.

It is known that many cells behave differently in 2D culture systems compared to 3D systems. However, no publications have been reported yet about the capacity of T cells subsets to infiltrate in a 3D human ECM environment without stimulations in vitro.

Thus, the phenotype of different subsets of T cells cultured in a 2D system was compared with the new 3D liver scaffold model obtained from both healthy and cirrhotic human liver ECM scaffolds. Multicolour flow cytometry was used to identify and quantify the T-cell subsets with the expression of cell surface markers (Fig. 30).

These data suggest that the 3D system is characterized by the presence of a higher percentage of T cells compared to the 2D system (Fig. 30). Additionally, an expansion of CD8+ cells infiltrating the liver 3D scaffolds was observed when compared to 2D. Importantly, the percentage of CD8+ cells infiltrating the cirrhotic 3D liver scaffolds was significantly increased in comparison to the same subset infiltrating the healthy 3D scaffolds (Fig.30).

In contrast to CD8 T cell behaviour, the percentage of $CD4^+$ T cell population was similar between 2D culture and non-infiltrating cells of 3D healthy and cirrhotic scaffolds. Notably, when analysing the CD4 to CD8 subpopulation ratio in both types of 3D scaffolds (Fig. 30), a striking difference was observed between CD4+/CD8+ infiltrating and non-infiltrating cells ratio indicating that CD8 T cells could have a particular advantage and capacity to infiltrate the 3D liver scaffolds. Overall, these data showed a preferential accumulation of $CD8^+$ T cells inside the 3D liver scaffold, with $CD4^+$T present in the supernatant as non-infiltrating cell subset. Thus, studying T cell infiltration in a 3D context by employing tissue- and disease-specific ECM scaffolds may provide insights that otherwise could not be studied in a 2D system.

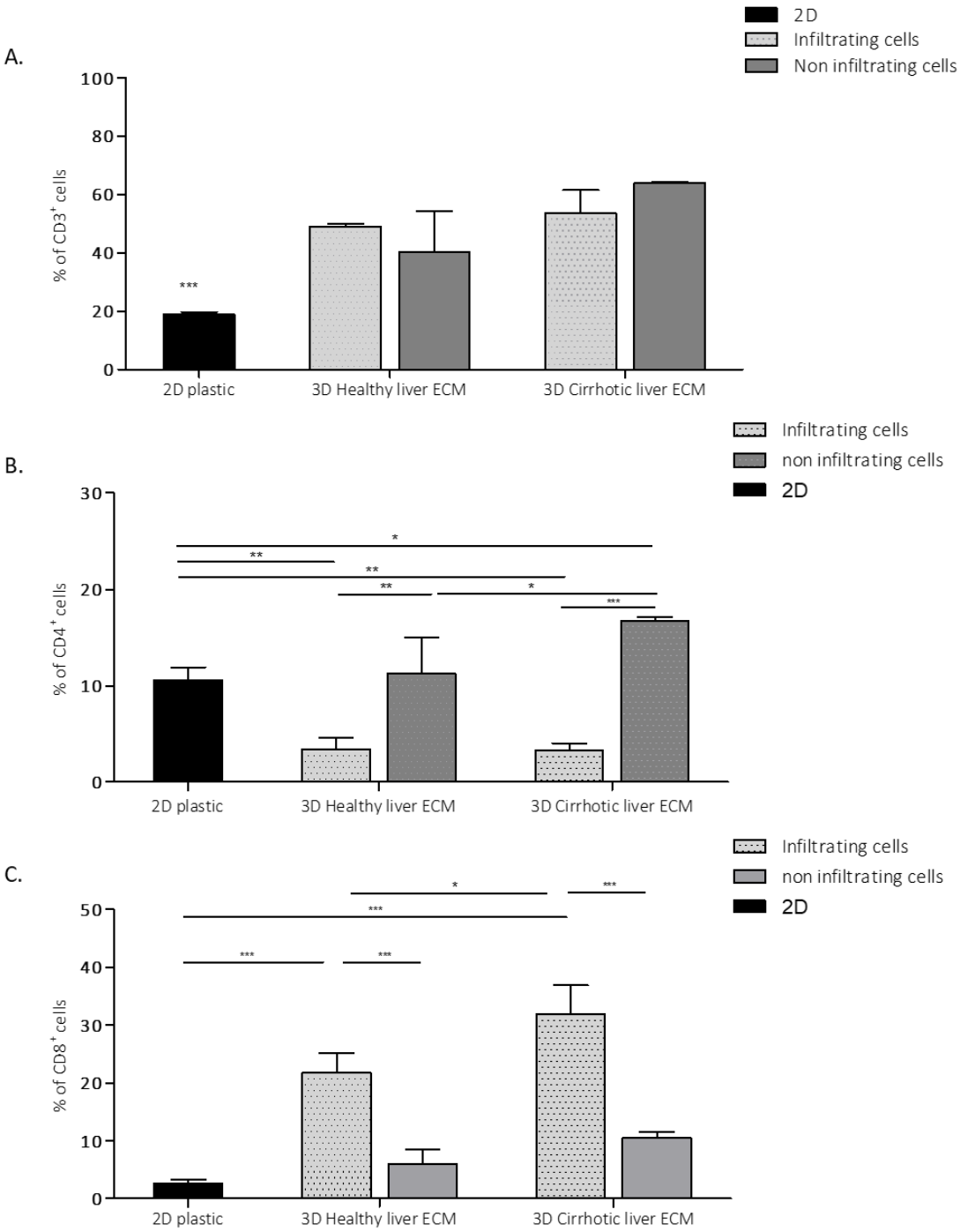

Fig. 30 percentage of T cell populations in 2D system compared to 3D ECM scaffolds.

T cell subsets were assessed by multi-parametric flow cytometry from peripheral blood of healthy donors in culture for 5 days in a 2D system and in 3D ECM scaffolds (healthy and cirrhotic). The gating strategy was as follows: (a) T cells: $CD3^+$ cells (b) T helper cells: $CD3^+CD4^+$; (c) cytotoxic T cells: $CD3^+CD8^+$. Bars represent the pooled data of n=3 scaffolds per condition (mean±standard deviation). In graph a all 3D conditions are statically significant compared to 2D. Statistical difference between groups was determined by Student t *test. * P<0, 01, *** P<0,001*

Next, experiments were performed to further investigate the changes within the immune cell subsets upon exposure to both types of 3D liver scaffolds. Conditioned media was used as control to assess the impact of secreted factors by the extracellular matrix into the culture medium. To this end, conditioned media was obtained by culturing decellularized healthy 3D liver scaffolds in the culture media used for culturing PBMCs for 48 h. Next, PBMCs cultured in 2D were exposed to either normal or conditioned medium for 5 days.

As illustrated in Fig. 31, flow cytometric analysis revealed that PBMCs cultured/exposed to the conditioned medium showed a statistically significant increase in the number of all T cells populations.

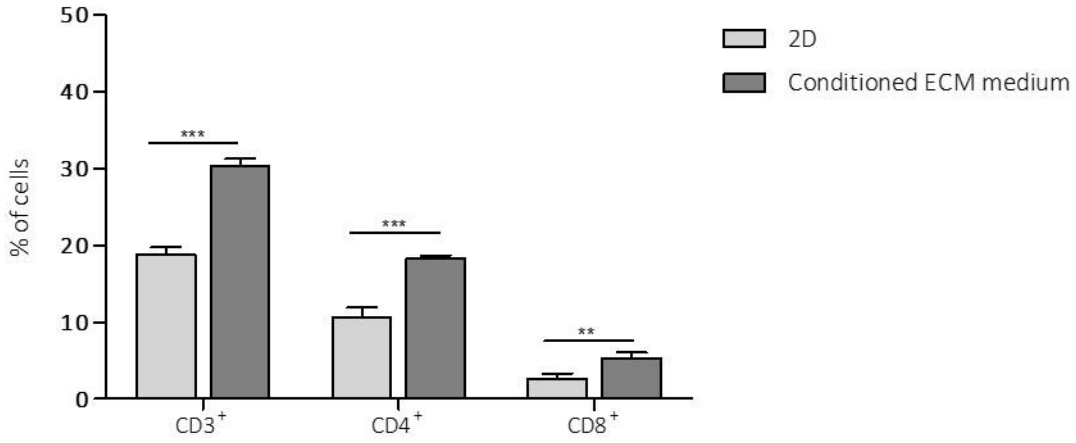

Fig. 31 Percentage of T cell populations in culture medium and conditioned "3D ECM scaffold" medium.

T cell subsets were assessed by multi-parametric flow cytometry from peripheral blood of healthy donors in culture for 5 days in 2D system in normal and in conditioned media. T cell subsets were defined as follows: (a) T cells: CD3+ cells (b) T helper cells: CD3+CD4+; (c) cytotoxic T cells: CD3+CD8+. Bars represent the pooled data n=x per condition (mean±standard deviation). Statistical difference between groups was determined by Student t *test. ** P<0, 01, *** P<0,001*

Next, different markers were used to assess the T cell specific populations between infiltrating and non-infiltrating cells in both healthy and cirrhotic scaffolds. FACS analysis was performed for the following markers $CD4^+CD25^+$ T cells and $CD8^+CD107a^+$.

A closer look into the T-cell subsets revealed that infiltrating CD8 T cells do not significantly increase the expression of the degranulation marker CD107a in the 3D liver scaffolds compared to non-infiltrating cells (Table. 7). These results suggest that $CD8^+$ T cells are prone to infiltrate but do not acquire the activation state once infiltrated into the 3D liver scaffolds. Furthermore, the co-expression of CD4 and the activation marker CD25 were found to be significantly higher in T cells infiltrating both types of 3D liver scaffolds (Table 7).

An overview of the percentages of immune-cell populations infiltrating and non-infiltrating healthy and cirrhotic 3D liver scaffolds (Table 7).

Marker	Infiltrating/non infiltrating cells	Results	Infiltrating/non infiltrating cells	Results
Healthy Liver ECM				
$CD3^+$	Infiltrating cells	49,1% ± 0,85%	Non Infiltrating cells	40,1% ± 4,6%
$CD4^+$	Infiltrating cells	3.4% ± 1.2%	Non Infiltrating cells	11,3% ± 3,7%
$CD4^+CD25^+$	Infiltrating cells	64,7% ±17,2	Non Infiltrating cells	15,9% ±5,2
$CD8^+$	Infiltrating cells	21,8% ± 3,2	Non Infiltrating cells	6,02% ± 2,4%
$CD8^+CD107a^+$	Infiltrating cells	2,1% ±0,6	Non Infiltrating cells	8,6% ±1,8
Cirrhotic Liver ECM				
$CD3^+$	Infiltrating cells	53,7% ±7,8%	Non Infiltrating cells	64% ±0,4%
$CD4^+$	Infiltrating cells	3,24% ±0,7%	Non Infiltrating cells	16,8% ±0,37%
$CD4^+CD25^+$	Infiltrating cells	84,3% ±5%	Non Infiltrating cells	2,8% ±0,08%
$CD8^+$	Infiltrating cells	31,87% ±5%	Non Infiltrating cells	10,48% ±1%
$CD8^+CD107a^+$	Infiltrating cells	8,55% ±1,8%	Non Infiltrating cells	7% ±1,5%

Table 7 Summary of T cell populations percentages in PBMCs cultured in 3D liver scaffolds.

PBMCs were cultured for 5 days in a healthy or in cirrhotic 3D liver scaffolds. The numbers represent the percentage of the PBMC stained positive for the corresponding anti-CD antibodies (average±SD). All the

cells, positive for CD4 or CD8, also express the pan-T-cell antigen CD3. CD25 and CD107a populations were calculated as a percentage of CD4 and CD8.

T cells are highly IL-2-dependent for their survival and function, express constitutively IL-2R (CD25) but are not able to produce IL-2[154]. As shown in table 7, the percentage of CD4CD25+ cells was dramatically higher in the infiltrating population compared to the non-infiltrating population in particular when those cells were obtained from cirrhotic scaffolds. To justify this finding, proteins were extracted from healthy and cirrhotic 3D ECM scaffolds and SDS-PAGE electrophoresis was employed to detect IL-2. Thus. The preliminary results showed the presence of IL-2 (Fig.32) in the cirrhotic scaffolds while this was not detected in the healthy scaffolds. According to, unpublished proteomics data (Mazza G. et al, unpublished data) of healthy and cirrhotic 3D liver scaffolds, it is known that cytokines and growth factors are embedded within ECM biomaterials and therefore a full characterization of those is needed to dissect the mechanisms behind immune cells infiltration.

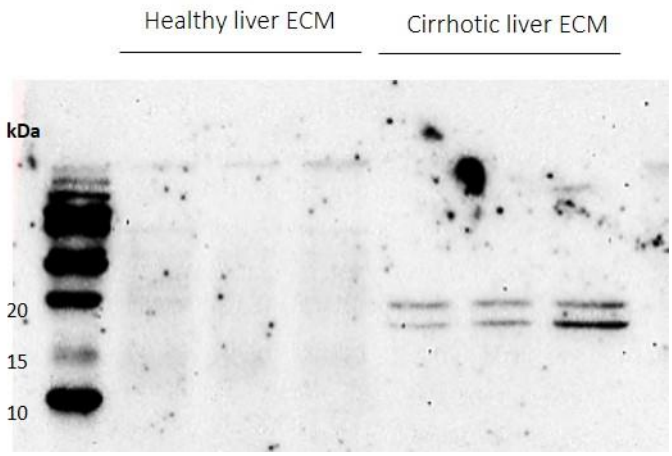

Fig. 32 Western blot of decellularized 3D healthy and cirrhotic ECM.

The protein lysate was obtained from empty liver scaffolds derived from healthy and cirrhotic livers and, the membrane was incubated with anti-IL-2 antibody. 10µg of protein was loaded for each sample.

9.1.5 Natural killer cells on 3D liver scaffolds

Further characterization of the 3D ECM model was performed in order to show the capability of the 3D liver scaffolds to modulate cell biology and prime cell phenotype towards an intra-hepatic like phenotype. Therefore, the impact of human liver ECM on natural killer cells (NK) was determined as the liver is particularly enriched with NK cells.

In contrast to NK cells in peripheral blood ($CD56^{dim}$ cells), NK cells in the human liver have a specific profile containing two different populations, $CD56^{bright}$ and $CD56^{dim}$ cells, that are present in equal proportions in the liver[155].

NK cells purified from PBMCs were cultured in 2D and reseeded in a healthy 3D liver scaffold for 48h without any exogenous stimuli. Cells were extracted from the 3D scaffold and in parallel collected from the 2D system. NK cells were stained with anti-CD3 and anti-CD56 antibodies conjugated to different fluorochromes. Next, a FACS gate was set on $CD3^{+}$ $CD56^{+}$ cells (NKT cells) and $CD3^{-}$ $CD56^{+}$ cells (NK cells). Gates on NK cell population indicated the $CD56^{bright}$ and $CD56^{dim}$ subpopulation. A comparison of the 2D culture and the 3D system showed the presence of different NK subpopulations ($CD56^{bright}$ and $CD56^{dim}$). Interestingly, NK cells cultured in 3D ECM showed an increase in the $CD56^{bright}$ (in line with intrahepatic NK) phenotype in comparison to 2D plastic culture (in line with population present in the peripheral blood) therefore suggesting a tissue-priming effect on NK cells provided by human ECM (Fig.33).

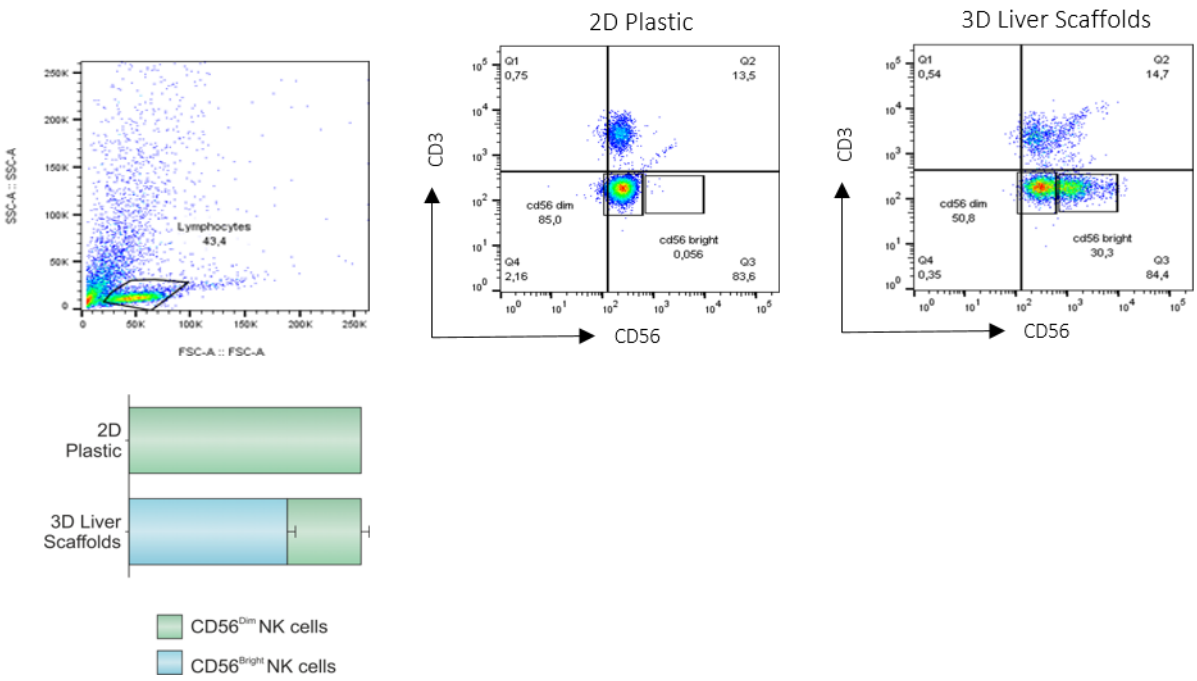

Fig. 33 phenotypical changes in circulating NK and infiltrating NKs.

Flow cytometry dot plot of NK cells after gating on lymphocyte, single cells, CD3 and CD56 population. The positivity of CD3 versus CD56 dot plot allows the identification and discrimination of human NKTs. The remaining CD3 negative cells were analysed for CD56 positive cells to identify the natural killer (NK) cells. $CD56^{dim}CD56^{bright}$ NK cells are clearly present in cells engrafted in the healthy 3D liver scaffolds (dot plot on the left) while the bright population is absent in cells cultured on 2D plastic (dot plot in the middle). Lower graph representing the comparison between $CD56^{dim}$ and $CD56^{bright}$ NK cells cultured in 2D plastic and in healthy 3D liver scaffolds (n=3), data are presented as the mean ± SD.

9.1.6 Monocyte macrophages population in 3D liver scaffolds.

The monocytes population is present in the peripheral blood and ultimately migrate into tissues where they can differentiate into macrophages. Macrophages are able to acquire and change accordingly to the microenvironment into different morphological types (Kupffer cells, histiocytes, alveolar macrophages etc.[156]).

In the following set of experiments the role of ECM on monocyte-macrophage differentiation was investigated with human peripheral blood mononuclear cells (PBMC) engrafted on healthy and cirrhotic 3D ECM scaffolds.

The results showed that monocytes undergo a differentiation into macrophages when engrafted into 3D liver scaffolds by analysing the expression of CD68 (pan macrophage marker) and CD11b (protein directly involved in cellular adhesion) markers after 5 days of culture (Fig. 34). CD11b protein is important not only for cellular adhesion of neutrophils and monocytes but its expression is induced during differentiation of monocytes into macrophages [157].

FACS analyses showed that cells infiltrating the healthy as well as cirrhotic 3D liver scaffolds were positive for CD68. Absence of a CD68+ cells population was found in those cells in suspension i.e. non-infiltrating the 3D scaffolds. An extra population was detected that expressed both CD68 and CD11b within the infiltrating cells which might indicate the presence of activated macrophages (Fig.34), it has also been shown to mediate macrophage adhesion, migration, chemotaxis and accumulation during inflammation [158]

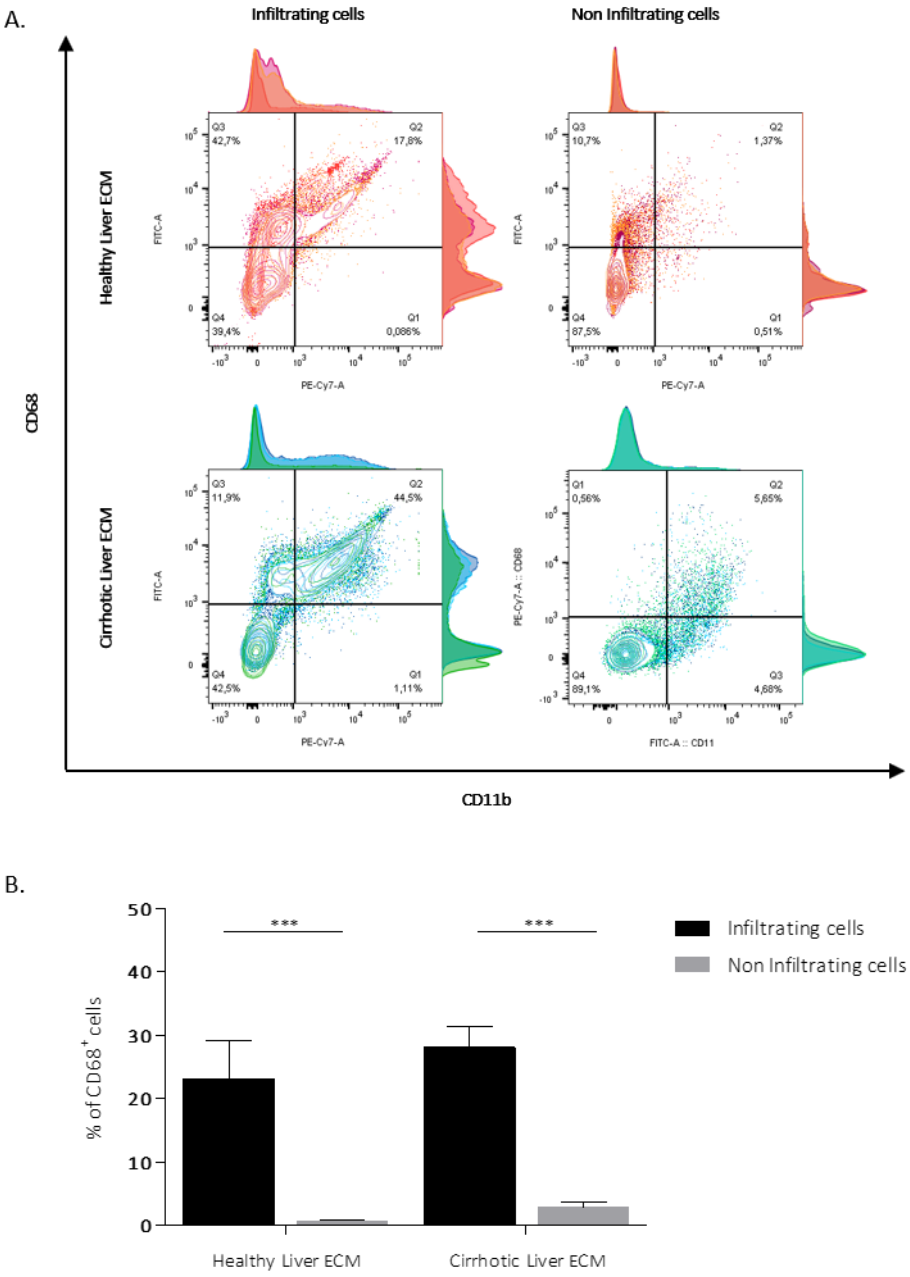

Fig. 34. Phenotypical changes during the culture of the monocytic lineage in 3D liver scaffolds.

CD68 and CD11b expression patterns in PBMCs, analysed by flow cytometry. A: Scatter plots and adjunct histograms shows the distribution of cells in CD68⁻/CD11b⁺ (Q1), CD68⁺/CD11b⁺ (Q2), CD68⁺/CD11b⁻ (Q3), and CD68⁻/CD11b⁻ (Q4) subpopulations of monocyte and macrophages growing and infiltrating the healthy (upper left plot) and cirrhotic 3D liver scaffolds (lower left plot) as well as non-infiltrating cells for both conditions (plots on the right). For each sample, 10.000 initially gated events were analysed. Graph shows pooled data from 3 biological replicates with n=3 scaffolds per biological sample. B: Percentage of CD68+

*cells, infiltrating the 3D liver scaffolds (black) and non-infiltrating cells (grey). All quantitative data are presented as the mean+SD. ***Represents student t test, p<0.001*

These results suggest that both types of liver 3D scaffolds could modulate monocyte–macrophage differentiation *in vitro* and that monocytes undergo a rate of differentiation towards CD68+ macrophages when engrafted in the 3D liver scaffolds in contrast to the monocytes non-infiltrated, which lack CD68+. More analysis are needed to fully dissect the role of ECM in modulating the monocyte differentiation as well as include more markers to evaluate whether the liver ECM can primer circulating monocytes towards a Kupffer cells-like phenotype.

9.1.7 Gene expression of remodelling genes and Integrins in immune cells in 3D scaffolds

In this set of experiments the gene profile of several genes involved in cell-ECM interaction and ECM remodelling were investigated. Cell adhesion molecules (CAMs) proteins orchestrate the interaction between immune cells and tissue resident cells and play a key role in modulating cell-ECM interaction. For instance, the intercellular adhesion molecule 1 (ICAM-1), involved in the binding of a cell-cell interaction and cell ECM interactions, was investigated. ICAM-1 plays a role in cell proliferation, differentiation, motility, trafficking, apoptosis and tissue architecture.

Moreover, possible changes in the expression profile of Metalloproteases (MMPs) and MMPs inhibitors were assessed to determine differences in tissue invasion properties between infiltrating and non-infiltrating cells. Therefore, gene expression of MMP-9 (tissue invasion) and TIMP-1 (inhibitor of metalloproteinases) was assessed at three different time points.

Furthermore, the expression of distinct chemokine receptors by immune cells is critical for their recruitment and infiltration in non-lymphoid sites. CXCR7 has been identified as an alternative receptor for CXCL12 and CXCL11[159]. It is known that CXCR7 is not

expressed in normal blood leukocytes. However, its expression seems to be critical for the immune cell infiltration[160].

In addition to chemokines receptors and adhesion molecules, integrin expression was analysed as their interaction with ECM proteins plays an important role in the recruitment, homing and activation of immune cells [161]. Thus, the expression of Integrin β1 - also known as CD29 - was investigated as it plays a key role in the migration, activation and adhesion of T cells. The gene expression profile of ICAM-1 showed a significant upregulation in infiltrated cells vs. non-infiltrated cells in 3D healthy scaffolds at 24hrs of incubation whereas ICAM1 was significant reduced at 120hrs in infiltrating cells compared to non-infiltrating cells (Fig.35A). In contrast, MMP-9 gene expression was dramatically upregulated after 72hrs and 120hrs in cells infiltrating both types of 3D liver scaffolds. MMP-9 mRNA expression did not change in non-infiltrating cells obtained from both healthy and cirrhotic while MMP-9 mRNA expression was statistically significantly higher in infiltrating cells obtained at 120hrs from cirrhotic scaffolds compared to healthy scaffolds (Fig.35B). Similar results were observed when analysing TIMP-1 gene expression with very low levels of TIMP-1 expressed by non-infiltrating cells with a significant increase at 5 days in cells infiltrating both types of 3D scaffolds (Fig.35C). Moreover, the capacity of cells to infiltrate healthy and diseased ECM correlated with a significant increase in CXCR7 mRNA levels across the different time points investigated (Fig.35E). Similar results and trends were detected for ITGβ1 mRNA expression in immune cells infiltrating the scaffolds while the ITGβ1 expression was significantly lower in non-infiltrating cells. (Fig.35D). There were not significant differences between infiltrating cells in healthy 3D scaffolds versus cirrhotic 3D scaffolds for the gene expression of ITGβ1.

A.

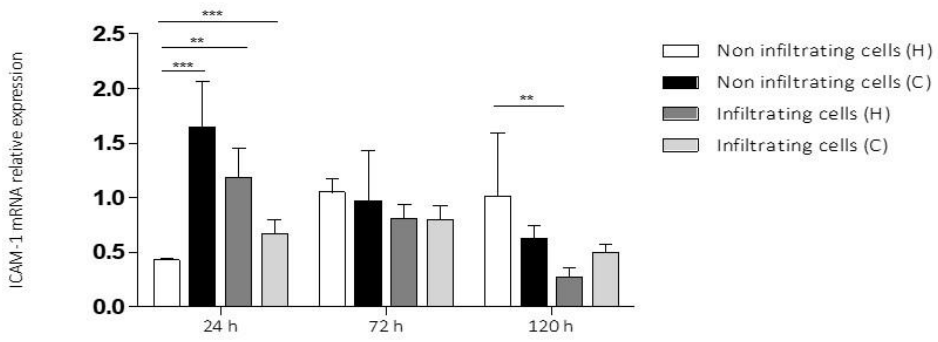
Non infiltrating cells (H)
Non infiltrating cells (C)
Infiltrating cells (H)
Infiltrating cells (C)
ICAM-1 mRNA relative expression
2.5
2.0
1.5
1.0
0.5
0.0
24 h
72 h
120 h

B.

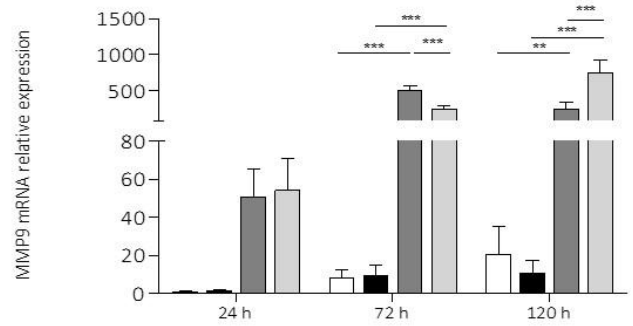
MMP9 mRNA relative expression
1500
1000
500
80
60
40
20
0
24 h
72 h
120 h

C.

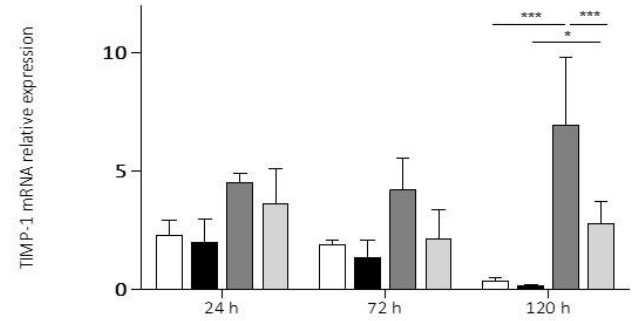
TIMP-1 mRNA relative expression
10
5
0
24 h
72 h
120 h

D.

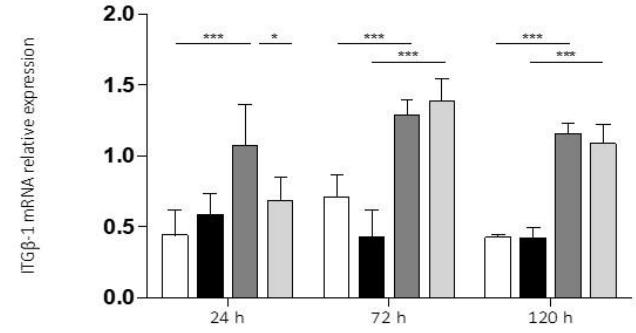
ITGβ-1 mRNA relative expression
2.0
1.5
1.0
0.5
0.0
24 h
72 h
120 h

E.

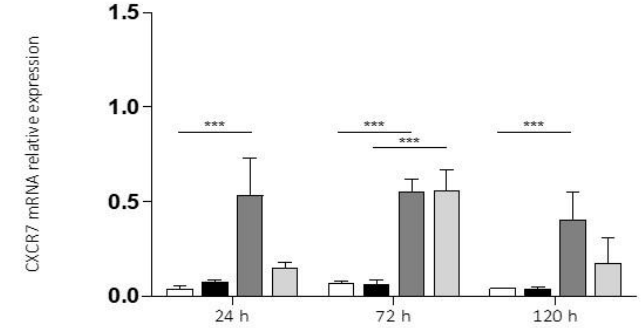
CXCR7 mRNA relative expression
1.5
1.0
0.5
0.0
24 h
72 h
120 h

Fig. 35 Graphs showing mRNA levels assessed by real time PCR in infiltrating and non-infiltrating cells in both types of 3D liver scaffolds.

*Messenger RNA expression of ICAM-1, MMP-9, TIMP-1, ITGβ1 and CXCR7 was assayed by RT-qPCR, time points settled at 24, 72 and 120 hours in culture, of PBMCs infiltrating or non-infiltrating the healthy (H) and cirrhotic (C) 3D scaffold, normalized to control GAPDH mRNA. Results are expressed as mean±s.d. ***Represents two-way anova test, p<0.001.*

9.2 The extracellular matrix derived from human cirrhotic liver strongly reduces the anti-cancer immune response in a 3D model of hepatocellular carcinoma

9.2.1 Introduction

Hepatocellular carcinoma (HCC) is a frequent complication of chronic liver diseases and is associated with high mortality rate and chemotherapy resistance. Immune oncology therapies represent the most promising avenue for the treatment of HCC. Conventionally, tumours can be divided into 'hot' (or 'inflamed') or 'cold' (or 'immune desert') according to the presence of immune cells. The "hot" phenotype is associated to a more favourable prognosis. The aim of this work was to introduce and validate a new 3D model employing healthy or cirrhotic human liver extracellular matrix (ECM) engineered with HCC cells to evaluate immune cell infiltration, T cell cytotoxicity and other phenotypic changes.

PBMC were then co-cultured in HCC 3D models obtained by pre-reseeding HCC cancer cells in either healthy or cirrhotic ECM scaffolds. PBMC co-cultured with HCC cells engrafted prior in both types of scaffolds were able to infiltrate healthy ECM scaffolds but were not able to infiltrate the HCC model based on cirrhotic ECM. This finding suggests that HCC cells cultured in cirrhotic ECM lead to a more aggressive "T cell exclusion phenotype".

9.2.2 HCC cell line in healthy and cirrhotic environment

The occurrence of HCC is associated with multiple factors as the result of distinct environmental risk factors each involving different genetic, epigenetic and gene mutations. Regardless of the aetiology, HCC commonly originates in a background of necroinflammation that sequentially progresses from fibrosis to cirrhosis that then culminates in HCC (this concept is discussed in section 3.1.1). The HCC microenvironment is composed of tumour cells and their tumour stromal cells such as activated hepatic stellate cells (HSC), cancer-associated fibroblasts (CAF), myofibroblasts and immune cells[162]. The majority of HCC patients with liver cirrhosis are asymptomatic, thus resulting in difficulties to diagnose early stages of HCC, which could explain the poor prognosis of HCC in patients. Detecting HCC when patients are in an advanced-stage HCC results in ineffective treatment despite recent progress in the therapeutic field [163].

Consequently, the tumour microenvironment has become an important target for HCC treatment. Since more than 80% of HCC cases rises from cirrhotic microenvironment [107], better understanding of the tumour microenvironment and the implication in the progression and metastatic potential might allow the development of effective therapies for HCC.

In this chapter, the new 3D ECM scaffold model was further explored and more specifically focus was laid on the cirrhotic liver 3D model as a tool to optimize an HCC *in vitro* model that could recapitulate the pathophysiological microenvironment of primary liver cancer.

The HCC cell line SNU-449 derived from a Korean patient prior to cytotoxic therapy[159],was employed due its mesenchymal and aggressive phenotype. Studies have shown that epithelial-mesenchymal transition (EMT) plays an important role in metastasis of malignant tumours, making the tumour cells more flexible, invasive and migratory, thus promoting tumour metastasis and spread[164].

In a first experiment, SNU-449 cells were seeded in both healthy and cirrhotic 3D liver ECM scaffolds and were cultured for 12 days (details in section 5.6.2).

H&E staining demonstrated the engraftment of SNU-449 cells into the scaffold over 12 days in healthy and cirrhotic 3D liver scaffolds (Fig.36) with a diffuse presence of proliferating cells as confirmed by employing immunohistochemistry for the Ki67 proliferation marker (Fig.37).

The histological analysis showed a gain in cellular mesenchymal morphologic features and a difference in topography and pattern of infiltration depending on the type of 3D ECM scaffolds i.e. healthy versus cirrhotic 3D liver scaffolds. These morphological changes prompted us to test the expression of a series of key EMT markers.

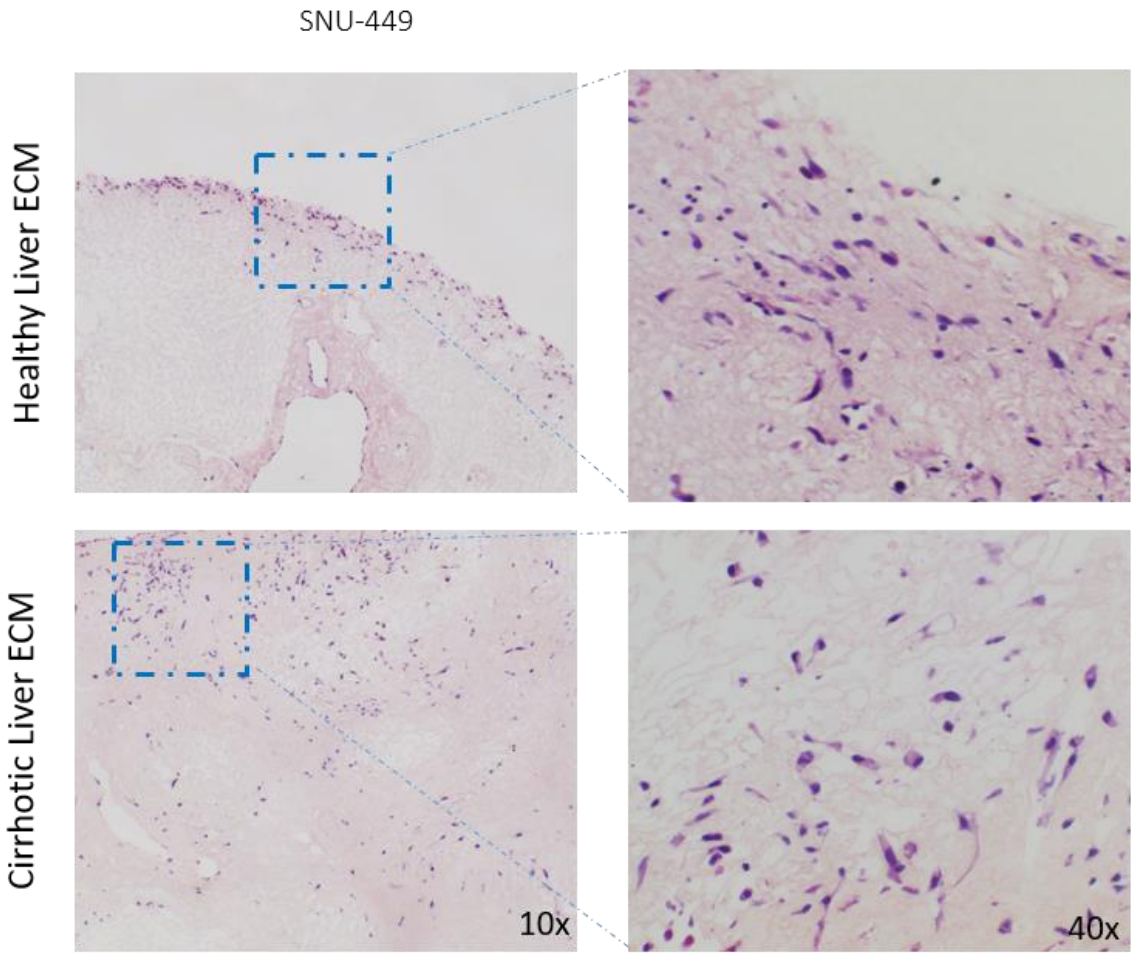

Fig. 36 Representative pictures of haematoxylin and eosin (H&E) of SNU-449 cells in healthy and cirrhotic 3D scaffolds.

Haematoxylin and eosin staining showing the engraftment of SNU-449 on the decellularized 3D liver scaffolds. Upper panel showing SNU-449 cells cultured in a healthy 3D liver scaffolds, bottom panel showing SNU-449 cells in a cirrhotic 3D liver scaffolds, after 12 days in culture. Magnification 10x (right) and 40x (left).

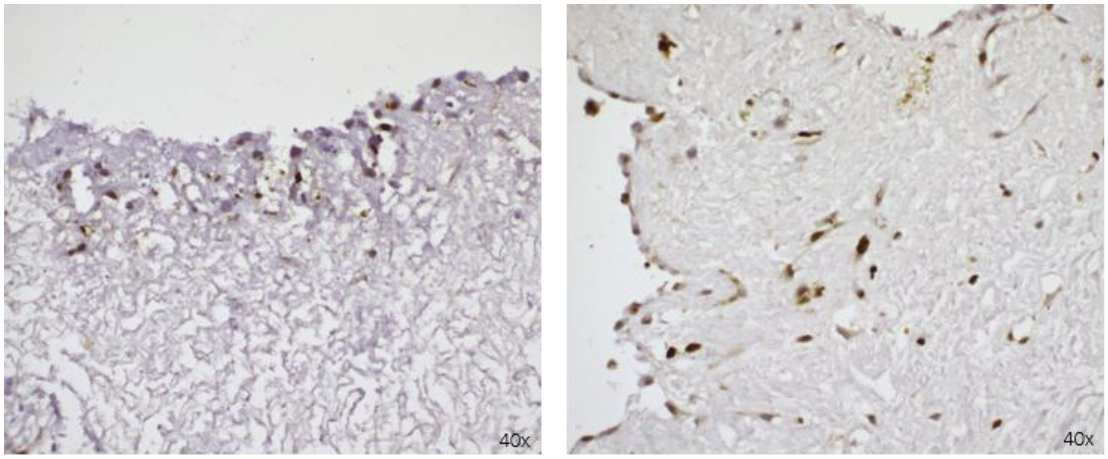

Fig. 37 KI-67 IHC staining of 3D healthy and cirrhotic 3D liver scaffolds repopulated with the SNU-449 cell line.

Formalin-fixed, paraffin-embedded SNU-449 cells in 3D liver scaffolds stained to detect Ki-67 proliferation marker. Note nuclear staining of proliferating cells (brown). SNU-449 cells engrafted after 12 days in healthy 3D liver scaffolds (right) and in cirrhotic 3D liver scaffolds (left). Magnification 40x.

During EMT, epithelial cells undergo a phenotypic switch to form mesenchymal cells that are similar in appearance to fibroblasts [161]. Thus, EMT is characterized by a gain of mesenchymal cell markers and a loss of epithelial markers, such as the adherence junction component E cadherin. During this process cells acquire molecular alterations that facilitate cell motility and tissue invasion [165].

In order to confirm the morphological modifications that were previously observed (H&E, Fig.36) were related to EMT, the differential expression of two main EMT markers was quantified in SNU-449 cells cultured in 2D plastic and compared with cells engrafting healthy and cirrhotic 3D liver scaffolds.

EMT status of SNU-449 cells in 2D, healthy and cirrhotic 3D scaffolds was determined by calculating the Vimentin/E-cadherin mRNA expression ratio. As expected, E-cadherin (CDH1) expression was significantly decreased in cells grown in the cirrhotic 3D

environment (Fig.38) thus suggesting a role of disease-specific ECM microenvironment in priming EMT.

Those findings are in line with the theory of HCC "aggressiveness" related to its coexistence of liver cirrhosis [166], as we found a direct association with the cirrhotic ECM and the increase in the main EMT related genes.

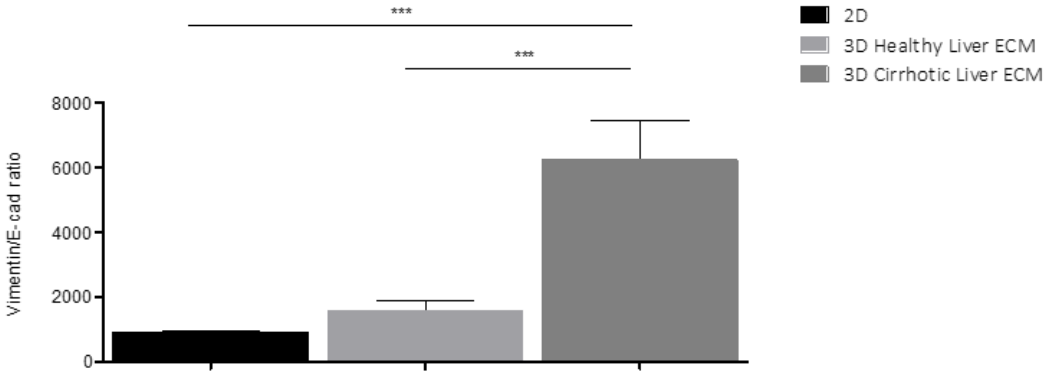

Fig. 38 EMT status of SNU-449 growing in 2D and 3D healthy and cirrhotic 3D liver scaffolds.

*Real-time q-PCR analysis demonstrates a different EMT status between all 3 conditions under investigation. SNU-449 cells cultured in 2D were less mesenchymal by V/E ratio (Vimentin/E-cadherin ratio) in contrast to cells engrafted in cirrhotic 3D scaffolds. Results were normalized to GAPDH mRNA. N=4 scaffolds per condition *** <p < 0,0001*

9.2.3 Sorafenib treatment of human hepatocellular carcinoma cells line SNU-449.

Next, the differences in treatment response to Sorafenib was investigated. Sorafenib (multikinase inhibitor) is the only molecular targeted drug approved for advanced-stage HCC, but unfortunately it provides a survival advantage of only 3 months [167].

Sorafenib concentrations in patients normally range between 6 and 12 µM (pharmacologic concentration) [168]) and different doses were tested first in 2D cultures

(Fig. 39). Next, viability of SNU-449 cells exposed to Sorafenib was investigated in 3D scaffolds and compared to 2D monolayer by using the Annexin/PI staining (Fig. 40).

To determine the IC50 of Sorafenib for these cells growing in different conditions, cells were exposed to different concentrations of Sorafenib, and cell survival was assessed (Fig.40).

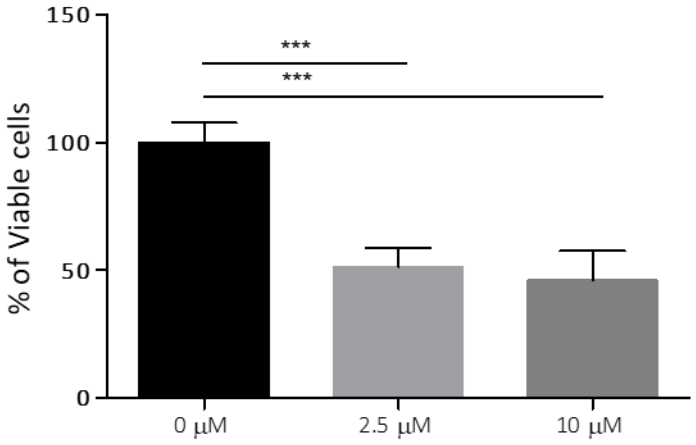

	2D
IC50	5.000

Fig. 39 Effect of Sorafenib on SNU-449 cell viability on 2D.

*Graph showing the percentage of viable cells lines SNU-449 cultured in 2D, IC_{50} were calculated with graph prism. Results are expressed as mean±S.D. ***Represents two-way anova test, p<0.001.*

Differences in Sorafenib IC_{50} were observed in SNU449 cells cultured in cirrhotic 3D scaffolds compared to healthy 3D scaffolds (25 µM vs. 16.9 µM), suggesting that the cirrhotic microenvironment may reduce sensitivity to Sorafenib (Fig.40). Notably, SNU449 cells cultured in 3D scaffolds were more resistant to Sorafenib compared to cells cultured in 2D (Fig.39) where the IC_{50} were 5 µM.

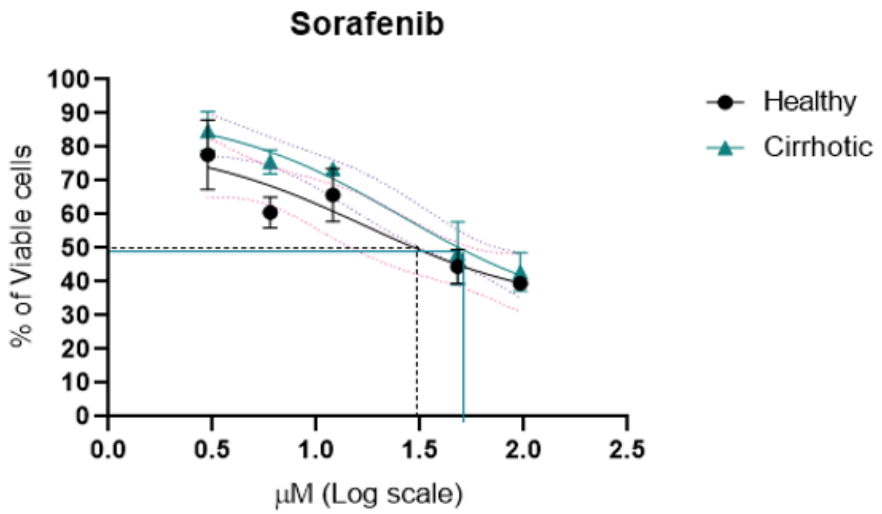

	Healthy	Cirrhotic
IC50	16.93	25.37

Fig. 40 Effect of Sorafenib on SNU-449 cell viability on 3D scaffolds.

Viability assay was performed by flow cytometry on SNU-449 cell line growing on healthy and cirrhotic 3D liver scaffolds after 48 hours of Sorafenib treatment. Graph showing difference in IC_{50} of Sorafenib in cells growing in a different ECM environment.

To examine whether cells undergo apoptosis or necrosis in response to therapy, untreated and Sorafenib-treated SNU-449 cells were stained with Annexin V and sytox blue. Flow cytometry analysis of stained cells can distinguish cells into four groups, namely viable (Annexin V^- $sytox^-$), early apoptosis (Annexin V^+ $sytox^-$), late apoptosis (Annexin V^+ $sytox^+$) and necrotic (Annexin V^- $sytox^+$) cells. As shown in Figure 41, different concentrations of Sorafenib (respectively 17 µM and 25 µM), resulted in a higher population of early apoptotic population (~26.9%) compared to untreated (<2%) in healthy and cirrhotic 3D liver scaffolds reseeded with HCC cell lines.

Our data showed that in the presence of Sorafenib for 2 days, 14% (SNU-449 reseeded in healthy scaffolds) and 10% (SNU-449 reseeded in cirrhotic scaffolds) of cells became apoptotic (Fig.41, panel b and d). However, the pre-apoptotic cells (26 %) in the healthy 3D scaffolds were not detected in the cirrhotic 3D scaffold, which remained at approximately 2%. On the contrary, a higher percentage of necrotic cells were detected in the cirrhotic 3D scaffolds (28.4%) compared to the counterpart in the healthy 3D scaffolds (3.27%).

Detection of different amount of apoptotic and necrotic cells after Sorafenib exposure suggested that the cell death mechanisms triggered by Sorafenib might be different for cancer cells growing in a specific ECM microenvironment.

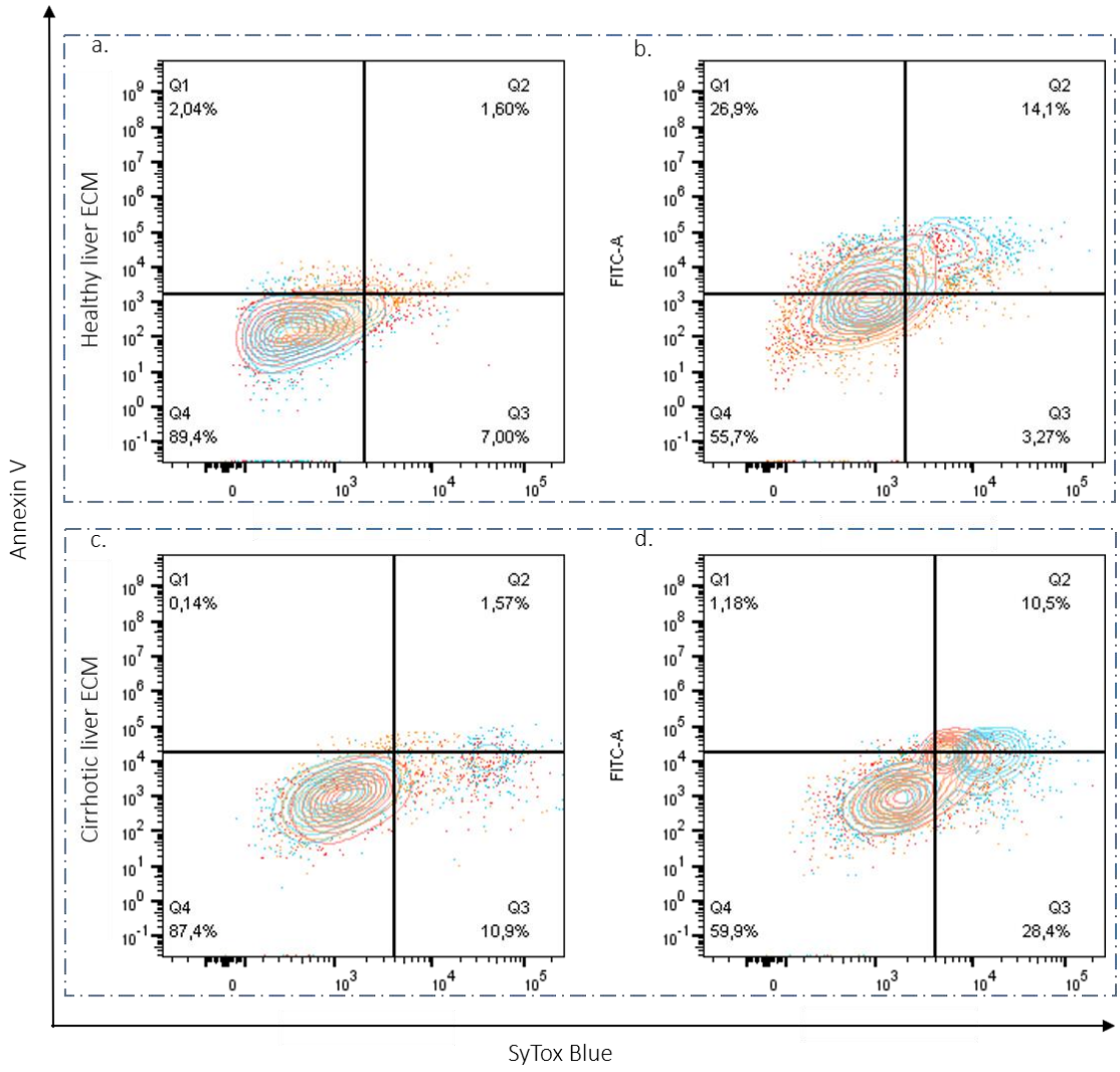

Fig. 41 Sorafenib-induced apoptotic effect on SNU-449 cells after 48 hours of exposure.

Apoptotic (Annexin V FITC+ and SYTOX-) and necrotic cells (Annexin V FITC+ and SYTOX+) were detected by flow cytometry analysis at 48 h following Sorafenib treatment. Results are displayed for SNU-449 cells untreated in (a) healthy and (c) cirrhotic 3D liver scaffolds treated with (b) 17 µM and (d) 25 µM of Sorafenib. Graph shows data of 3 biological replicates and each condition contained 3 scaffolds (n=9). ~5,000 events per condition.

9.3 Co-culture: human HCC cell line SNU-449 with PBMCs in 3D scaffolds

Immune checkpoint inhibitors and CAR-T cell therapies promote T cell-mediated killing of cancer cells, however not all patients benefit from the treatment. A possible explanation for this limitation may be that the tumour microenvironment (TME) is immune privileged, which may exclude cytotoxic T cells from the vicinity of cancer cells[169].

Previous findings (Mazza G et al. unpublished) together with the results described in figure 38 showed that 3D cultures of SNU449 cells in a cirrhotic 3D microenvironment induced a higher EMT phenotype. Therefore, co-cultures including both cancer cells and PBMCs were optimized in both healthy and cirrhotic 3D liver scaffolds and the immune cells status was assessed in those conditions.

9.3.1 Co-culture: HCC cell lines and PBMCs in 3D liver scaffolds

Next, $1^{\wedge}10^{6}$ cells of PBMCs purified from peripheral blood of healthy donors were added to each scaffold previously repopulated with SNU-449 cells for an additional 5 days (as explained in Fig.42). The ratio between cancer cells and immune cells was established as 2:1 effector versus target cell (PBMCs: SNU-449).

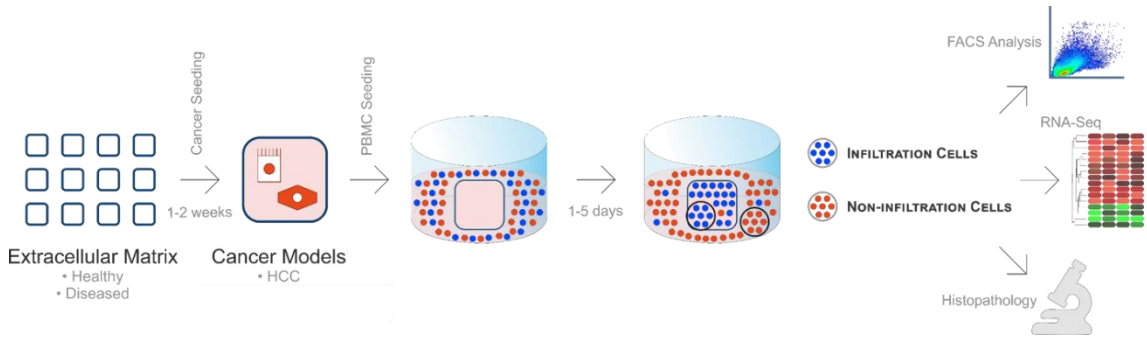

Fig. 42 schematic representation of the experimental protocol for the co-culture.

After the decellularization of scaffolds derived from both healthy and cirrhotic ECM, HCC human cancer cell line (SNU-499) were seeded for 12 days. PBMCs (previously purified from peripheral blood of healthy

donors), were incubated up to 5 days with SNU-499 engrafted 3D scaffolds. The presence of cells infiltrating the 3D scaffolds and the non-infiltrating cells were evaluated with different techniques.

Histological analysis (H&E) showed regions in the healthy 3D scaffolds repopulated with PBMCs ('T cell inflamed' or hotspots). In contrast, PBMCs were not detected in the cirrhotic 3D scaffold i.e. 'immune exclusion' (Fig.43).

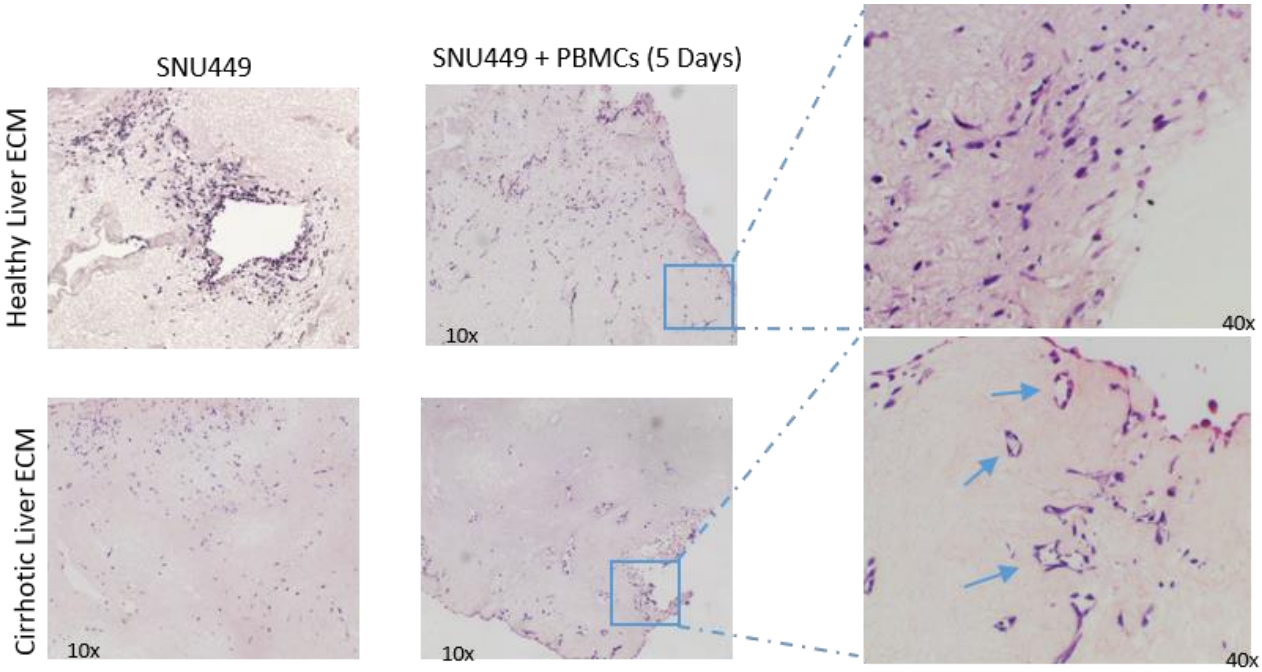

Fig. 43 Morphological changes of SNU-449 cells in single culture and in co-culture with PBMCs growing in healthy and cirrotic 3D liver scaffolds.

Haematoxylin and eosin staining showing the engraftment of SNU-449 cells on the decellularized 3D liver scaffolds showing differences in cell distribution and morphology. Left upper panel SNU-449 cells cultured in a healthy 3D liver scaffold, left bottom panel showing cells engrafted in a cirrhotic 3D liver scaffold after 12 days in culture. Right, Left upper panel: co culture of SNU-449 cells and PBMCs for additional 5 days. Insets show a higher magnification with specific distribution and cell morphology. Magnification 10x (right) and 40x (left).

The mechanisms involved in the immune escape of cancer cells are one of the key missing information in oncology. Indeed, it is still not clear how cancer cells develop specific

escape mechanisms against the immune system by employing inflammatory cells for their own advantage[170]. As already explained in chapter 4.4, one of the key strategies of cancer cells is to inhibit the immune signalling, to enhance the number of immunosuppressive cells and thereby to inhibit immune cells infiltration which in turns it allows for tumour cell proliferation[171].

Moreover, histological analysis of tumour-infiltrating lymphoid cells has been proven to be a reliable and prognostic marker further emphasizing the importance of a classification based on the host immune response using the so called Immunoscore[48].

As mentioned in chapter 4.1.4, tumours can be divided into 'hot' (T cell inflamed) or 'cold' (T cell non-inflamed) according to the presence of immune cells. Hot tumours are characterized by the abundance of tumour infiltrating lymphocytes (TILs) and exhibit an initial immune response that can be dampened by upregulation of immune checkpoints or increased numbers of immunosuppressive cells. In contrast, cold tumours are defined by the absence of TILs, and can be further characterized into the immune-excluded phenotype and the immunologically tolerogenic phenotype [172, 173].

Thus, to confirm the previous observations obtained by H&E staining, CD45 (leukocyte common antigen, LCA) was used for identifying hematopoietic cells. $CD45^+$ positive cells were identified in both healthy and cirrhotic 3D scaffolds when cultured without cancer cells (Fig.44). In contrast, $CD45^+$ cells were detected close to $CD45^-$ cells (cancer cells) when co-cultured in healthy 3D liver scaffolds. Notably, $CD45^+$ cells were not present after 5 days of PBMC co-culture with the cancer cells grown in the cirrhotic 3D scaffolds.

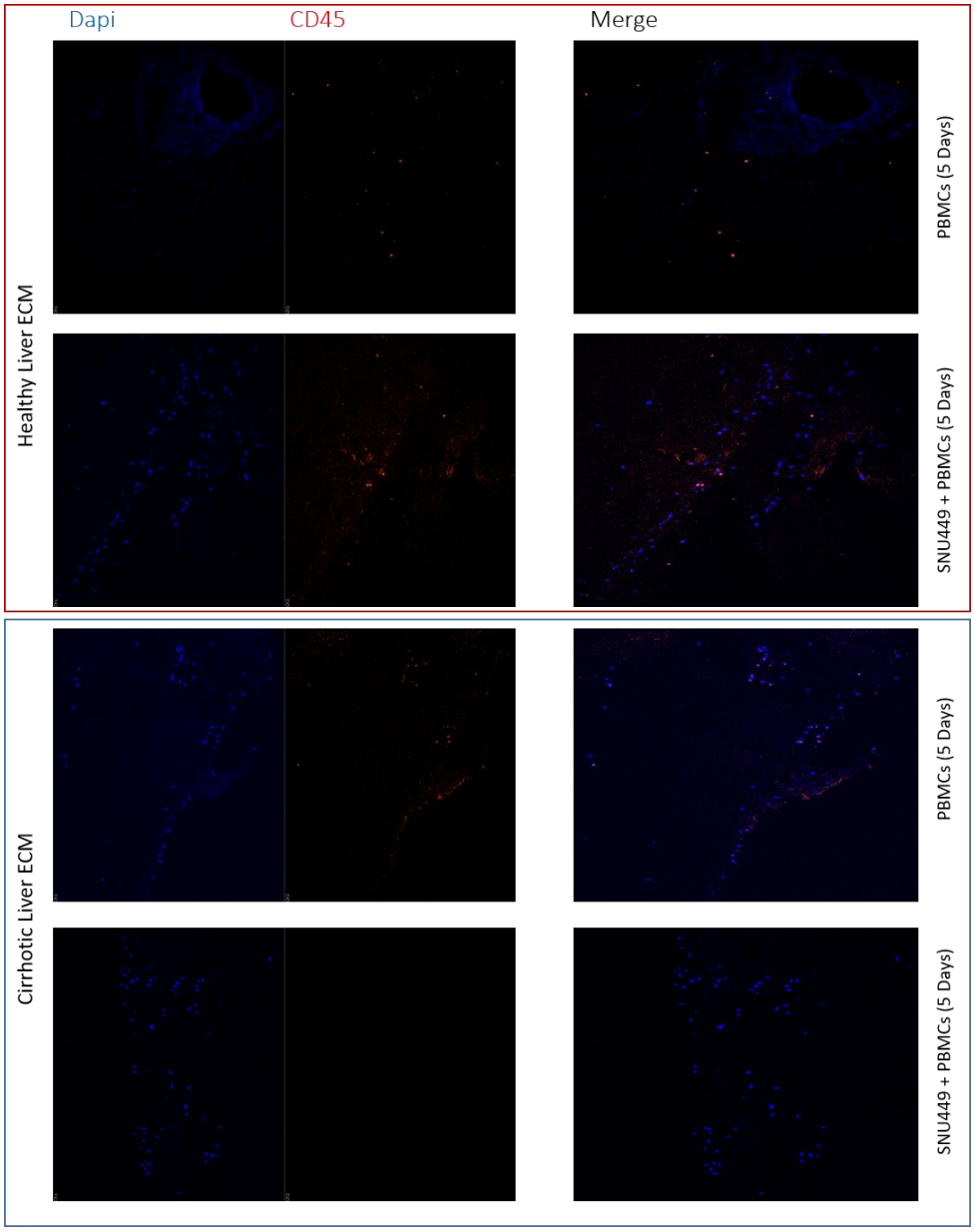

Fig. 44 Immunofluorescence image for PBMCs infiltrating Healthy and Cirrhotic 3D liver scaffolds.

Infiltrating PBMCs were identified as CD45+ cells, Dapi (blue) was used for nuclear counterstain. Representative image showing the presence of infiltrating PBMCs after 5 days in monoculture in healthy and cirrhotic 3D liver scaffolds. Presence of immune infiltrates is confirmed in the co-culture with SNU-449 cells repopulating the healthy 3D scaffolds. In contrast CD45+ cells are absent in the co-culture performed in the cirrhotic 3D scaffold. Yokogawa CQ1 confocal.

Immunofluorescence and H&E staining showed the histological context of the immune cells without determining their viability, lineage and immune cells populations.

Therefore, T cell subsets and the immune checkpoint expression were analysed by FACS analysis to provide additional information about a possible mechanism involved in the exclusion of immune cells from the tumour bed. Indeed, the prognostic importance of the immune cell infiltration is well known for different tumour types. Tumour-infiltrating immune cells are highly relevant for prognosis and identification of immunotherapy targets in hepatocellular carcinoma (HCC) [119].

To further confirm these histological data, the percentage of $CD3^+$ cells were compared in both co-cultures of SNU449 cells with PBMCs in healthy and cirrhotic 3D scaffolds (Fig.45). The infiltrating T cells have been evaluated by flow cytometry, as displayed in the plots in Fig. 45. A distinct population of CD3+ cells was detected in the co-culture performed in healthy 3D scaffolds (represented in red, ~ 40%), while a very small percentage of T cells were detected in the cirrhotic 3D scaffolds (represented in pseudo-green, ~7%). These results suggest that T cells were able to infiltrate only the healthy ECM reseeded with cancer cells and not when exposed to cancer cells reseeded in cirrhotic liver ECM scaffolds.

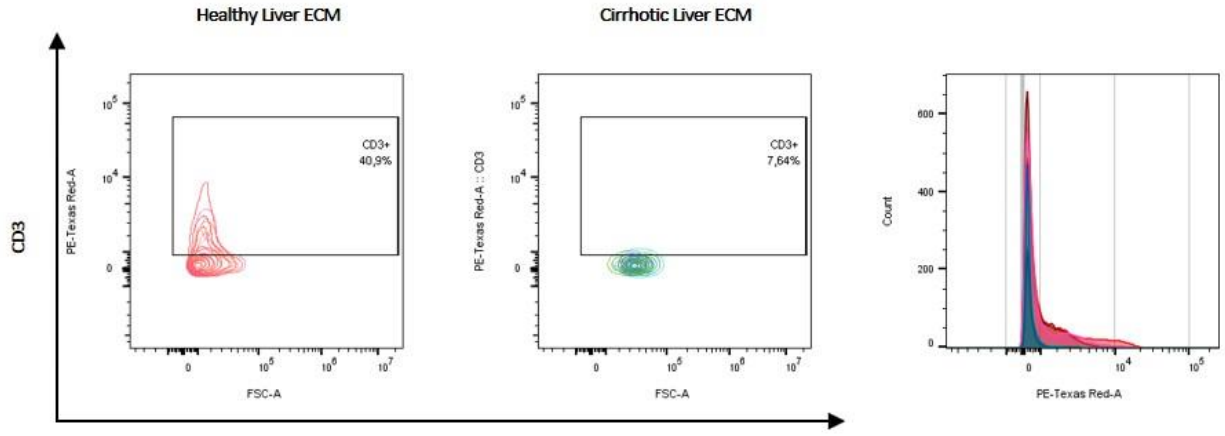

Fig. 45 Flow cytometry of CD3 T cell population of SNU-449 cells co-cultured with PBMCs.

Histogram profiles of PBMCs in co-culture with SNU449 cells, extracted from healthy 3D scaffold (light blue) and from the cirrhotic 3D scaffolds (Violet).

Further characterization of the model was performed in order to depict its resemblance to a “hot” and “cold” human tumour tissue. For this purpose, infiltrated and non-infiltrated cells were further analysed for the presence CD25 and CD107a as markers for activated T cells.

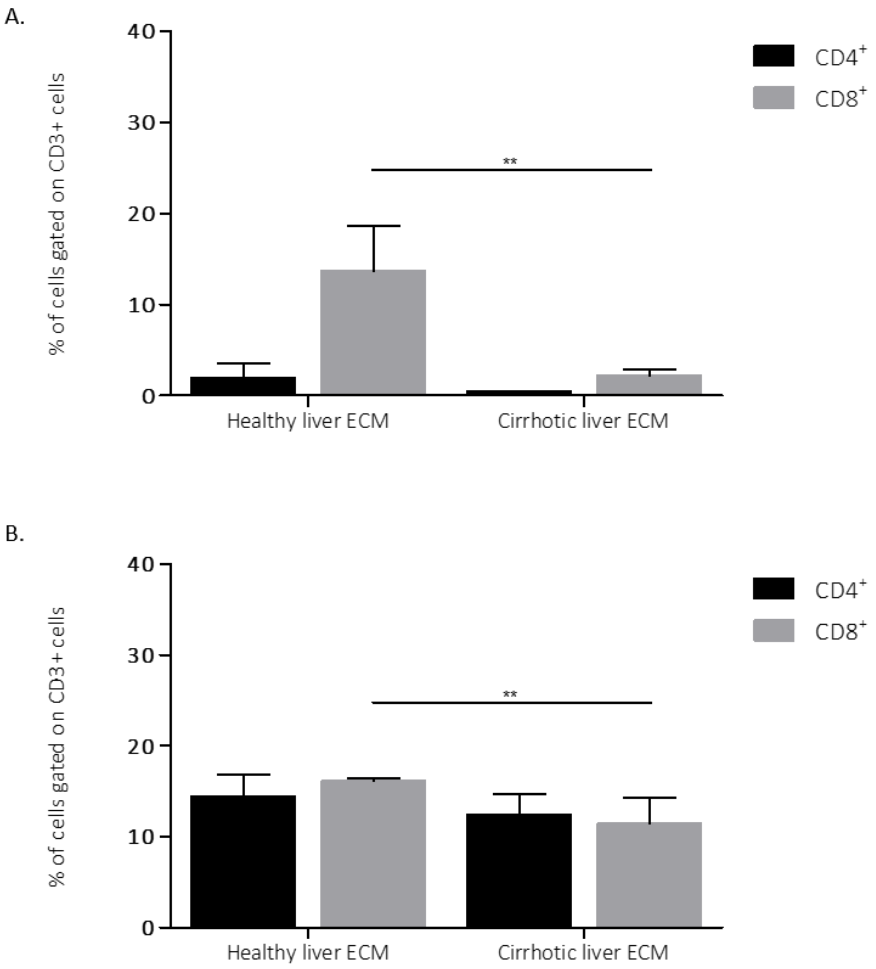

Fig. 46 immunophenotypic analysis of T cell in 3D cancer models.

Immunophenotypic analyses of T cells were performed in CD3+ cells extracted from healthy and cirrhotic 3D scaffolds in co-culture with HCC cancer cell line (SNU-449). (A) Expression of CD4+ CD8+ cells exposed to cancer cells infiltrating the scaffolds and (B) non-infiltrating the tumour tissue. Statistical difference between groups was determined by paired 2-tailed Student t *test. ** <p 0.05. Data are presented as three biological repeats with each 3 scaffolds (n=9).*

Studies show that CD107a (LAMP-1) may be a marker for degranulation of activated CD8+ T cells[174]. In our study, the expression of CD107a as well as CD25, marker for activated T cells, has been determined after exposure of cells in a healthy and cirrhotic 3D scaffolds (Fig.47). CD107a upregulation by infiltrating CD8+ cells it might indicate T-cell reactivity to HCC cell lines. However, the upregulation was less than 2% within the infiltrating population while was not relevant in the non-infiltrating population thus confirming the low amount of activated cytotoxic CD8+ T cells. (Fig47 A, B, grey bars). Similar results were detected for the CD4 infiltrating and non-infiltrating cells, as shown in Fig.47 (C, D) by gating the cells for CD4+ and CD25.

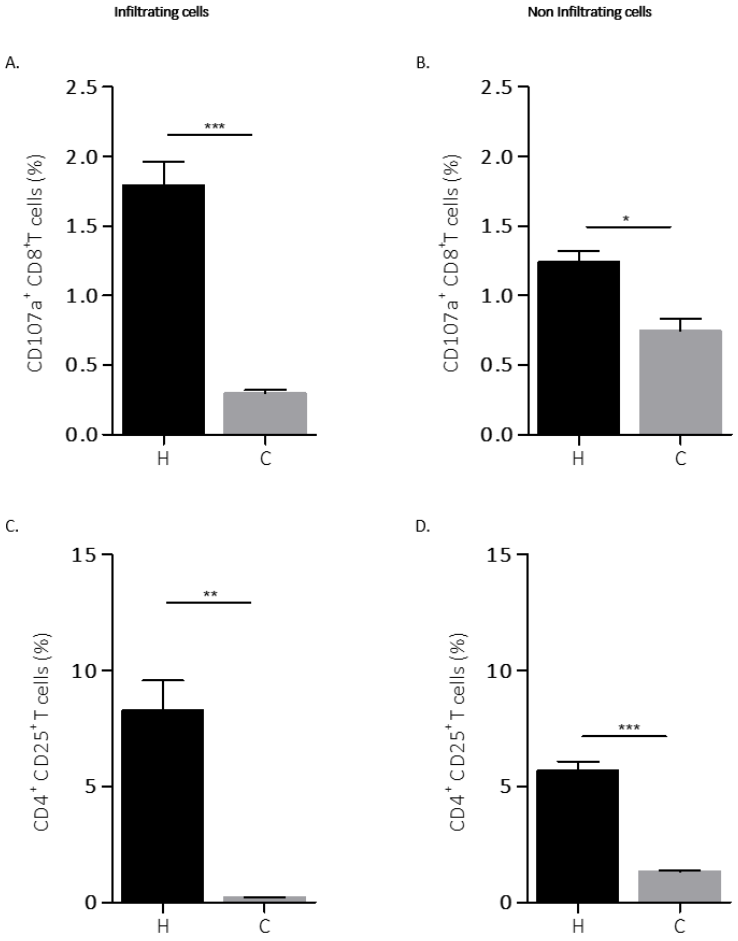

Fig. 47 Immunophenotypic analysis of T cell infiltrating 3D cancer models.

Flow cytometric analysis was performed in CD3+ T cells in healthy (H) and cirrhotic (C) 3D liver scaffolds repopulated with HCC cell line (SNU-449). (A, B) Killing activities were assessed by CD107a staining on CD8+ cells (graph upper panel). (C, D) In the lower panel, graphs showing the percentage of T regulatory cells (CD4+CD25+ cells). For both staining analysis of infiltrating cells was performed on extracted cells (A, C) as

*well as (B, D) non-infiltrating cells. Statistical difference between groups was determined by paired 2-tailed Student t test. Percentages with bars representing the mean of triplicates ± SD, **p< 0, 0033; *** p< 0, 0005.*

Moreover, Cytokeratin expression was employed as a tumour cell marker of SNU449 cells as cytokeratin (Pan-CK) provide to be useful markers for epithelial malignancies, and allows to discriminate between cancer cells and immune cells (that are negative for cytokeratin) (Fig.48).

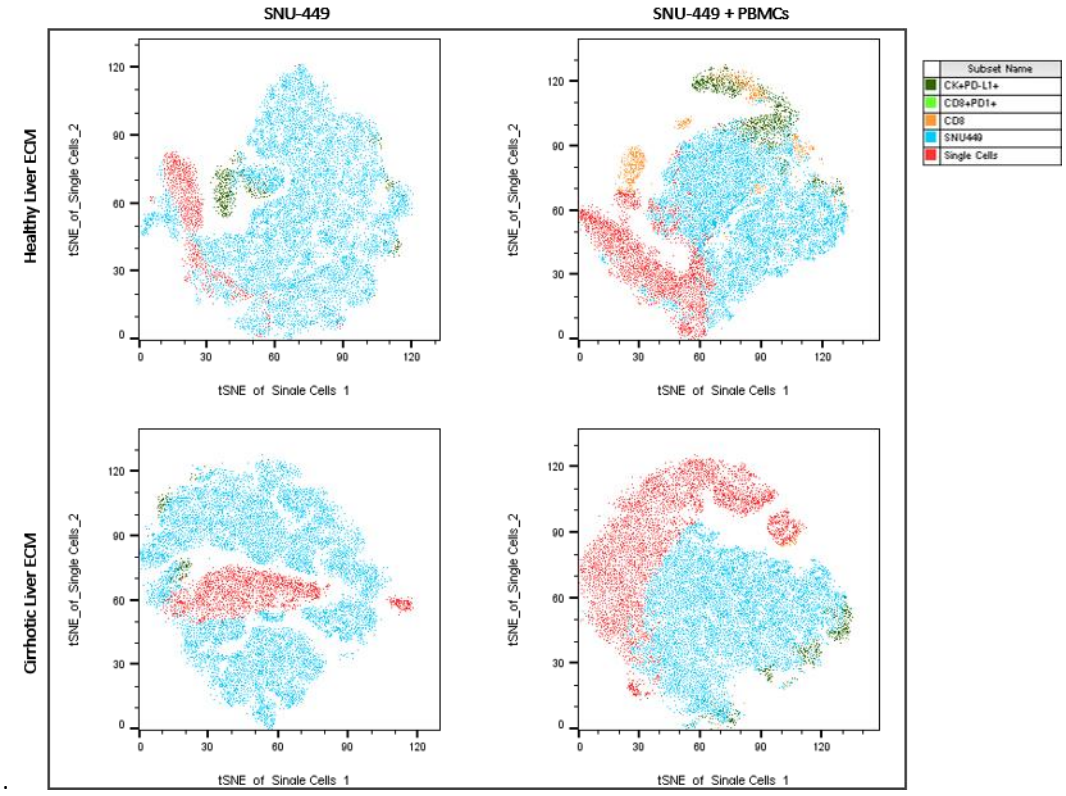

Fig. 48 Distinct phenotypic subset infiltrating the 3D liver scaffolds.

T-SNE plot based on the expression of 5 markers for PBMCS and cancer cells. Representative samples for each condition where each population was overlaid onto the tSNE space in the FlowJo Layout editor, revealing how specific phenotypic subsets of events cluster together. Cell populations are indicated by different colours, in blue HCC cell line SNU-449 marked with a Pan-cytokeratin marker and analysed for the expression of PD-L1 (dark green), in orange $C8^{+}$ cells, in green $CD8^{+}$ population expressing PD-1, in red the cells negative for all 5 markers.

Given that PBMCs infiltration was only detected in healthy liver 3D scaffolds repopulated with the HCC cell line, we then assessed whether PBMCs were able to infiltrate an empty scaffold placed in the close vicinity to a recellularised scaffolds by using SNU-449.

This experiment was performed with both healthy and cirrhotic 3D scaffolds in order to evaluate whether the cancer cells create a physical barrier against immune cells when reseeded into cirrhotic scaffolds or whether cancer cells reseeded in cirrhotic scaffolds modulate immune cells infiltration via paracrine factors. The presence of immune cells was assessed by histology. As shown in Fig. 49, immune cells exposed to healthy 3D scaffold were more attracted towards the cancer cells than to the empty 3D scaffold (Fig.49 indicated with E). Importantly, this effect was not observed when using a cirrhotic 3D scaffold and immune cells were not able to infiltrate the empty cirrhotic scaffolds placed in close vicinity to a recellularised scaffold by using SNU-449 cells

Notably, in the cirrhotic 3D liver scaffolds repopulated with cancer cells and upon exposure to PBMCs, after exposing SNU449 cells reseeded into cirrhotic scaffolds to PBMCs, cancer cells migrated towards the vessels of decellularized cirrhotic scaffolds (cells indicated by the arrows in figure.49).

H&E staining showed also an increased eosinophilia in cancer cells (i.e. indicating apoptosis) and, these cells were located on the external surface of the cirrhotic 3D scaffolds when exposed to PBMCs.

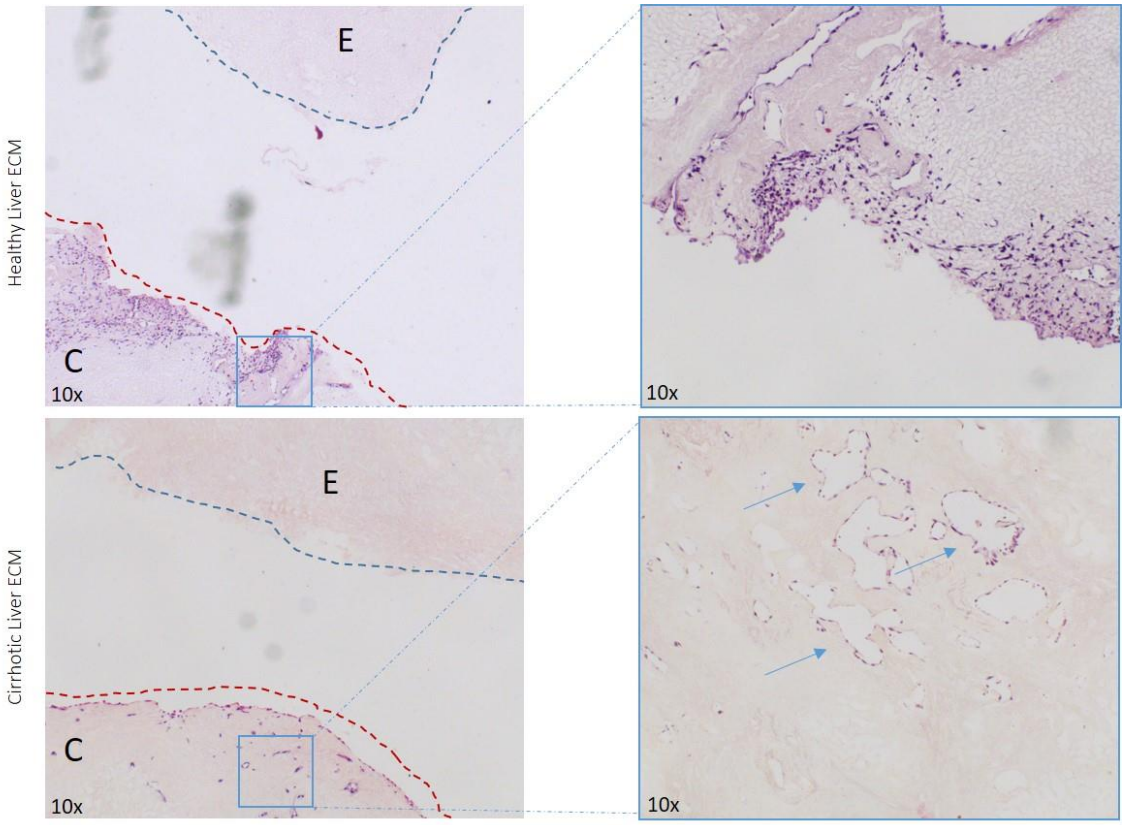

Fig. 49 Morphological changes of SNU-449 cells in co-culture with PBMCs growing in healthy and cirrotic 3D liver scaffolds.

Haematoxylin and eosin staining shows SNU-449 cells cultured in a healthy 3D liver scaffold (indicated in the picture with "C"). Bottom panel SNU-449 cells repopulated a cirrhotic 3D liver scaffold, after 12 days in culture. Co culture was performed exposing at the same time and in the same well PBMCs to a decellularized acellular 3D scaffold (indicated with "E") and a 3D scaffold repopulated with SNU-449 for additional 5 days. Arrows indicating changes in localization of SNU-449 in the cirrhotic 3D scaffold after co-culture. Magnification 10x (right) and 40x (left).

These data suggest that cancer cells find ways to avoid immune cells and to escape immune-mediated killing i.e. immune excluding phenotype. In future experiments, a further assessment of the transcriptomic profile of those new 3D models as well as secretomics could clarify the mechanism(s) behind the immune exclusion phenotype by addressing cell-cell interaction and secreted factors in those different systems.

As highlighted in the previous section, the presence of tumour-infiltrating lymphocytes is used as a prognostic tool for patient survival for many solid tumours. Indeed, low intra-

tumoral T cell infiltration may be a limiting aspect for effective cancer immunotherapy such as checkpoint inhibition. Even if the clinical benefit of checkpoint inhibition in various cancers such as melanoma, non-small cell lung cancer, and renal cell cancer has been demonstrated, only a minority of patients benefit from these treatments. A possible explanation for tumour resistance to checkpoint inhibitors such as anti–PD-1 is the failure of cytotoxic T cells to physically reach the cancer cells at the tumour site.

For these reason in the next set of experiments, the frequencies of PD-L1^{+} cancer cells and the correlation with the presence of PD-1^{+} positive infiltrating CD8 cells was determined (Fig. 50,51).

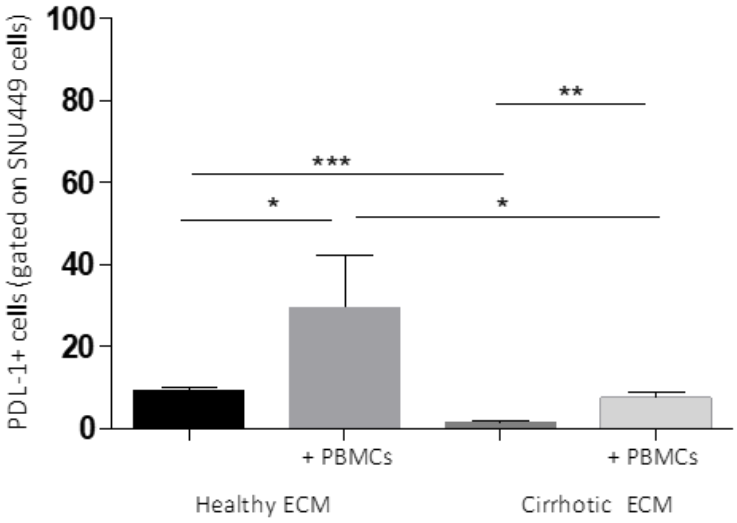

Fig. 50 PD-L1 expression on SNU-449 cancer cells repopulating 3D liver scaffolds.

The surface expression of PD-L1 on SNU-449 cells growing in healthy and cirrhotic 3D liver scaffolds was tested by FACS analysis. Percentage of PD-L1+ cancer cells, in monoculture and co-culture with PBMCs in a healthy or cirrhotic environment, by gating CK positive cells, percentages with bars representing the mean of triplicates ± SD. Statistical difference between groups was determined by paired 2-tailed Student t test * p< 0,02, ** p< 0,0016; *** p< 0,0001

Expression of PD-L1 in the SNU449 cells was assessed by flow cytometry and demonstrated a higher expression in SNU-449 cells growing in healthy 3D liver scaffolds in comparison to cirrhotic 3D scaffolds (Fig. 50). Interestingly, the presence of PBMCs in the co-culture significantly increased the expression of tumour cell surface PD-L1, especially in SNU-449 cells engrafted in healthy 3D scaffolds. This seems to recapitulate

a “hot” tumour phenotype with potential favourable response to therapy Interestingly, PD-L1 expression was statistically significantly lower in reseeded cirrhotic scaffolds compared healthy liver scaffolds and therefore potential novel mechanisms could be involved in the immune exclusion phenotype provided by cancer cells reseeded into cirrhotic scaffolds.

. Next, the percentage of CD8+ cells expressing PD-1 was analysed by FACS in single culture and in co-culture with cancer cells.

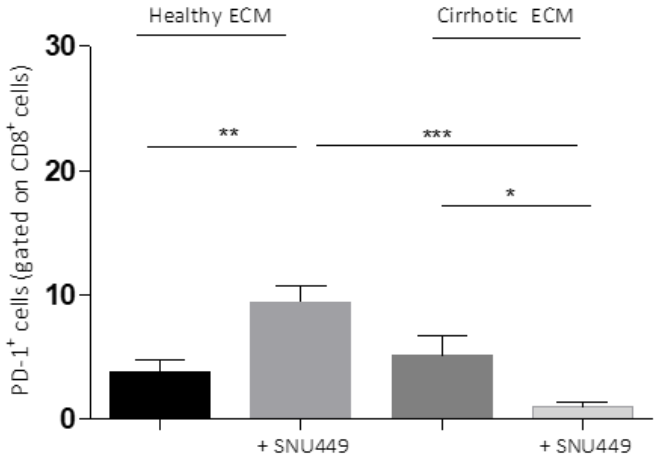

Fig. 51. PD-1 expression on CD8+ cells infiltrating the 3D liver scaffolds.

Graphs on the left show the surface expression of PD-1 on CD8+ cells. Percentage of PD-1+ T cells, in monoculture and co-culture with HCC human cell line SNU-449 in a healthy or cirrhotic environment, by gating CD8+ cells, percentages with error bars representing SD. Statistical difference between groups was determined by paired 2-tailed Student t *test. *** p< 0,0002*

No significant difference in the expression of PD1 was observed between PBMCs cultures in healthy or cirrhotic 3D scaffolds (Fig 51). In contrast, PD-1 expression was statistically significantly up-regulated in CD8+ T cells by SNU-449 cells, compared to CD8+ T cells alone when cultured in a healthy 3D liver scaffold. This up-regulation was not detected in co-culture experiments by employing cirrhotic 3D scaffolds.

Several studies and meta-analysis have shown that PD-L1 expression of cancer cells was associated with a high number of CD8+ PD1+ cells infiltrating the tissue [175, 176]. Based on these premises, a possible correlation between the presence of PD-1 CD8+ cells and

PD-L1 expression on cancer cells reseeded in both healthy (Fig 52 left panel) and cirrhotic (Fig 52 right panel) scaffolds was determined.

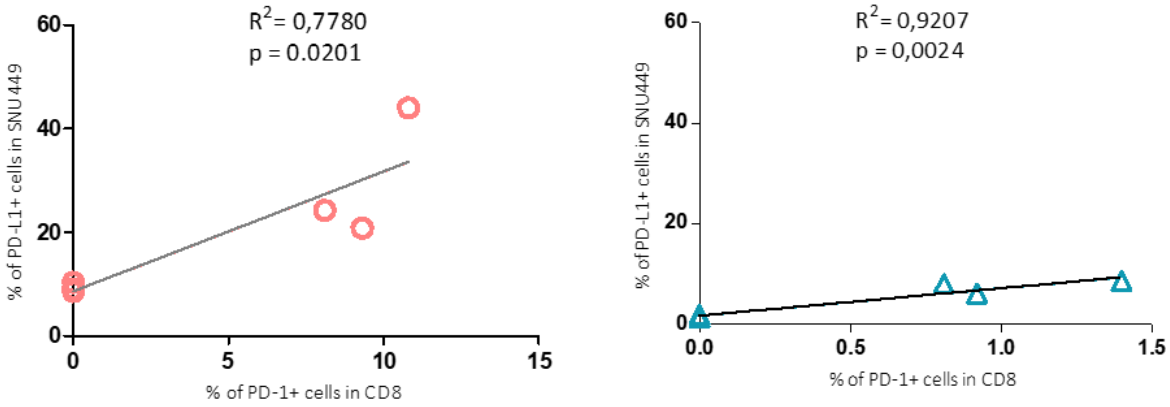

Fig. 52. PD-L1 expression on SNU-449 cells positively correlates with infiltrating CD8⁺ T cells frequencies in healthy ad cirrhotic 3D liver scaffolds.

SNU-449 cells and PBMC co-cultured in healthy (n=6) and cirrhotic 3D scaffolds (n=6) were extracted and stained for PD-L1 and PD-1 markers, cell subsets were analysed by flow cytometry. Correlative analysis of frequencies of SNU-449 cells expressing PD-L1 with $CD8^{+}PD\text{-}1^{+}$ in healthy (red) and cirrhotic (blue) 3D liver scaffolds. Significance testing was carried out using the Pearson correlation coefficient and was deemed significant.

A significant correlation between the absence/presence of $CD8^{+}$ cells and the expression of PD-L1 in response to co-culture with SNU-449 cells was determined (Fig.52). The correlation between the expression of PD-1/PDL-1 and immune cell infiltration is in line with previous studies on HCC patients in which the microenvironment-based immune clusters defined an active or exhausted immune response [177]..

9.3.2 Modulation of PD-1 and PDL-1 expression in 3D co-cultures treated with Sorafenib

To understand whether the expression of PD-L1 by tumour cells was an important factor affecting the response to treatment in a healthy or cirrhotic ECM environment, we then analysed the expression of PD-L1after Sorafenib treatment.

Sorafenib (already describe in section 4.1.1) is an antiangiogenic tyrosine multikinase, mainly targeting RAF and VEGFR. Several studies have suggested that Sorafenib may also differentially affect immune cells, although it is not known whether it can have an impact on immune modulation [178]. Remarkably, the upregulation of PD-L1 in HCC cells upon exposure to, or in resistance to Sorafenib, has been recently reported in HCC mouse model [179].

To understand PD-L1 expression patterns in tumour cells and tumour-infiltrating immune cells in HCC 3D ECM models after Sorafenib treatment, the following conditions were analysed: pre- and post-Sorafenib treated SNU-449 cells in 3D liver scaffolds (healthy and cirrhotic) with or without the immune cells by using flow cytometry.

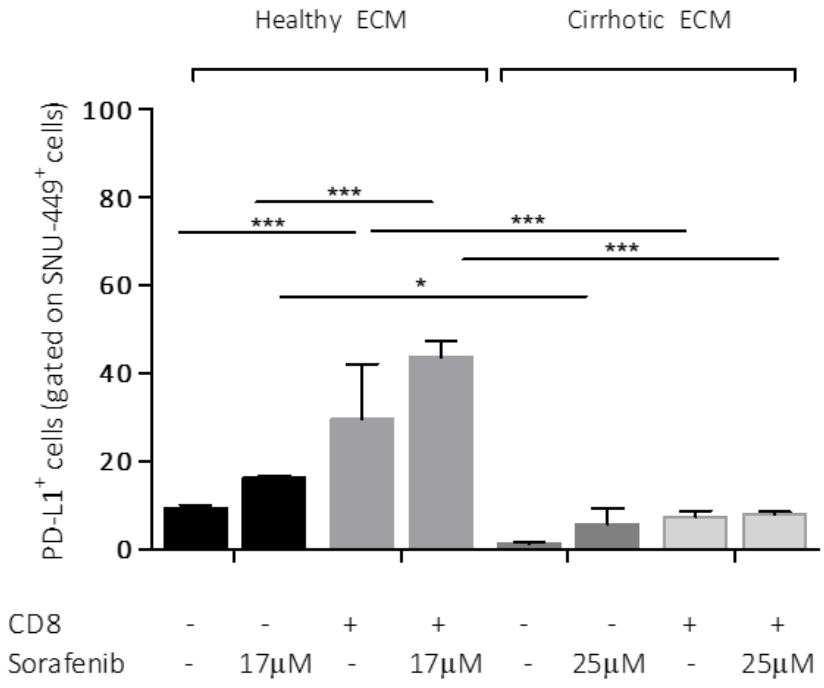

Fig. 53 Differential expression of PD-L1 in HCC cancer cell line SNU-449 engrafted in healthy and cirrhotic 3D scaffolds, in single culture and co-culture with PBMCs before and after Sorafenib treatment.

Immunophenotypic analyses of the immune inhibitory receptor ligand PD-L1 were performed in SNU-449 cells extracted from healthy and cirrhotic 3D scaffolds. Expression of PD-L1 in HCC cells exposed to PBMCs compared with mono culture of cancer cells (black and dark grey bars for monoculture growing in healthy

and cirrhotic 3D scaffolds with or without Sorafenib treatment. All compared w/o Sorafenib treatment (48h). Statistical significance between groups was determined by paired 2-tailed Student t*. * p< 0,05, *** p< 0,001*

The PDL-1 expression was not significantly different between pre- and post-Sorafenib exposure in SNU449 cells engrafted in healthy and cirrhotic 3D scaffolds.

However, PD-L1 expression in HCC cells in co-culture with PBMCs was significantly higher in post-Sorafenib treated cells than in pre-Sorafenib treatment for cells cultured in the 3D healthy liver scaffolds compared to cirrhotic 3D ECM. No difference in PDL1 expression was observed in SNU-449 cells reseeded into cirrhotic 3D liver scaffolds with or without PMBCs in the presence or not of Sorafenib (Fig.54).

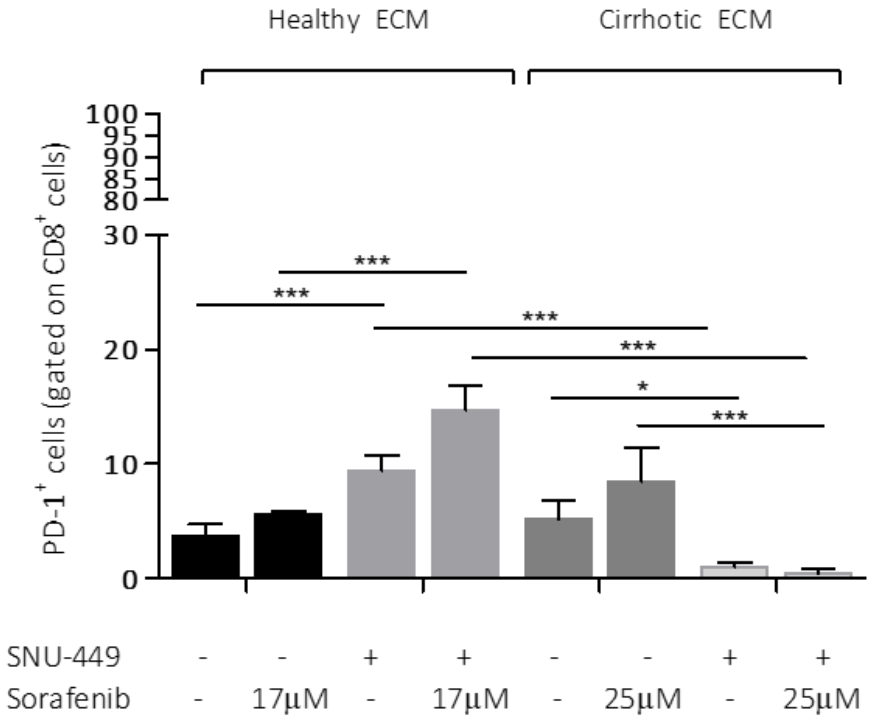

Fig. 54 Differential expression of PD-1 in CD8+ infiltrating the 3D scaffolds, in single culture and co-cultured with cancer cells before and after Sorafenib treatment.

Immunophenotypic analyses of the immune receptor ligand PD-1 were performed in CD8 T cells extracted from healthy and cirrhotic 3D scaffolds. Expression of PD-1 in PBMCs after exposure of HCC cells compared with monoculture of cancer cells (black and dark grey bars for monoculture growing in healthy and cirrhotic 3D scaffolds with or without Sorafenib treatment). All compared w/o Sorafenib treatment (48h). Statistical significance between groups was determined by paired 2-tailed Student t*. * p< 0, 05, *** p< 0,001*

All of the above presented data underline the important implication of the cirrhotic microenvironment in priming a tumour characterized by the absence of T cells ("cold tumour"). Considering all the advantages made in the cancer immunotherapy field during last years, the treatment of a cold tumour is still one of the main therapeutic challenge[180]. However, as discussed in section 3.4.1, many therapeutic approaches are currently under investigation to revert this unfavourable context. The model herein described could help in understanding the mechanisms involved in the immune exclusion of T cells, which is crucial for the development of effective treatments for aggressive tumours. Therefore, more analyses are still needed in order dissect the role of cirrhotic ECM microenvironment in modulating cancer cell phenotype which in turns affect immune cells infiltration. Among all possible reasons for the immune-privileged tumour microenvironment that is presented in this thesis by employing cirrhotic liver 3D scaffolds, it is hypothesized that the T cell exclusion may be due to the production of soluble mediators or cell-surface mediators expressed by the aggressive SNU-449 cancer cells.

9.3.3 Conclusions

This chapter provides more insights in the optimization of healthy and diseased ECM microenvironment-based models to be proposed as a potential new tool for exploring and better understanding immune cell involvement in HCC progression. The herein described 3D HCC model will allow to study and dissect in more details the role of ECM in modulating cancer cell aggressiveness, the role of immune cells in modulating HCC phenotype and the effect of aggressive HCC phenotype in driving immune exclusion. In addition, the 3D ECM platform represents a more suitable and physiological system to screen mono or combinational therapies in HCC.

This work provides compelling technical evidence on the possibility of generating “hot” and “cold” tumours in vitro by reseeding HCC cells into 3D healthy and cirrhotic human liver ECM, respectively. The system represents a more realistic immune oncology model to investigate the relationship between ECM and immune cells in HCC and it might ultimately lead to more effective treatment strategies.

9.4 Modelling the liver metastasis immune microenvironment using three-dimensional human liver extracellular matrix scaffolds.

9.4.1 Introduction

Liver metastases are common in many types of cancer, including tumors derived from the gastrointestinal tract, breast, lung, and pancreas [181].

Two main mechanisms have been proposed to justify the high incident of liver metastases. Firstly, the hepatic circulation plays a key role in this because the blood supply from the portal and systemic circulation increases the chance of metastatic spread in the liver. Secondly, the anatomy of the liver sinusoid and the presence of endothelial fenestrations makes easier the extravasation and invasion of metastatic cells into the liver parenchyma[182].

The development of therapeutic drugs (including immune oncology therapies) against metastatic tumour has been limited by the lack of preclinical models that recapitulates the metastatic microenvironment. Since the majority of pancreatic cancer cells metastasize to the liver and the immune system has impaired function to overcome tumour growth, a co-culture system was developed that mimics the liver metastatic microenvironment using tissue-specific human ECM liver scaffolds reseeded with PK-1 and PBMC. PK-1 cells are a human pancreatic cancer cell line isolated from liver metastasis of pancreatic cancer[183]. Previous findings have shown the capability of human liver ECM in priming a metastatic phenotype in PK-1 cells compared to the same cells reseeded into pancreatic ECM scaffolds (Al-Akkad W. et al., unpublished). Next, the response of metastatic cancer cells to immunotherapy (Bispecific T Cell Engager approach) was investigated in 2D and 3D cultures. This study was in collaboration with Professor Nathwani (UCL Institute of Immunity & Transplantation) which kindly provided the treatment compound. Notably, cancer cells reseeded in their original ECM

microenvironment showed a higher resistance toward therapies compared to 2D cultures, thus recapitulating limited therapeutic response in patients with liver metastasis.

9.4.2 Recreating a metastatic microenvironment

In order to mimic a metastatic liver microenvironment from a pancreatic origin, PK1 and PBMCs cells were co-cultured within healthy 3D liver ECM scaffolds.

First, the capability of PK-1 cells to engraft in the 3D liver scaffolds was assessed. The in vitro experiment was performed by reseeding the decellularized healthy 3D scaffold with $0.5\text{^}10^6$ Pk1 cells/scaffold and cultured for 12 days.

H&E staining was used to analyse cell integrity and morphology and showed that PK-1 engrafted the 3D scaffolds over 12 days. Immunohistochemistry for Ki67 confirmed the presence of proliferating cancer cells within the healthy ECM scaffolds after 12 days of in vitro culture and therefore this time point was selected for further experiments. (Fig.56).

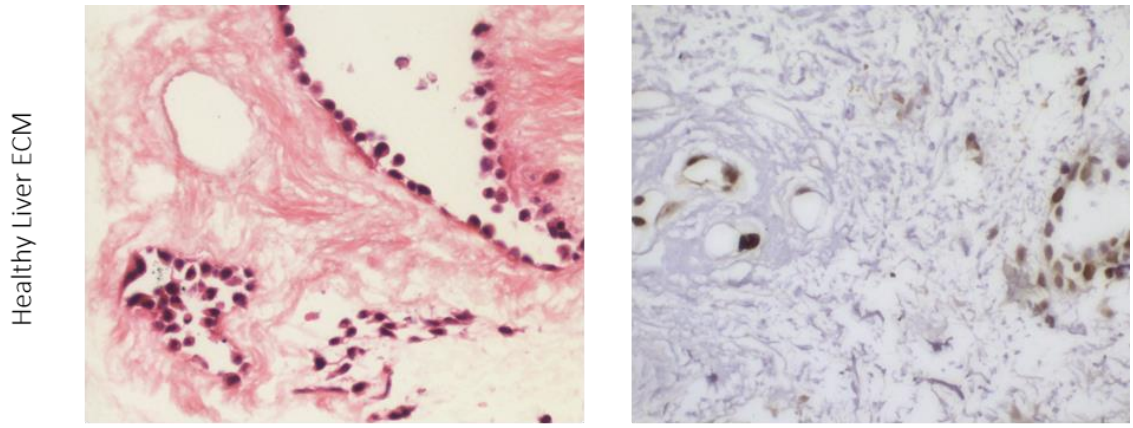

Fig. 55. Section of healthy 3D liver scaffolds repopulated with the metastatic cell line PK-1.

Haematoxylin and eosin staining shows PK-1 cells engrafting the 3D liver scaffolds. Cells migrated and attached preferentially to vessels after 12 days in culture. On the right, Formalin-fixed, paraffin-embedded PK1 cells in 3D liver scaffolds stained to detect Ki-67 as nuclear staining of proliferating cells (brown).

The focus of the work described in this chapter was to establish a 3D metastatic tumour model for studying infiltration of T cells and response to treatment. To study T cell infiltration, PBMCs were added to the 3D liver scaffolds engrafted with PK-1 cell line for 5 days.

The ratio of PBMCs and PK-1 in co-cultures was 2:1. Even if most of the studies that involve co-cultures of PBMCs with cancer cells used the ratio of 10:1 [184], a ratio of 2:1 was preferred as this would be more realistic to seek interactions between PK-1 and peripheral immune cells. As control, cultures monocultures of the metastatic cell line (PK-1) and PBMCs were used. After 5 days of co-culture, the infiltration of PBMCs in the 3D scaffold repopulated with the metastatic cell line PK-1 was assessed.

Haematoxylin and eosin staining demonstrated that PK-1 morphology was not affected by co-culture with T lymphocytes (Fig.57 indicated by arrows).

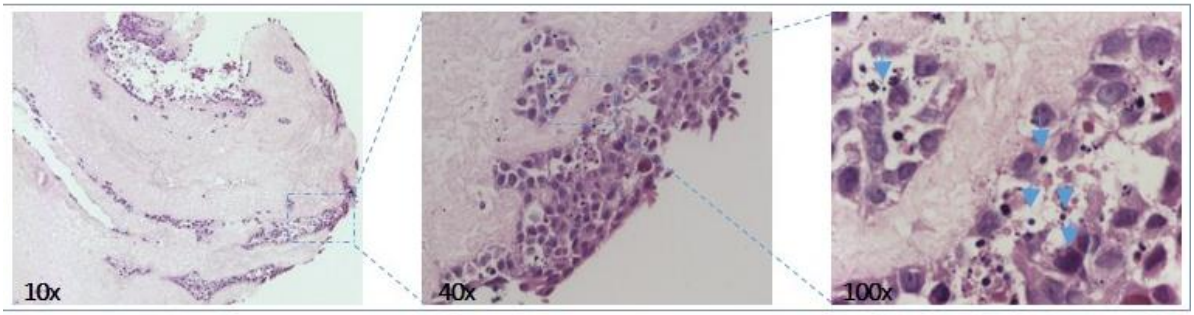

Fig. 56 Immune cells are detectable within the healthy 3D liver scaffolds repopulated with metastatic cell line.

Localization of immune cells and metastatic cell line PK-1 by H&E on paraffin-embedded in 3D liver scaffolds sections. Magnification: ×10 (A) or ×40 (B) and x100 (C). Arrows are indicating immune cells infiltrating the tissue after 5 days of co-culture.

Interestingly, immune cells infiltrating the metastatic tumour were observed by H&E staining and for this reason, immunofluorescence was used to further characterize the cellular composition in the engineered healthy 3D scaffolds by assessing the expression of $CD8^+$ cells for immune cells and tubulin for cancer cells (Fig.58).

These data showed that $CD8^+$ T cells localise in close proximity to cancer cells and they do not spread through the empty areas within the ECM tissue (Fig.59, Z-stack reconstruction).

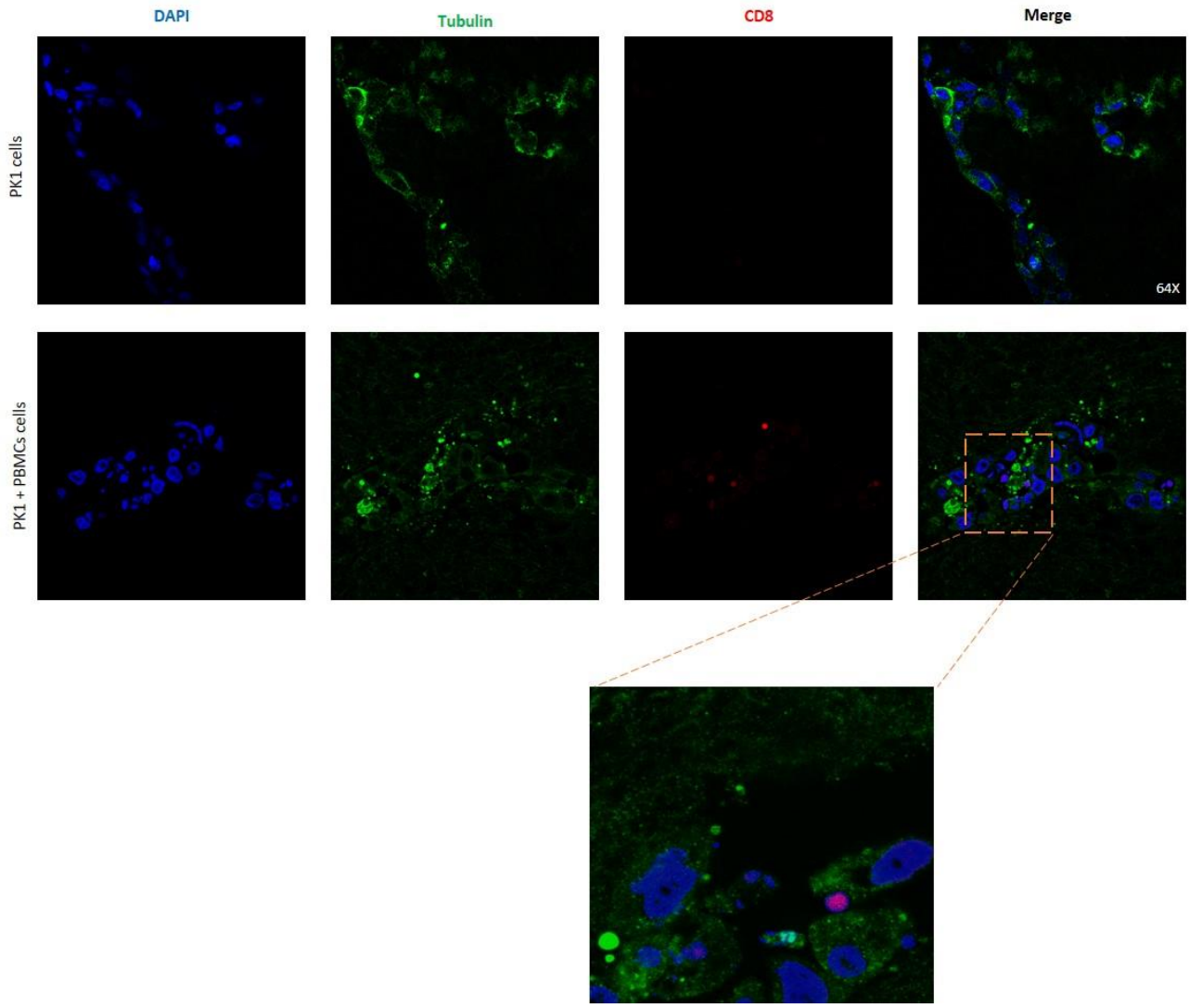

Fig. 57 . Immunofluorescent analysis was performed on 3D liver scaffolds repopulated with PK-1 (12 days) and cultured with PBMCs for additional 5 days.

Tubulin (green) was used for staining of PK-1 microtubules, DAPI was used to identify the nuclei (blue), and CD8 antibody (red) to identify cytotoxic T cells. Magnification 64X

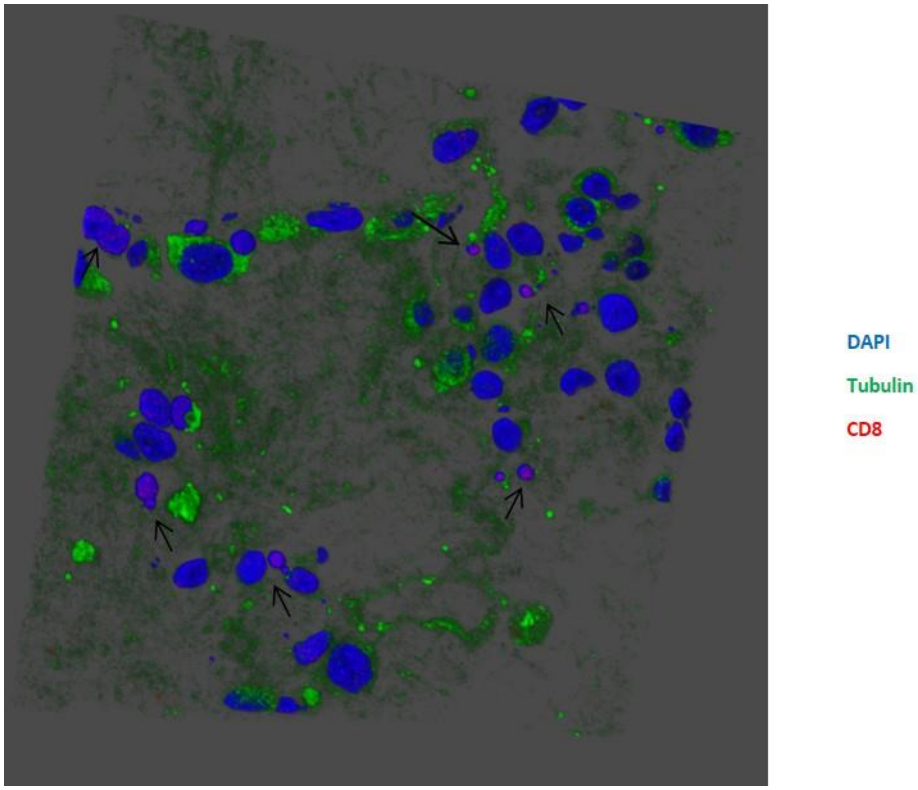

Fig. 58. Confocal Z-stack of Healthy 3D liver scaffolds repopulated with PK-1 cells and PBMCs.

Images of the middle section of the scaffold were taken as 0.5 µm slices and this to analyse the distribution of both cell types in the co-culture system without any stimulus. Images were then used to generate the 3D composite images shown with the ImageJ. Blue: all nuclei (DAPI), red: CD8⁺cells, green: Tubulin.

Next, the immunophenotype of cells infiltrating the 3D liver scaffolds repopulated with PK-1 and in the same conditions in 2D was assessed by flow cytometry. Analysis of $CD4^+$ and $CD8^+$ cells was performed for both 2D and 3D cultures and showed significant reduction in $CD4^+$ cells in 3D accompanied by an increase in the percentage of $CD8^+$ cells. Interestingly, this trend was opposite in 2D culture (Fig.60).

This further confirms the previous data obtained in the HCC 3D model (Section 7.3.1) where a tendency of CD8 to infiltrate the ECM was observed in comparison to the CD4 cells.

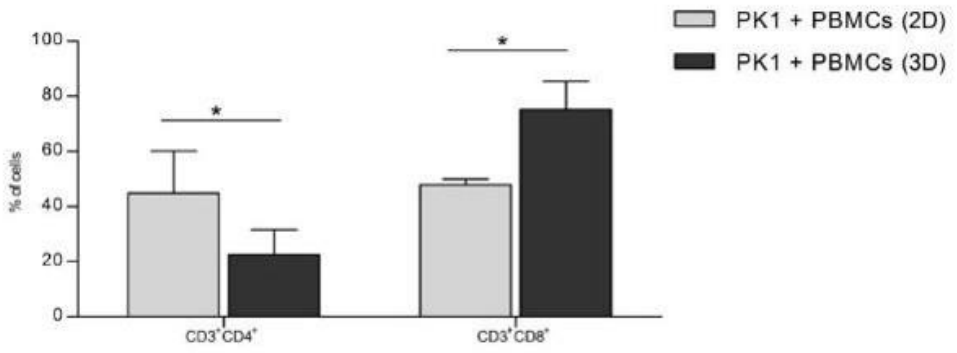

Fig. 59. Percentage of T cell subpopulations in 2D compared to 3D metastatic cancer model.

T cell subsets were assessed by multi-parametric flow cytometry from peripheral blood of healthy donors in co-culture for 5 days in a 2D system with PK-1 cells and in healthy 3D scaffolds repopulated with PK-1. Briefly, the gating strategy was as followed: T helper cells: $CD3^+CD4^+$ and cytotoxic T cells: $CD3^+CD8^+$. Bars represent the pooled data (mean±standard deviation). Statistical difference between groups was determined by Student t *test.*

Therefore, the ratio between CD4/CD8 in the 3D metastatic model is significantly lower compared to the 2D (Fig.61). It is possible that PBMCs retained their starting phenotype in 2D culture and the cells maintain the same ratio identified in the peripheral blood. In contrast, the same peripheral cells behave differently in the 3D ECM environment when in contact with cancer cells by acquiring a more immune-cancer phenotype. Indeed, the ratio in the 3D ECM model is unbalanced by the presence of a high percentage of $CD8^+$ cells able to infiltrate and reach the cancer cells growing within the liver 3D liver scaffold.

Along these lines, it has been shown that the $CD4^{+/}CD8^+$ ratio in the solid cancer is accompanied by increased frequency of $CD8^+$ T cells infiltrating the tumour[185, 186].

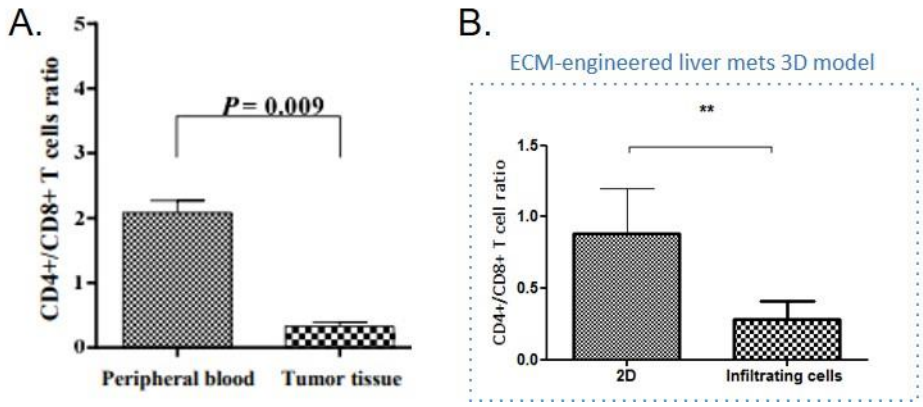

Fig. 60. CD4/CD8 comparison of human cancer and 3D metastatic cancer model.

A) Representative graph of human breast cancer showing the changes in T cells ratio between peripheral blood and the tumour tissue [187].B) $CD4^+/CD8^+$ ratio at Day 5. Determined by flow cytometric analysis of T cells extracted from the 3D scaffolds repopulated with PK-1 cells and PBMCs. The same condition was performed in 2D. Data are shown as mean± SD. Student's t test was used to analyse significance.

9.4.3 T-cell-based cancer immunotherapy: BiTe treatment in 3D scaffolds.

The immune microenvironment in secondary liver cancer is characterized by immunosuppressive features [188] and therefore several therapeutic approaches are undergoing to overcome this problem.

Among others, tissue specific T cell engager represent one of the most advanced field of research for restoring the appropriate immune response against tumour cells by bringing and activating tumour cells close to the cancer cells. Bispecific T-cell Engagers (BiTEs) are bispecific antibodies that are specific for CD3 (expressed on T cells) on one arm and a tumour antigen on the second. As such, BiTEs functions by recruiting and activating T-cells at tumour sites without the conventional co-stimulation or MHC recognition[189].

The use of BiTe in therapeutic settings has demonstrated remarkable anti-tumour activity in patients with blood malignancies but still without clear clinical improvements shown in solid tumours. Therefore, the work described in this chapter relates to evaluate the

capability of these therapies within a physiological tumour models using 3D ECM scaffolds.

Previous work from our collaborators in the Prof. Natwani's group demonstrated the efficiency of BiTe in killing a range of solid tumour cell lines. The collaborators have developed a humanized Bi-specific T cell engager targeting the surface antigen receptor-tyrosine-kinase like orphan receptor 1 (ROR1)[190]. This receptor has been shown to be overexpressed and associated with poor prognosis in several tumours [191]. Briefly, ROR-1 BiTe is composed of a humanized anti-ROR1 single-chain antibody and a human CD3-specific single-chain antibody.

First, the expression of ROR-1 in PK-1 cells was confirmed by flow cytometry (Fig.62). Figure 62 demonstrates the positivity of metastatic cells to the RoR-1 antibody.

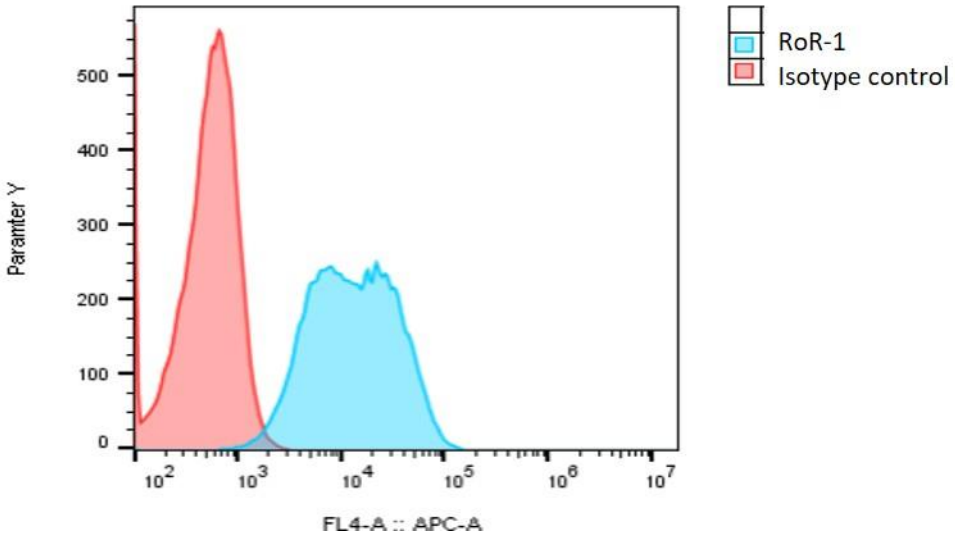

Fig. 61. Measurement of the amount of ROR-1 antigen by flow cytometry.

An anti-ROR-1 antibody was used to detect the expression levels of ROR-1 in PK-1 cells. Representative histogram plot showing surface expression of ROR-1 on PK-1 compared to the matched isotype controls. PK-1 cells expressed ROR-1 at medium levels.

In order to assess the therapeutic potential of ROR1 BiTe, T cells were purified from PBMCs of healthy donors, sorted for CD3+ cells and expanded in vitro. Freshly isolated T cells were expanded using or 200 IU/mL of IL-2, and kept in culture for between 24 h and 1 week before co-culture. The ratio of T cells and PK-1 in co-cultures was 2:1.

The outline of the co-culture procedure is described in Fig.63 and include the flowing steps: PK-1 cells were cultured into the 3D scaffolds for 11 days prior to the start of the co-culture with T cells to allow cancer cells engraftment. PK-1 cells were reseeded in 2D two days before adding T cells to let cancer cells adhere to the plastic. Before performing co-cultures, the number of cancer cells growing in 3D liver scaffolds was tested in order to estimate the number of T cells for co-culture experiments for maintain the same ratio effector cells: target cells compared to 2D cultures. A total of 500,000 cancer cells were counted after 11 days of culture in 3D and therefore 1 million of T cells were added in the 3D ECM co-culture experiment (2:1 effector: target cells).

At day 12, different conditions were tested as follows: BiTe treatment, PD-1 inhibitor, the combination of these treatment or no treatment (daily treatment). Every 24h, for 3 days, 1ml of medium was centrifuged, the pellet was resuspended with fresh medium with or without treatment (Fig. 63).

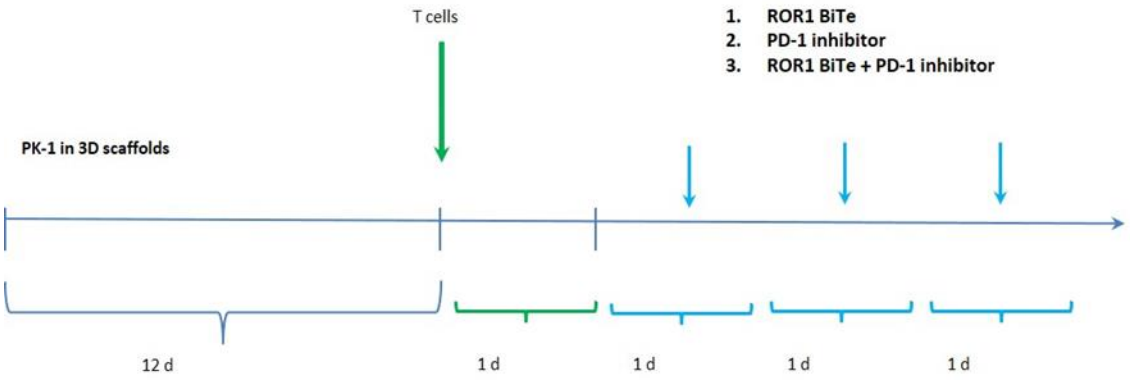

Fig. 62. Outline of 3D experiment.

Representation of the 3D in vitro culture conditions for PK-1 cells in co-culture with T cells. From day 0 to day 11, PK-1 cells were cultured in normal growth medium. T cells were added at day 11. ROR1 BiTe (final concentration 1µM), PD-1 inhibitor (final concentration 1µM) and their combination was then added to the media at day 12 for 72 hours repeated every 24 hours. The control group (A) was cultured in normal media and no BiTe or inhibitor was added.

The percentage of T cells subpopulation ($CD4^+$ and $CD8^+$) were analysed by flow cytometry to determine if blood T cell subpopulations cultured in a 3D scaffold could reflect the typical immune ratio observed in tumours.

Indeed, results showed a higher frequency of $CD4^+$ T cells in the supernatants compared to the $CD4^+$ cells infiltrating the tumour. Thus, reflecting the incapacity of $CD4^+$ T cells to reach the tumour (Fig.64).

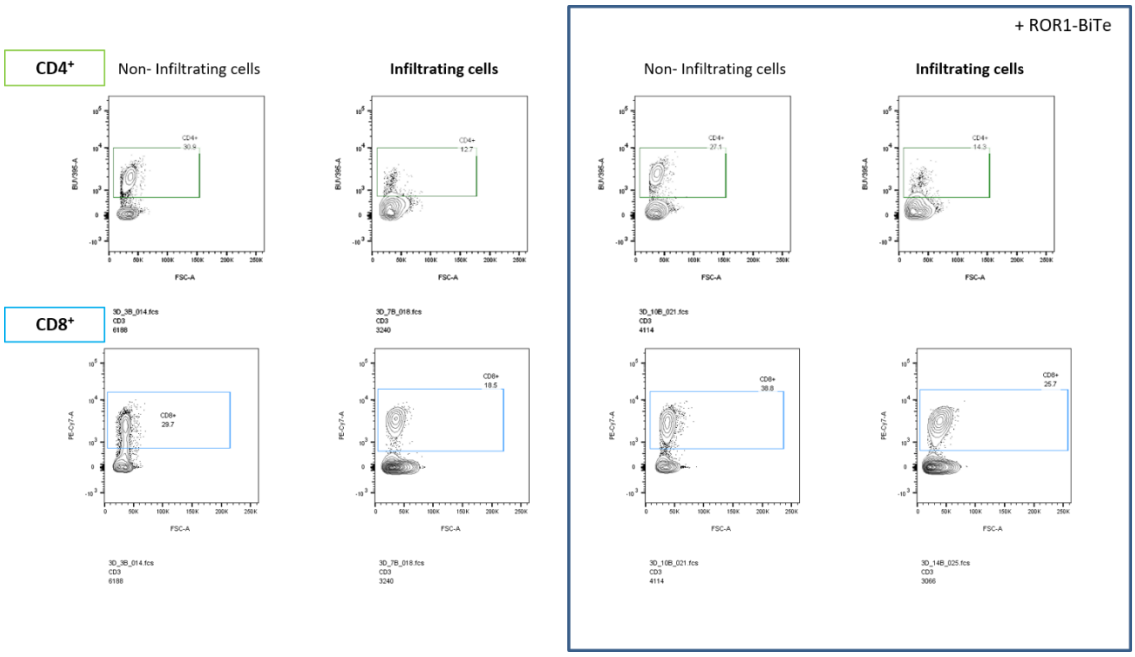

Fig. 63 T cell subpopulations in 3D liver scaffolds repopulated with PK-1 human metastatic cell line before and after treatment (ROR-1 BiTe)

T cell subsets were assessed by multi-parametric flow cytometry T cells in culture for 24 hours in 3D liver scaffolds repopulated with Pk-1 cells. Briefly, the gating strategy was as follows: T helper cells: $CD3^+CD4$ (upper panel) and cytotoxic T cells: $CD3^+CD8^+$ (bottom panel). In the blue panel (right) conditions 24 hours after ROR-1 BiTe treatment.

These results are aligned with all previous experiments described in this thesis showing that the percentages of CD4 and CD8 T is modulated by the 3D ECM scaffolds reseeded with cancer cells.

Next, the effect of BiTe treatment was assessed in all experimental conditions. Histochemical analysis of 3D liver scaffolds repopulated with PK-1 cells and co-cultured with T cells was performed and in parallel light microscopic pictures were taken of the respective 2D culture. The effect ROR1 BiTe treatment in PK-1 cultured in 2D demonstrated a cell cytotoxicity after 24h (Fig. 65). In contrast, histological examination of treated and untreated 3D scaffolds demonstrated infiltration of T cells within the tumour aggregates during all experimental time points (Fig. 66). However, based on histological findings, cancer cells were still viable after 24h treatment in 3D liver ECM scaffolds. After 72h treatment it was possible to appreciate some cellular death in PK-1 reseeded into3D scaffolds (Fig.66)

A clear reduction in the number of cancer cells was observed of cells in 2D culture compared to those in 3D culture after exposure to T cells and the BiTe treatment.

To further confirm these findings, cell death and apoptosis was determined by calculating the percentage of PI^+ cells and Annexin V^+ cells by flow cytometry. In line with the histological results, the percentage of apoptotic cells was lower in treated cells cultured in 3D compared to the same settings performed in 2D cultures (Fig.67). An overview of this analysis is summarised in Table 8.

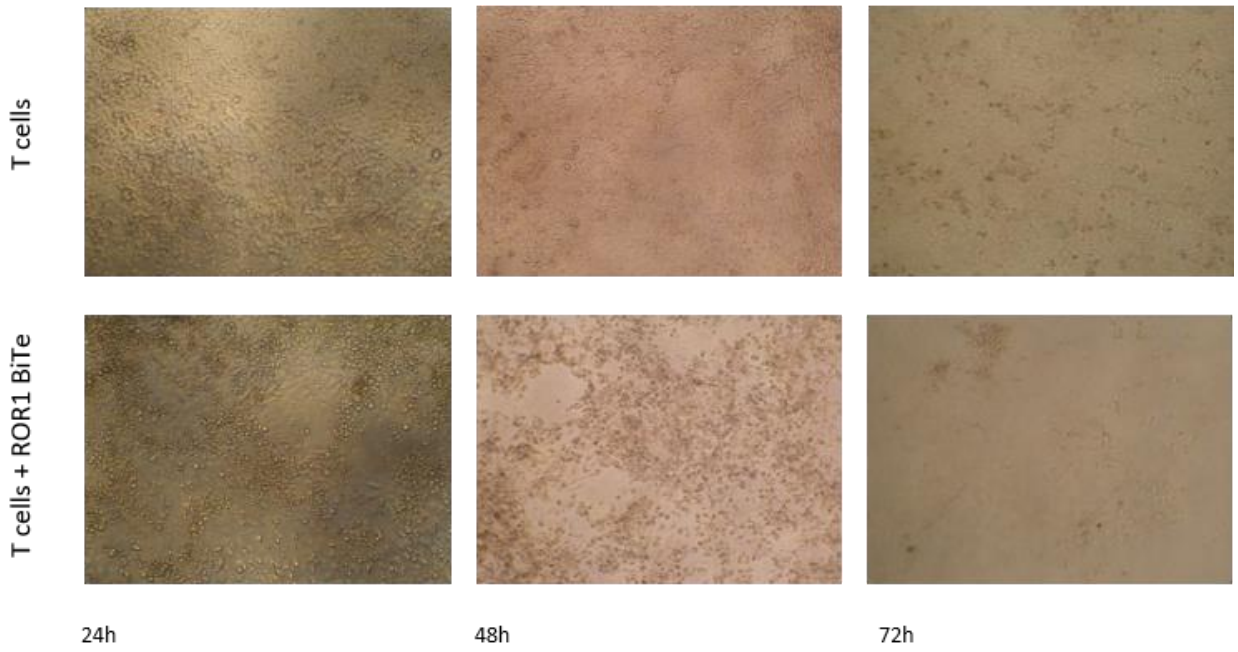

Fig. 64. Morphologic appearance of PK-1 and T cells in co-culture following repeated treatment with ROR-1 BiTe (1µm) or control.

Representative microphotographs of co-culture of PK-1 and T cells, and treatment with ROR-1 BiTe (1um) at three different time points, as specified in the picture (24,48 and 72 hours). Images showing the morphological changes of PK-1 treated with T cells alone or in combination ROR-1 BiTe. (Magnification 10x)

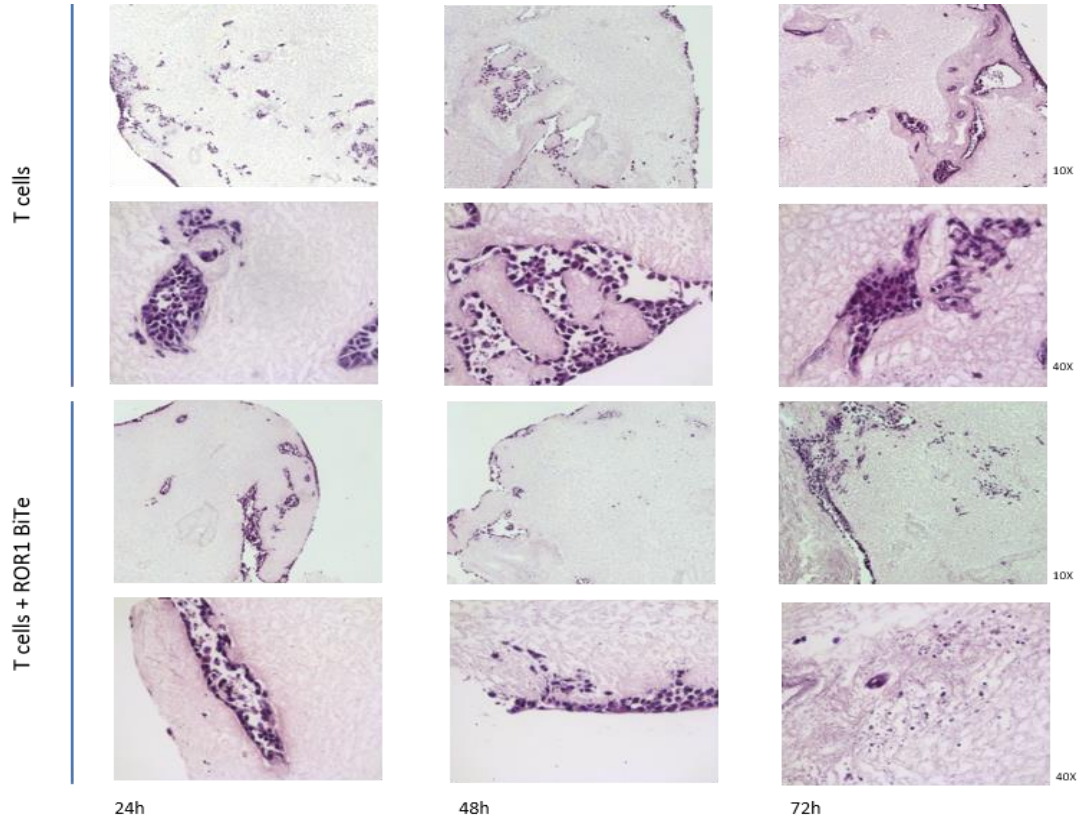

Fig. 65. PK1 repopulation with T cells treated and untreated with ROR1-BiTe in healthy 3D scaffolds.

Haematoxylin and eosin (H&E) showing PK-1 cells in co-culture with T cells in co-culture and untreated (upper panels, indicated with T cells only). Cells exposed daily to ROR1 BiTe for 24, 48 and 72 hours (bottom panels). For each condition, 10x and 40x magnification are shown.

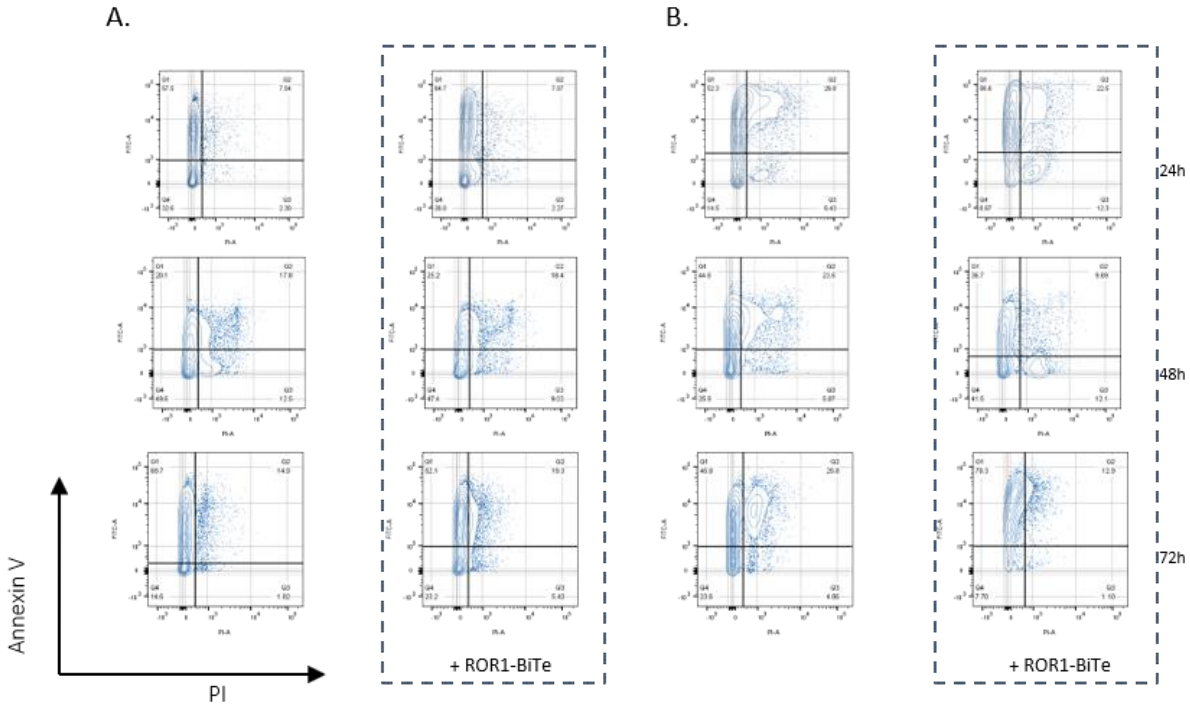

Fig. 66 Differential viability of PK-1 cells co-cultured with T cells in 2D and 3D after 3 cycles of ROR1 BiTe treatment.

Representative plot of Viability staining performed on 3D scaffolds and 2D cultures. Apoptotic (Annexin V FITC+ and PI+) and necrotic cells (Annexin V FITC- and PI+) were detected by flow cytometry analysis at 24, 48 and 72 h following ROR1 BiTe treatment (as indicated in figure). Results are displayed for PK-1 cells in co-culture with T cells, untreated and treated with 1 µM of ROR-1 BiTe added to the media daily in 3D scaffolds (A) and in 2D cultures (B).

24 hours	2D		3D	
	T cells	T cells + ROR-1 BiTe	T cells	T cells + ROR-1 BiTe
Alive (%)	11.77	6.6	28.27	19.30
Pre-apoptotic (%)	53.10	58.43	50.90	57.00
Apoptotic (%)	25.37	28.53	15.42	17.00
Necrotic (%)	9.147	6.42	5.36	7.277

48 hours	2D		3D	
	T cells	T cells + ROR-1 BiTe	T cells	T cells + ROR-1 BiTe
Alive (%)	50.63	22.67	52.80	49.30
Pre-apoptotic (%)	26.87	44.87	16.90	24.08
Apoptotic (%)	8.73	28.57	15.64	17.23
Necrotic (%)	13.73	3.13	14.60	9.457

72 hours	2D		3D	
	T cells	T cells + ROR-1 BiTe	T cells	T cells + ROR-1 BiTe
Alive (%)	24.34	9.927	38.47	17.77
Pre-apoptotic (%)	46.73	65.27	42.67	55.57
Apoptotic (%)	22.70	21.50	13.43	22.13
Necrotic (%)	5.577	3.290	5.397	4.77

Table 8 Summary of Viability staining in 2D and in 3D liver scaffolds before (T cells) and after treatment (T cells + ROR-1 BiTe).

The numbers represent the percentage of cells expressed as mean of triplicates (n=9) of alive (Annexin V FITC- and PI-), Pre apoptotic cells (Annexin V FITC+ and PI-), apoptotic (Annexin V FITC+ and PI+) and necrotic cells (Annexin V FITC- and PI+) were detected by flow cytometry analysis at 24, 48 and 72 h before and after ROR1 BiTe treatment (as indicated in the table).

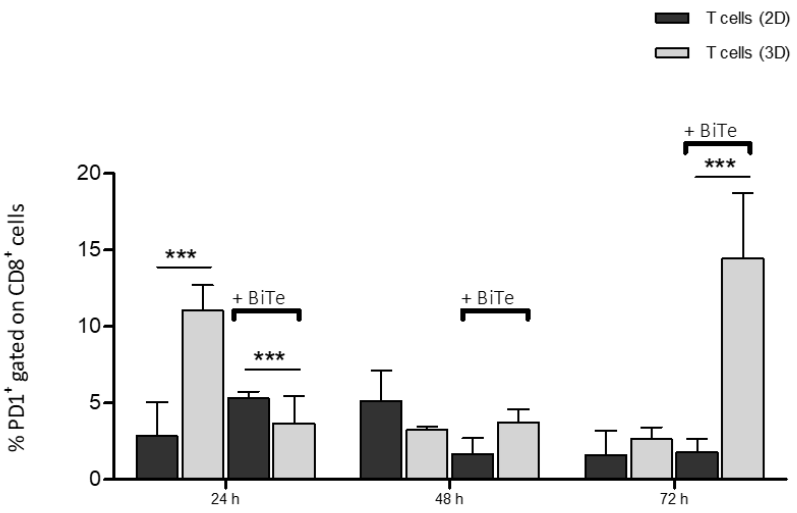

Fig. 67. Changes in cell surface expression of PD-1 and PK-1 cells after ROR1 BiTe treatments in 2D and 3D scaffolds.

Flow cytometric analysis was performed on a co-culture of PK-1 cells and T cells growing in 2D and 3D liver scaffolds at three different time points with or without treatments. The graph is showing the percentage of $CD8^+$ cells expressing PD-1 at 24, 48 and 72h treatment. The results are presented as column bar graphs and statistically analysed using ordinary one-way ANOVA with the Tukey's multiple comparisons post-test.

Next, we investigated the expression of PD-1 in $CD8^+$ cells to explore the activated or exhausted phenotype of those cells. Indeed, PD-1 expression was downregulated in CD8+ cells cultured in 2D after ROR-1 BiTe treatment, although this receptor was upregulated by CD8+ T cells infiltrating the 3D liver scaffolds after 72 hours in response to treatment (Fig. 68).

Considering the higher therapeutic resistance provided by 3D ECM scaffolds as well as the increased levels of PD-1 observed in infiltrating T cells, the therapeutic potential of ROR1-BiTE in combination with PD-1 Inhibitor was investigated in both 3D and 2D at 72h. As shown in Fig. 69 and 70, the anti-PD1 antibody alone had no effect on tumour growth compared with control, while ROR1 BiTe treatment significantly reduced viability of cells, especially for cells cultured in 2D. Furthermore, repeated doses of PD-1 antibody in combination with ROR1BiTe demonstrated the highest

killing efficiency at 24h in 2D. In contrast, the same therapeutic window did not affect tumour cells viability when those were cultured in 3D (Fig.71). For this latter, tumour-killing efficiency started to be evident at 72 hours post-combinational therapy.

Although the experimental settings were identical between 2D and 3D, cells cultured in 2D were much more sensitive to the treatments and, as shown in figure 70, the combinational treatment in 2D was stopped at 24h due to the high cell mortality. Only the data shown for this condition (combinational treatment: PD-1 inhibitor plus ROR1 BiTe) from now on will be referring to the 24h time point of treatment.

At the final time point, cells were collected and processed into single-cell suspensions. FACS staining with Annexin V (marking apoptotic cells) and sytox (marking cells with damaged/porous plasma membrane, i.e. late apoptotic and necrotic cells) quantified the induction of cell death and apoptosis. After ROR1 BiTe and PD-1 treatment, only the cells cultured in 2D displayed a significant increase in apoptotic and necrotic cells (Fig.70), whereas cells cultured in 3D were largely resistant to the treatments (fig.71).

For the 2D cultured, the photographed images of cell amounts using a light microscope showed that viability of cells treated with PD-1 only it was comparable to that of untreated controls. Importantly, ROR1 BiTe treatment induced cell death as clearly shown on photographed images (Fig.70) and a further increase in cell death after the combinational treatment with PD-1 inhibitor (Fig.70F).

Similar results, but with much less impact on cell viability, were detected by Haematoxylin and eosin staining of 3D scaffolds (Fig. 72). Overall, these results are consistent with previous findings described in this thesis showing that 3D systems tumour models are particularly refractory to treatments compared to 2D culture

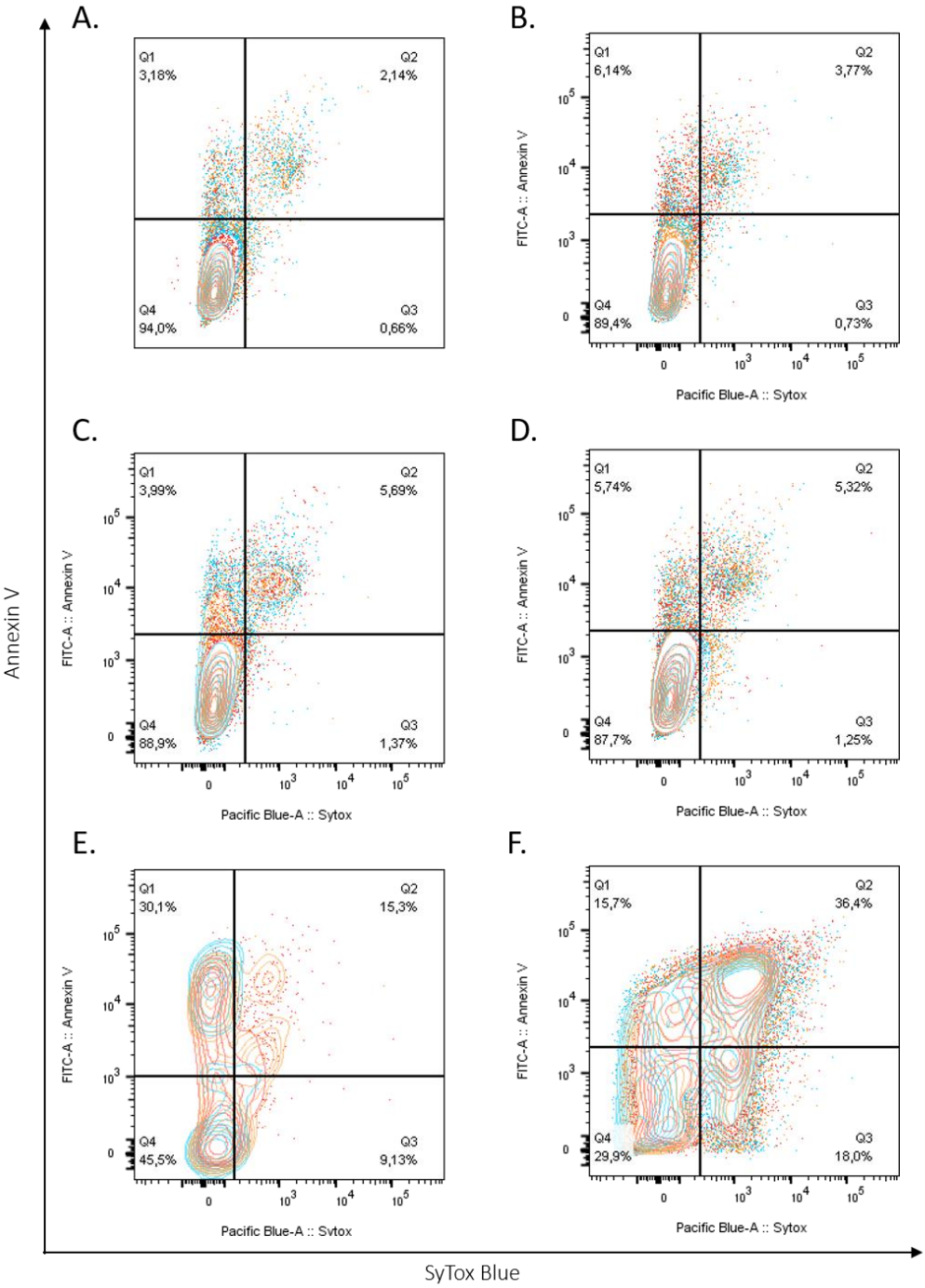

Fig. 68. Viability of PK-1 cells and T cells cultured in two-dimensional (2D) conditions.

Apoptotic (Annexin V FITC+ and SYTOX-) and necrotic cells (Annexin V FITC+ and SYTOX+) were detected by flow cytometry analysis of 2D conditions at 72 h following different treatments. Results are displayed for (A) single culture of PK-1 cells in 2D (B) treated with 1 µM of PD-1. Plot showing the co-culture of PK-1 and T cells, C) untreated (and (D) treated with ROR1 BiTe, (E) PD-1 antibody, (F) combinational treatment of ROR1 BiTe + PD-1 antibody. the last condition (F) is shown at 24h. Graph shows pooled data from 3 biological replicates each of it is a pool of 3 samples, ~5,000 events per condition.

Fig. 69. Phase contrast of PK-1 cells and T cells cultured in two-dimensional (2D) conditions.

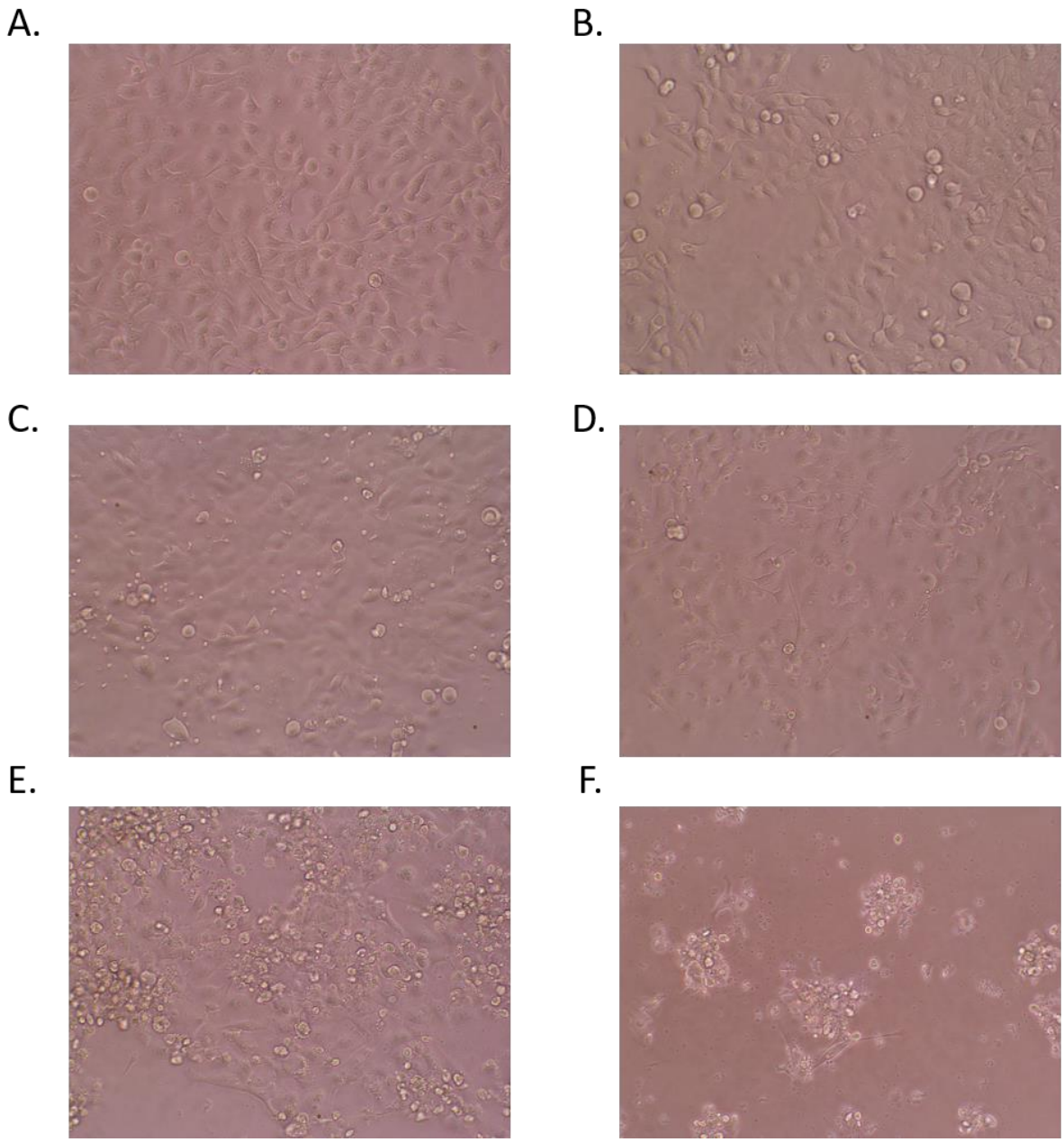

Morphology of PK-1 cells in different conditions. Phase contrast micrographs of PK-1 cells cultured in monolayer (2D). (A) Photographs of single culture of PK-1 cells in 2D (B) a treated with 1 µM of PD-1. Plot showing the co-culture of PK-1 and T cells, (C) untreated, (D) treated with ROR1 BiTe, E) PD-1 antibody (, and (F) combinational treatment of ROR1 BiTe + PD-1 antibody. the last condition (F) is shown at 24h of treatment.

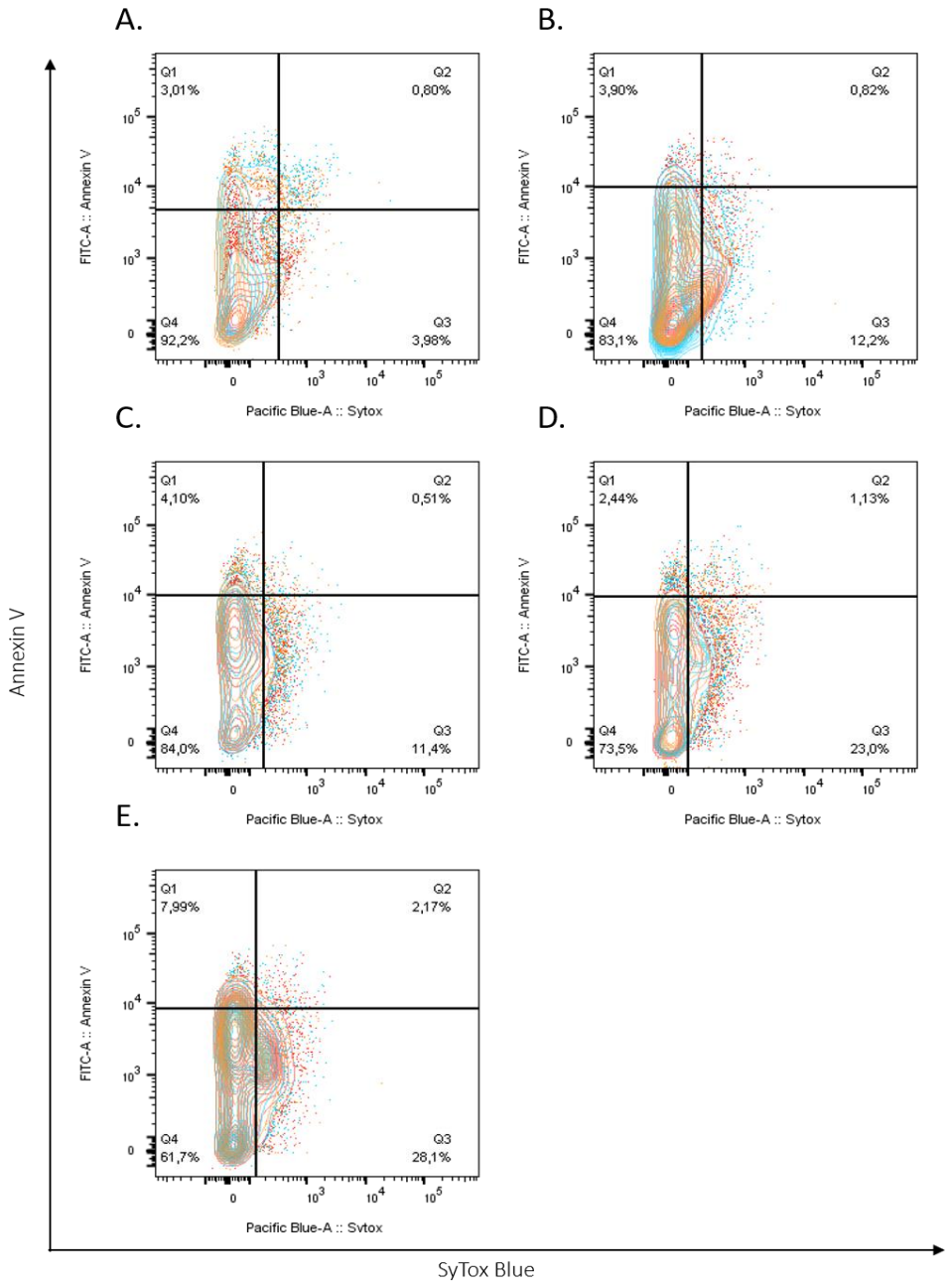

Fig. 70. Viability of PK1 cells and T cells cultured in 3D scaffolds.

Apoptotic (Annexin V FITC$^+$ and SYTOX$^-$) and necrotic cells (Annexin V FITC$^+$ and SYTOX$^+$) were detected by flow cytometry analysis of 3D scaffolds at 72 h following different treatments. Results are displayed for single culture of PK-1 cells in (A)single culture, the remaining plots showing the co-culture with T cells, untreated (B) and treated with ROR1 BiTe (C), PD-1 antibody (D), combinational treatment of ROR1 BiTe + PD-1 antibody (E). Graph shows pooled data from 3 biological replicates each of it is a pool of 3 samples, ~5,000 events per condition.

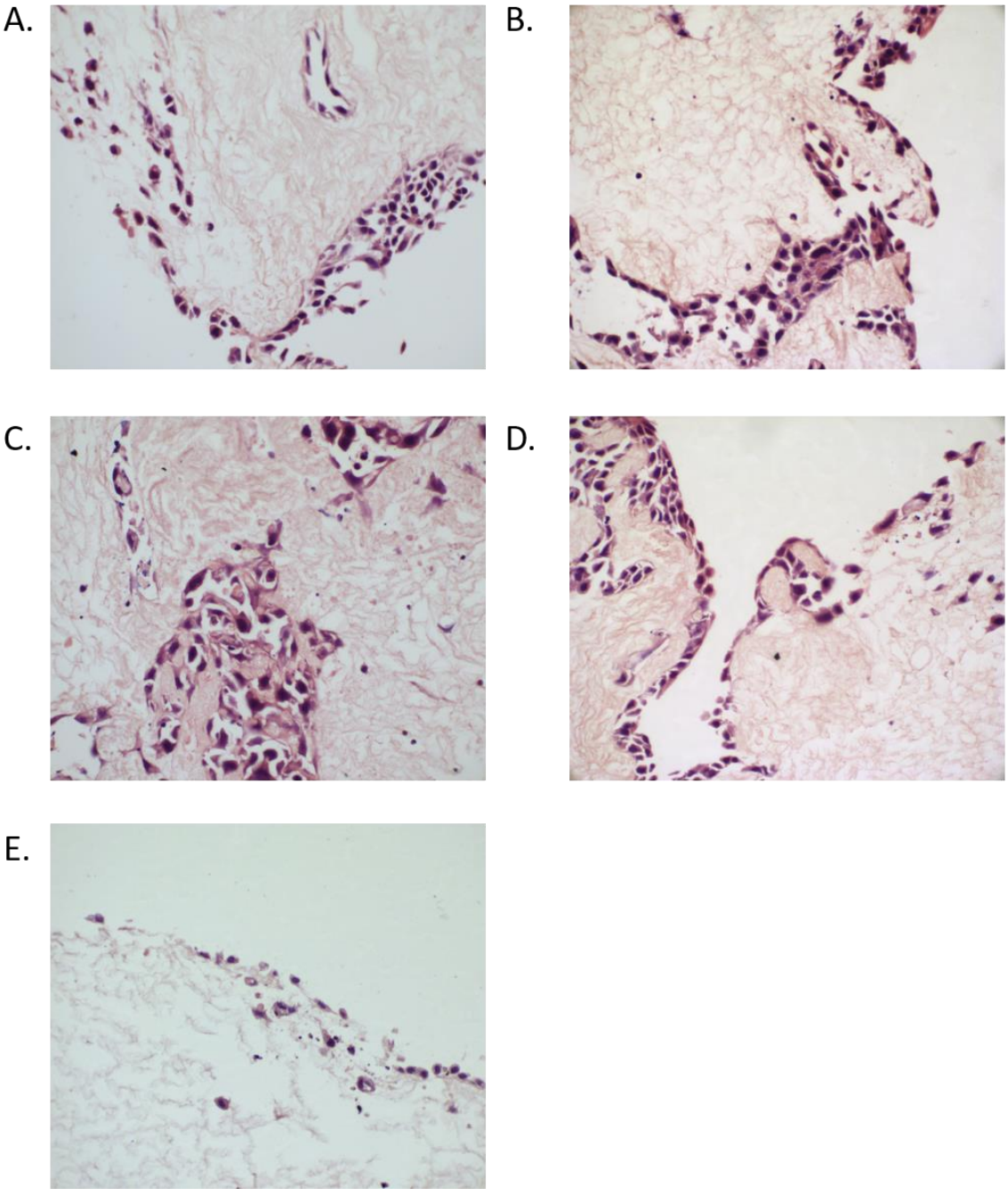

Fig. 71. Anti-tumour capacities of ROR1 Bite and PD-1 inhibitors in 3D scaffolds.

Haematoxylin and eosin (H&E) showing PK-1 cells in (A) single culture in (B) co-culture with T cells. The cells in co-culture exposed daily to (C) ROR1 BiTe, (D) PD-1 antibody and the (E) combination of ROR1 BiTe and PD-1 treatments after 72h. The last condition (E) revealed necrotic areas. Magnification 40x.

Next, tumour-infiltrating T cells were analysed by flow cytometry. In the 3D metastatic model, treatments with PD-1 administered alone or in combination with the ROR-1 BiTe led to an increase in infiltrating T cells compared to untreated condition (Fig.73). The treatment with anti PD-1 promoted higher number of infiltrating cells within the 3D ECM scaffolds with approximately 30% CD3+ cells, whereof 10% were activated (CD107a positive cells, Fig.74). Notably, the combinational treatment enhances even more the infiltration of T cells within the 3D scaffolds.

A.

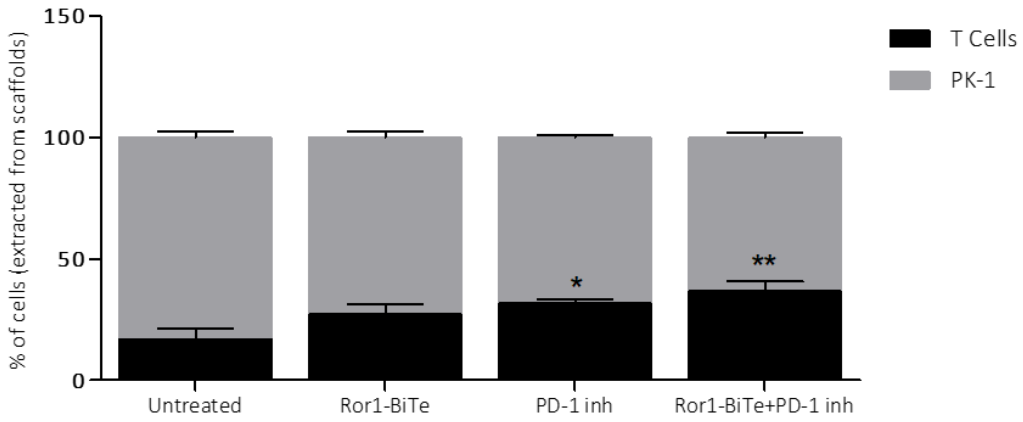

B.

	Untreated	Ror1-BiTe	PD-1 inh	Ror1-BiTe+PD-1 inh
PK-1	80,89% ±2,46	72,73% ±2,51	68,24% ±0,92	63,01% ±2,12
T Cells	17,11% ±2,4	22,3% ±2,51	31,8% ±0,92	37% ±2,4

Fig. 72. Percentage of immune cells infiltrating the scaffolds after treatments.

(A) Stacked-bar graph shows distribution of T cells and PK-1 cells. Black indicates T cells while dark grey indicates cancer cell line PK-1. Percentages were measured by flow cytometry after 72 hours of treatments as indicated in the graph. (B) Summary of percentage of T cell and cancer cells cultured in 3D scaffolds and treated for 72h. The numbers represent the percentage of the PBMC stained positive for the corresponding anti-CD antibodies (average±SD). Graph shows pooled data from 3 biological replicates each of it is a pool of 3 samples, ~5,000 events per condition.

According to previous results described in this chapter (Fig.71, 72), the combinational therapy increased the T cell killing efficiency of cancer cells in 3D cancer model and therefore the activation status of T cells was next addressed.

T cell activation marker CD107a, whose behaviour is known to change upon activation, was assessed by flow cytometry to investigate the activation of T cells upon exposure to cancer cells within the 3D ECM scaffold. In cytotoxic lymphocytes (CD8+), lytic granules are secretory lysosomes that contain a dense core, including various proteins that are involved in cytotoxic function (e.g., perforin, granzymes)[192]. T cells cultured in 3D liver ECM scaffolds upregulated CD107a in the presence of cancer cells at 72h (Fig.74). However, CD107a expression was not modulated by the different treatments.

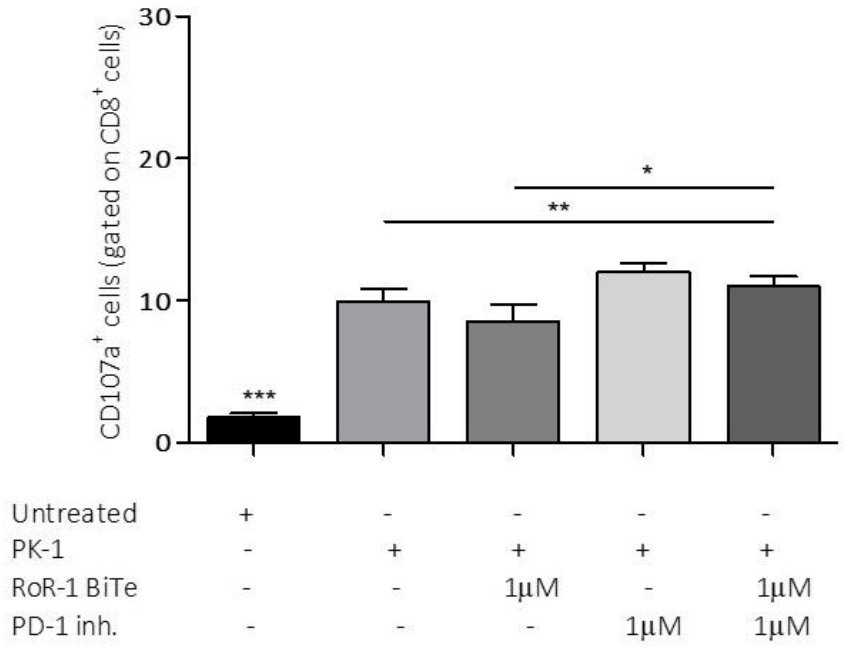

Fig. 73. Cell surface CD107a on T cells 72h after treatments.

Flow cytometric analysis was performed in CD8+ T cells in 3D liver scaffolds repopulated with or without (black bar) liver metastatic cell line (PK-1). Killing activities were assessed by CD107a staining on CD8+ cells. For the staining analysis of the infiltrating cells was performed on extracted cells. Statistical difference between groups was determined by paired 2-tailed Student t test.

Next, the expression of PD-1 and PD-L1 was measured by FACS. PD-1 was significantly more expressed on $CD8^+$ T cells exposed to PK-1 in 3D cultures after ROR1 BiTe treatment. As expected, the expression of PD-1 was downregulated by the blocking antibody, thus confirming the selectivity of the therapeutic approach (Fig.75A). Considering that, cancer cells can downregulate the immune response by expressing PD-L1, the expression of this receptor was evaluated in cancer cells reseeded in 3D in the same experimental settings described above.

As shown in Fig 75B, the co-culture of cancer cells with T cell led to a significantly increased expression of PD-L1 in cancer cells and this upregulation was sustained in response to treatments. Overall, these results are in line with clinical findings observed in patients [80].

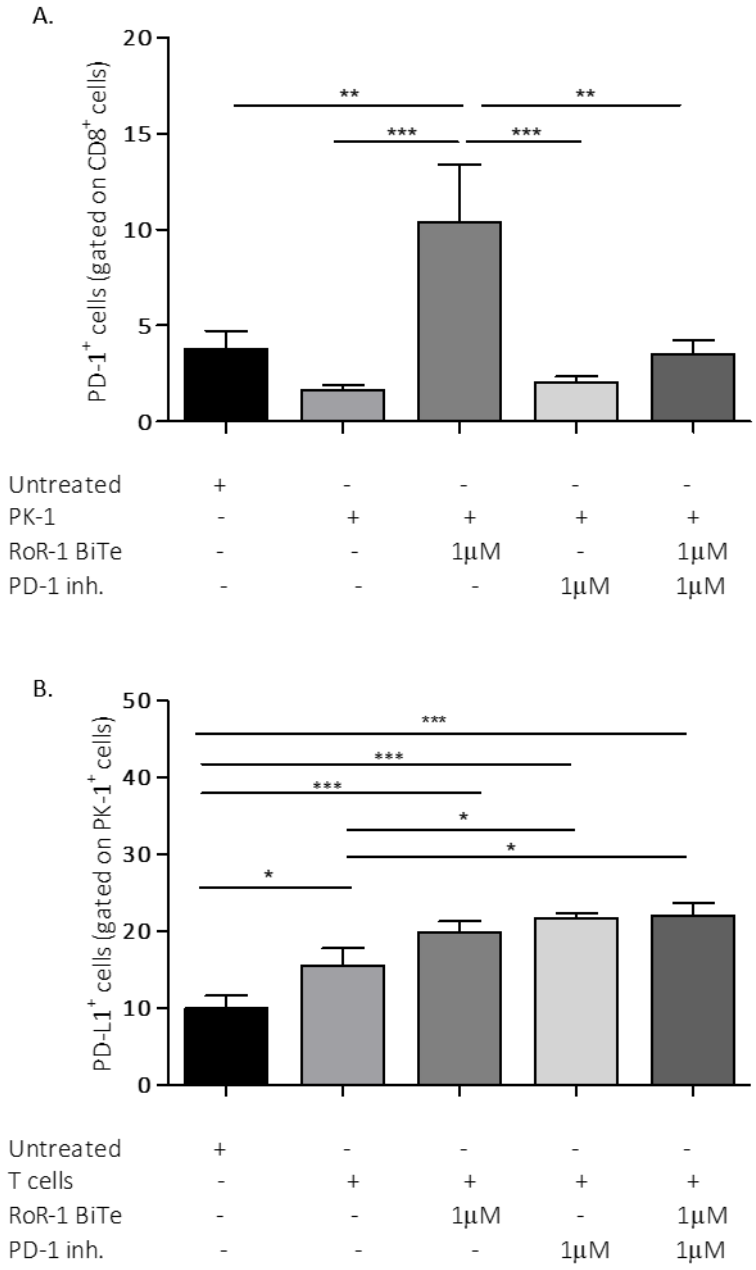

Fig. 74 *Changes in cell surface expression of PD-1 and PD-L1 after treatments.*

Flow cytometric analysis was performed in 3D liver scaffolds repopulated with single culture (T cells or PK-1, black bar in A and B graphs respectively) or co-culture with or without treatments after 72h. Upper graph (A) showing the percentage of CD8⁺ cells expressing PD-1, the graph in the bottom (B) refers to

PDL-1 + cells gated on PK-1 cells. The results are presented as column bar graphs and statistically analysed using ordinary one-way ANOVA with the Tukey's multiple comparisons post-test.

Overall, these findings indicate the relevance of using 3D complex model for recapitulating the therapeutic resistance commonly identified in patients. Indeed, according to the results described in this chapter combination of ROR1 and PD-1 antibody significantly reduced the viability of cancer cells, suggesting that the PD-1 inhibition can enhance immunotherapy's response.

However, complete tumour killing was not achieved in 3D ECM model while this was detected in 2D. One of the possible mechanisms of tumour resistance is linked to the possibility of cells to acquire escape mechanisms and detach from their original niche. Indeed, if the tumour is not sensitive to therapy, there can be a higher risk of developing metastatic disease [193, 194]. Considering this clinical observation, the presence of cancer cells was also assessed in the culture medium within the non-infiltration pool as potentially detached from the 3D scaffolds after treatment.

Interestingly, CK^+ cells (PK-1 cells) were identified by FACS in the supernatant of 3D scaffolds (Fig.76) treated with the ROR1 BiTe only as well as when combined with PD-1 antibody. The former finding might indicate that upon exposure to ROR1 BiTe cancer cells might have changed their cell adhesion protein profile and detached from their original microenvironment. The latter, in which it was shown stronger tumour killing, might indicate some escaping mechanisms driven by the inflammatory background. Future experiments are needed in order to characterize these "detached" cells and establish possible working mechanisms.

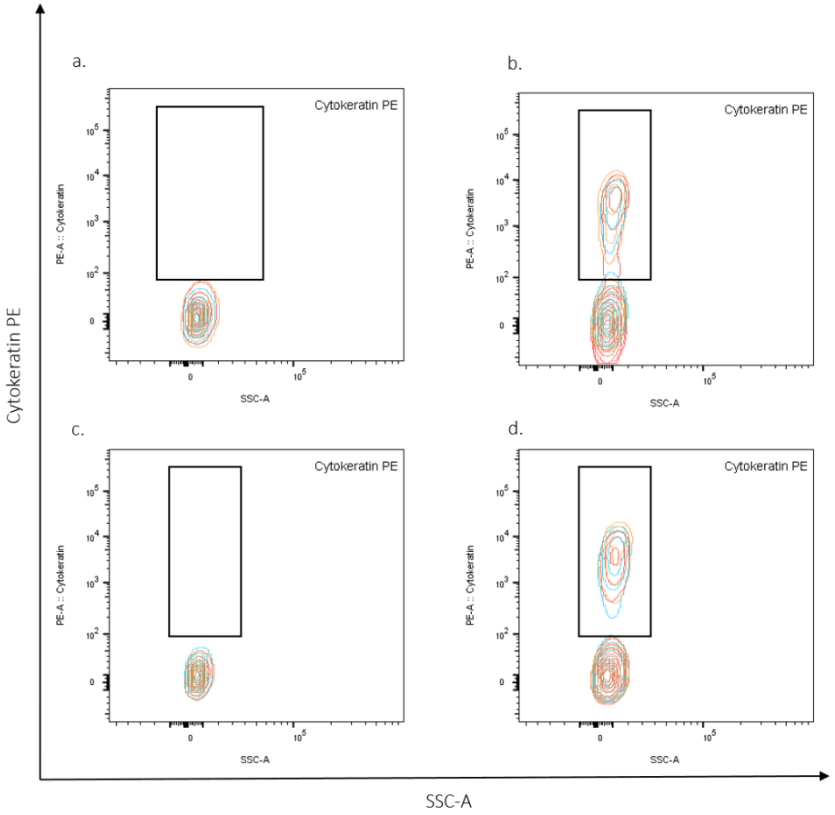

Fig. 75. Flow cytometry staining for Cytokeratin⁺ cells in the supernatants.

Flow cytometric plots showing PK-1 cells and T cells collected from the supernatants/media of 3D scaffolds after 72h of treatments. Cells were stained with pan-CK antibodies. Results are displayed for supernatants collected from the following 3D conditions: (A) PK1 and T cells untreated (B) treated with ROR1 BiTe, (C) treated with PD-1 antibody, (D) combinational treatment of ROR1 BiTe + PD-1 antibody. Graph shows pooled data from 3 biological replicates, each of which was a pool of 3 samples, ~10,000 events per condition.

9.4.4 Conclusion:

Therapeutic benefit of relevant ROR1-BiTE in the in the metastatic 3D model was modest especially if compared to the 2D.

BiTe therapies are based on the concept of directing T cells to tumour cells and activation of T cells by BiTEs is strictly dependent upon target cell binding [136].

This linkage is essential to the BiTe cytotoxic mechanism, as it must bind simultaneously to both the T cell and the tumour to induce a cytotoxic activity from the T cell. In this 3D setting, the number of cells available and their activation is impaired by the capacity of T cells to infiltrate the ECM compared to 2D. This may explain why in those models we do not have the dramatic effect after treatments in 2D. Moreover, despite their presence in the tumour, T cells in 3D are probably exposed to immunosuppressive environment within the tumour microenvironment that rendered them functionally inert.

The results in this chapter underline the advantages of a model that could reproduce the 3D ECM microenvironment where also the infiltrating capacity of T cells could be tested.

Unlike haematological malignancies, solid tumours present many obstacles to T cells resulting in an insufficient infiltration.

We herein propose a system that allows to evaluate the infiltration and response to therapy in a solid tumour context that is one of the main challenges in engineered T cell therapy.

10. Discussion

The ECM plays a key role in orchestrating cell-cell interaction and cell-microenvironment signalling. In turn, these signals affect cellular functional behaviours in 3D such as proliferation, differentiation, morphology especially when compared to cells cultured on a 2D system [17, 195].

Therefore, when drug candidates are being discovered and tested using cell-based assays, the culture methods used should mimic the most natural in vivo condition as much as possible. Nowadays, 3D culture systems are recognized as the most optimal approach for in vitro drug discovery applications as they tend to mimic the more natural tissue.

While several methods of complex 3D spheroid generations exist[196], it appears that especially the immunology field still requires a further search for its most optimal 3D in vitro model.

The work described in this thesis illustrates the development and the validation of a new 3D culture system based on tissue-specific and disease-specific human ECM scaffolds that allow immune cells co-culturing with tumour cells in order to recapitulate key findings observed in patients.

In the results section the use of 3D co-cultures has been demonstrated to effectively bridge the gap between in vitro 2D assessment and clinical observations in tumour development and treatment resistance in patients.

An extensive set of evidence has demonstrated that immune cells plays a crucial role in carcinogenesis[170]. Previously, most data available on cancer and immune system interactions in humans were obtained by culturing cells isolated from peripheral blood or cancer tissues together with established cell lines in conventional bi-dimensional in vitro conditions. However, this approach has failed to take into account critical aspects of the tumour-immune microenvironment, such as immune cell infiltration and unique disease-associated microenvironment.

Indeed, findings and observations made by using 2D cell culture methods hardly predict outcomes of clinical trials given the unique characteristics of the tumour and its immune composition[197]. In addition to the 2D studies also in vivo mouse models are used to test different therapeutic strategies. Although mouse models of cancer reproduce more the features of human tumours, differences between mouse and human immune mechanisms and lack of cross reactivity limit the application of these models. In the results section we showed how the use of 3D co-cultures might effectively bridge the gap between in vitro 2D assessment and animal models of cancer disease.

In the first part of the results (Chapter 9.1), the application of 3D liver scaffolds in studying immune cells infiltration was described. We showed that human ECM derived from a specific organ was able to modulate the phenotype of immune cells. For instance, we noticed that NK cells could acquire a more hepatic-like phenotype when exposed to a human liver ECM (Chapter 9.1.5). The influence of ECM on monocyte-macrophage differentiation was investigated using human PBMCs without using any other stimuli. The results presented indicate that the differentiation was induced in 3D liver scaffolds, as assessed by the expression of CD68 and CD11b in cells infiltrating compared to the one in suspension (non-infiltrating) (Fig.34).

The initial research activities described in this thesis were aimed at optimizing a model for infiltration and survival of the peripheral immune system and investigating its effect on engineered 3D tumour models.

According to previous reports, PBMCs do not proliferate in culture without interleukins stimulation. Most human T lymphocytes isolated from peripheral blood or other sources are in a quiescent state. They can be stimulated to proliferate in culture by mitogens and IL-2 [198]. In our 3D system, we demonstrate that lymphocytes can proliferate as confirmed by ki67 staining (Fig. 23).

We have demonstrated that PBMCs survive up to 5 days in 3D scaffolds, reflecting the importance of the natural environment provided by extracellular matrix on cell viability and function. Comparison between PBMCs cultured in 2D and 3D, showed an

increase in the percentage of both subpopulation of T cells ($CD4^+$ and $CD8^+$ cells) in 3D scaffolds. This result correlates with the positive expression of proliferation marker and implied the initial survival of T cells.

The results described in this thesis suggest that different cells have the capability to infiltrate within 3D ECM scaffolds without any prior stimulation. This capacity is reflected by the increase in gene and protein expression for pathways related to cell-ECM interaction (ITGβ1) and ECM remodelling/invasion (i.e. MMP9).

This unique capability of ECM scaffolds to allow for spontaneous immune cells infiltration can have tremendous implication in understanding molecular aspect of immune biology in the context of solid tumours.

Many groups have demonstrated that solid tumours may be classified based on T cell infiltration and indeed the localization of T cell within the tumour (high "immunoscore") it correlates with improved patient prognosis[48].

To date, the immunological status of a tumour is not reproducible using normal 2D technologies. The 3D co-culture tumour-immune cells models described in this thesis is the first in kind allowing us to recapitulate the cold and hot tumour features of human HCC. This was achieved by using two different ECM substrates deriving from a healthy and a cirrhotic human liver reseeded with HCC cancer cell line. Notably, while immune cells gene and protein expression of cell-ECM interaction pathway was modulated upon exposure to healthy or diseased ECM liver scaffolds, the immune exclusion phenotype ("cold tumour") was only achieved when cancer cells where introduced in the 3D system. Indeed, cancer cells reseeded into cirrhotic ECM scaffolds showed a more aggressive phenotype linked to EMT signatures that in turn promoted the exclusion of immune cells within the tumour model.

The expression of EMT markers such as Vimentin and E-cadherin was studied in 3D cultures. Cancer cells downregulated epithelial markers at genes and protein levels and upregulate the expression of mesenchymal markers when reseeded into cirrhotic ECM scaffolds.

The possibility to induce EMT by switching from a healthy to a cirrhotic substrate can allow a better understanding of the molecular process eventually leading to new therapeutics against this.

For cancer research, investigating the tumour cell microenvironment and the interaction with other cells types requires the establishment of such 3D co-culture models involving more than two or even three cell types [199]. To address this issue, we designed a 3D heterotypic co-culture model involving HCC cells and PBMCs. The established 3D co-culture model may lead to better understanding of cellular mechanism between different cell types within the tumour microenvironment and can provide solutions to help overcome tumour resistance and metastasis. We noticed that by adding immune cells to the 3D system repopulated with cancer cells in a cirrhotic ECM (i.e. cold tumour), the presence of immune cells drives the migration of the cancer cells towards blood vessels. This specific migration and localization of cancer cells in the vessels could indicate and important step in the process of metastasis (Fig.43, represented in the cartoon in Fig.77).

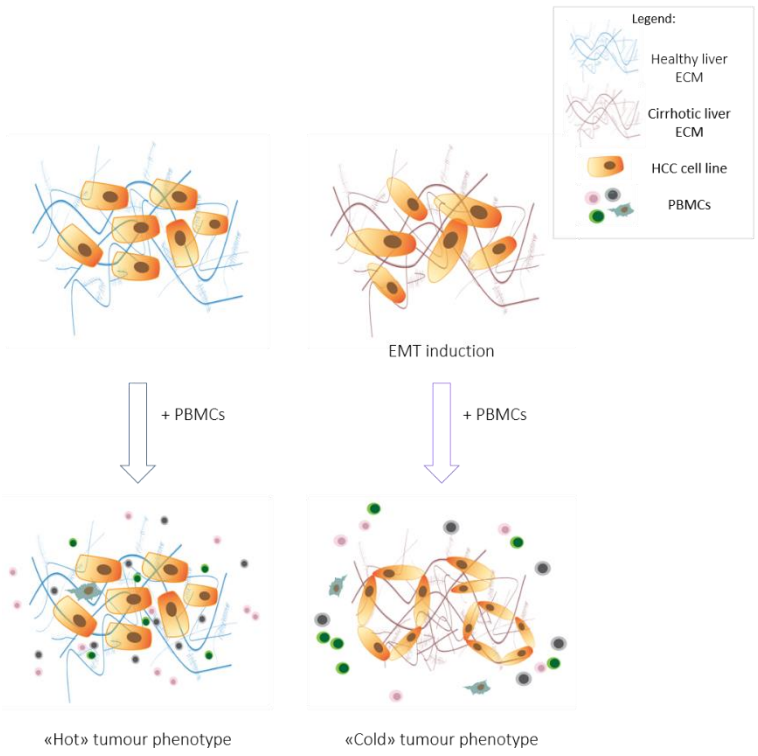

Fig. 76 Schematic representation of 3D scaffolds-based model for Hot and Cold tumour.

Important, PBMCs exposed simultaneously to bioengineered HCC cirrhotic scaffolds and cancer cell –free ECM cirrhotic scaffolds do not infiltrate, indicating that PBMCs lose their capacity to infiltrate (Fig. 49). This is in strong contrast when healthy 3D ECM was used as biomaterial, as PBMCs exposed to 3D cirrhotic scaffolds (without cancer cells) were able to infiltrate and proliferate (Fig.22-23). Within the cold phenotype, the tumour microenvironment lacks immune-effector T cells because the immunogenicity functions are inhibited. This results in lack of T cell priming or activation and as a consequence T cells cannot penetrate to attack tumours[172]. Further studies on this model will potentially explain the phenomena of T cell exclusion from the tumour site. Indeed, a complete analysis of the crosstalk between tumour cells, immune cells and the surrounding tissue microenvironment and consequently their immunological features could provide better understandings of the development and progression of cancer malignancies.

Immune cell infiltration depends on a complex cytokine and chemokine milieu within the tumour microenvironment, which allows and regulates activation and suppression of the immune system[200]. Understanding whether a tumour is immunologically cold or hot is therapeutically relevant because unlike cold tumour phenotypes, immune hot tumours seem to be more sensitive and responsive to cancer treatment with an immune checkpoints blockade.

Efforts have been made in order to understand the efficacy of combinational immunotherapies or by using chemokines which convert cold tumours into hot tumours by reverting the tumour micro environment, in that way immune efficiency could be enhanced [66]. For all these reasons, we herein propose and describe two different models based on cirrhotic and healthy liver ECM, which reproduce the variability among HCC derived from a different aetiology in response to immune cells and recapitulate the features of a cold and hot tumour.

It is known that the T-cell effector function can be restrained by the expression of PD-1 and its engagement with their ligands and to block the anti-tumour activity. This

marker was upregulated in our co-culture model when T cells were co-cultured with HCC cell lines growing in a healthy scaffold but not when co-cultured in a cirrhotic environment. Our results show the upregulation of PD-L1 is a feature that characterized the hot and cold tumour. The lymphocyte infiltration and presence of IFN-γ produced by T cell leads to an increase of PDL-1 in the hot tumours [172]. In contrast, there is no increase of PD-L1 in our model of cold tumour reflecting the feature typical of a cold tumour lacking T cells infiltration. This may be key factors for the effective anti-PD-1/-L1 treatments in hot and cold tumours.

Previous studies have also suggested that the increased expression of PD-L1 in the TME of HCC was associated with tumour aggressiveness or recurrence in patients with HCC [81, 201, 202]. Although Sorafenib is a multikinase inhibitor mainly targeting RAF and vascular endothelial growth factor receptors, many studies have suggested that Sorafenib may exhibit a variety of immunomodulatory effects [178]. Notably, upregulation of PD-L1 in HCC cells upon exposure to, or in resistance to Sorafenib, has been recently reported in preclinical studies [202]. Our results clearly show an increased expression of PD-L1 after Sorafenib treatment (Fig.54) which was further increased by the presence of immune cells.

This underlines the role of Sorafenib treatment and immune cells in affecting PD-L1 expression in the TME in our HCC model which recapitulates clinical findings in HCC [202].

Comparing the result of the efficacy of Sorafenib on HCC cells lines in 2D or 3D we confirmed the different sensitivity. The dosage response of Sorafenib was evaluated in 3D cultures and compared with 2D cultures following a 72-hour treatment. Specifically, we found a higher IC_{50} in the 3D than in the 2D-culture, suggesting that the 3D-environment was anti-apoptotic after the treatment. Moreover, the dose was different for the same HCC cell line growing in two different 3D scaffolds. For example, we found a higher IC_{50} in the SNU449 cultured on the cirrhotic 3D scaffolds, confirming the aggressiveness of cells and their acquired resistance to treatment that correlates with the finding of EMT induction.

To the best of our knowledge, we are the first to demonstrate the hot and cold phenotype within a 3D in vitro model. Elucidating the mechanisms that determine why a given tumour is characterized by a hot or cold phenotype should enable the development of therapeutic solutions to eradicate resistance for both canonical and immunotherapy.

To date, immunotherapy represents a promising approach for the treatment of cancers and metastatic disease. Checkpoint blockers (such as anti–PD-1 and anti–PD-L1), vaccines, and chimeric antigen receptor (CAR) T-cell therapies, antibodies-based therapies (BiTe), work primarily by activating T cells that have already reached the tumour. In immunologically cold tumours, the problem is that the efficacy of those therapies is limited by the absence of T cells.

In recent years, novel treatments combining cancer immunotherapy together with existing anticancer treatments have gained significant attention and have been extensively investigated in preclinical or clinical studies. In fact, it appears that giving standard doses of chemotherapy along with checkpoint inhibitors may be the optimal way to push the immune T cells into action[203].

We demonstrated in an experimental setting of liver metastases that the combination checkpoints inhibitors and immunotherapy could be beneficial for reducing tumour growth.

In addition, our new 3D co-culture systems were able to provide critical insights into the role of tumour microenvironment and interaction between immune cells in cancer therapy response and resistance in a superior way compared to 2D monolayers. This is in line with previous work published from other groups showing higher resistance to therapies in 3D spheroids tumour models. [204].

To this end, we analysed the differences in 2D vs. 3D culture looking at the interaction of liver metastatic cells with T cells. We explored the BiTe activity on 3D scaffolds, more specifically the strategy is based on T cell retargeting as cancer therapy. The linkage of T cells to tumour cells is central to the BiTE's cytotoxic mechanism. BiTEs must bind simultaneously to the T cell as well as the TAA, in this case ROR-1, to elicit

cytotoxic activity from the T cell. It has been shown that activation of T cells by BiTEs is strictly dependent upon target cell binding and consequently on T cell density [136].

Major differences were found when performing experiments in 2D and 3D. In 2D, T cells do not need to invade any solid tissue hence cancer cells treated with the BiTe in 2D were quite sensitive to the treatment showing a good killing capability. In contrast, when the same cells where applied into the 3D system, we found a reduced sensitivity to the treatment as well as an anti-apoptotic response compared to 2D.

The increased number of infiltrating T cells was detected after Bite treatment, PD-1 treatment and their combination (Fig.72). Considering that also from a translational point of view, one of the major problems for treating solid tumours with Bite is the density and type of T cells already present in the tumour bed. In addition, the T cells may already have an exhausted or a regulatory phenotype. We tested the efficacy of a combination of ROR-1BiTe with a PD-1 blocking antibody treatment to avoid possible T cell exhaustion and therefore boosting the efficacy of BiTe. The administration of PD-1 alone, did not affect cell viability nor the combination with BiTe. Importantly, cells in 2D treated with the combination showed a significant increase in apoptotic and necrotic cells after 24 hours of treatment, while cells grown in 3D showed still trace of resistance to treatment even after 72 hours.

One of the major reported escape mechanisms during treatment include the increased frequencies of regulatory T cells (Tregs) and increased levels of PD-L1 expression on cancer cells. Our model reflects what has already been demonstrated in other cancer cells where an upregulation of PD-L1 post-Bite treatment was reported [205].

The differences shown in 2D and 3D in the HCC model were confirmed also for the metastatic model. Indeed, the metastatic cell line PK-1 reseeded in 3D ECM scaffolds were relatively insensitive to these compounds compared to the 2D settings.

Interestingly, cancer cells were found outside the 3D scaffolds post-BiTe treatment thus suggesting this phenomenon could be related to the cancer cells response to

treatment. Evaluation of the viability and metastatic capacity of cells will be evaluated in future work to address possible underlining mechanisms.

Overall, we observed differences in the response to canonical and novel immunotherapy treatments in 3D versus standard 2D cultures. While the underlining mechanisms needs to be further explored, those findings may explain the differences in response to treatments found in patients.

The idea is that even if the generation/optimization of 3D immune-cancer models requires more labour than 2D culture, the routine use of these 3D systems in in vitro drug efficacy and toxicity applications will most probably generate more accurate results than the use of monolayer cultures alone. Therefore, the new 3D systems could better predict the efficacy of candidate compounds effects on target cells.

Our experiments confirm that the 2D system fails to recapture key features of cancer development and cancer-related immune environment and this might have caused the high rate of failure in therapeutic translation. Therefore, the development of realistic models for target identification, drug screening and development is extremely important to increase the chances of success in clinical trials.

11. References:

1. Bray, F., et al., *Global cancer statistics 2018: GLOBOCAN estimates of incidence and mortality worldwide for 36 cancers in 185 countries.* CA Cancer J Clin, 2018. **68**(6): p. 394-424.
2. McGlynn, K.A., J.L. Petrick, and W.T. London, *Global epidemiology of hepatocellular carcinoma: an emphasis on demographic and regional variability.* Clin Liver Dis, 2015. **19**(2): p. 223-38.
3. Marquardt, J.U., J.B. Andersen, and S.S. Thorgeirsson, *Functional and genetic deconstruction of the cellular origin in liver cancer.* Nat Rev Cancer, 2015. **15**(11): p. 653-67.
4. El-Serag, H.B. and K.L. Rudolph, *Hepatocellular carcinoma: epidemiology and molecular carcinogenesis.* Gastroenterology, 2007. **132**(7): p. 2557-76.
5. Pinzani, M., M. Rosselli, and M. Zuckermann, *Liver cirrhosis.* Best Pract Res Clin Gastroenterol, 2011. **25**(2): p. 281-90.
6. Zhou, W.C., Q.B. Zhang, and L. Qiao, *Pathogenesis of liver cirrhosis.* World J Gastroenterol, 2014. **20**(23): p. 7312-24.
7. Desai, A., et al., *Hepatocellular carcinoma in non-cirrhotic liver: A comprehensive review.* World J Hepatol, 2019. **11**(1): p. 1-18.
8. Scaglione, S., et al., *The Epidemiology of Cirrhosis in the United States: A Population-based Study.* J Clin Gastroenterol, 2015. **49**(8): p. 690-6.
9. Younossi, Z.M., *The epidemiology of nonalcoholic steatohepatitis.* Clin Liver Dis (Hoboken), 2018. **11**(4): p. 92-94.
10. Adams, L.A. and K.D. Lindor, *Nonalcoholic fatty liver disease.* Ann Epidemiol, 2007. **17**(11): p. 863-9.
11. Ascha, M.S., et al., *The incidence and risk factors of hepatocellular carcinoma in patients with nonalcoholic steatohepatitis.* Hepatology, 2010. **51**(6): p. 1972-8.
12. Hanahan, D. and R.A. Weinberg, *Hallmarks of cancer: the next generation.* Cell, 2011. **144**(5): p. 646-74.
13. Hanahan, D. and R.A. Weinberg, *The hallmarks of cancer.* Cell, 2000. **100**(1): p. 57-70.
14. Budhu, A. and X.W. Wang, *The role of cytokines in hepatocellular carcinoma.* J Leukoc Biol, 2006. **80**(6): p. 1197-213.
15. Mbeunkui, F. and D.J. Johann, Jr., *Cancer and the tumor microenvironment: a review of an essential relationship.* Cancer Chemother Pharmacol, 2009. **63**(4): p. 571-82.
16. Tahmasebi Birgani, M. and V. Carloni, *Tumor Microenvironment, a Paradigm in Hepatocellular Carcinoma Progression and Therapy.* Int J Mol Sci, 2017. **18**(2).
17. Bonnans, C., J. Chou, and Z. Werb, *Remodelling the extracellular matrix in development and disease.* Nat Rev Mol Cell Biol, 2014. **15**(12): p. 786-801.
18. Sorokin, L., *The impact of the extracellular matrix on inflammation.* Nat Rev Immunol, 2010. **10**(10): p. 712-23.

19. Fausto, N., J.S. Campbell, and K.J. Riehle, *Liver regeneration.* J Hepatol, 2012. **57**(3): p. 692-4.
20. Greuter, T. and V.H. Shah, *Hepatic sinusoids in liver injury, inflammation, and fibrosis: new pathophysiological insights.* J Gastroenterol, 2016. **51**(6): p. 511-9.
21. Hernandez-Gea, V., et al., *Role of the microenvironment in the pathogenesis and treatment of hepatocellular carcinoma.* Gastroenterology, 2013. **144**(3): p. 512-27.
22. Pickup, M.W., J.K. Mouw, and V.M. Weaver, *The extracellular matrix modulates the hallmarks of cancer.* EMBO Rep, 2014. **15**(12): p. 1243-53.
23. Lu, P., V.M. Weaver, and Z. Werb, *The extracellular matrix: a dynamic niche in cancer progression.* J Cell Biol, 2012. **196**(4): p. 395-406.
24. Levental, K.R., et al., *Matrix crosslinking forces tumor progression by enhancing integrin signaling.* Cell, 2009. **139**(5): p. 891-906.
25. Arii, S., et al., *Overexpression of matrix metalloproteinase 9 gene in hepatocellular carcinoma with invasive potential.* Hepatology, 1996. **24**(2): p. 316-22.
26. Egeblad, M. and Z. Werb, *New functions for the matrix metalloproteinases in cancer progression.* Nat Rev Cancer, 2002. **2**(3): p. 161-74.
27. Crispe, I.N., *The liver as a lymphoid organ.* Annu Rev Immunol, 2009. **27**: p. 147-63.
28. Crispe, I.N., *The Liver as a Lymphoid Organ.* Annual Review of Immunology, 2009. **27**(1): p. 147-163.
29. Kubes, P. and C. Jenne, *Immune Responses in the Liver.* Annual Review of Immunology, 2018. **36**(1): p. 247-277.
30. Racanelli, V. and B. Rehermann, *The liver as an immunological organ.* Hepatology, 2006. **43**(S1): p. S54-S62.
31. Freitas-Lopes, M.A., et al., *Differential Location and Distribution of Hepatic Immune Cells.* Cells, 2017. **6**(4).
32. Jenne, C.N. and P. Kubes, *Immune surveillance by the liver.* Nat Immunol, 2013. **14**(10): p. 996-1006.
33. Kurioka, A., et al., *MAIT cells: new guardians of the liver.* Clin Transl Immunology, 2016. **5**(8): p. e98.
34. Fasbender, F., et al., *Natural Killer Cells and Liver Fibrosis.* Front Immunol, 2016. **7**: p. 19.
35. Klein, I. and I.N. Crispe, *Complete differentiation of CD8+ T cells activated locally within the transplanted liver.* J Exp Med, 2006. **203**(2): p. 437-47.
36. Thomson, A.W. and P.A. Knolle, *Antigen-presenting cell function in the tolerogenic liver environment.* Nat Rev Immunol, 2010. **10**(11): p. 753-66.
37. Pennock, N.D., et al., *T cell responses: naive to memory and everything in between.* Adv Physiol Educ, 2013. **37**(4): p. 273-83.
38. Tay, S.S., et al., *Intrahepatic activation of naive CD4+ T cells by liver-resident phagocytic cells.* J Immunol, 2014. **193**(5): p. 2087-95.
39. Balmer, M.L., et al., *The liver may act as a firewall mediating mutualism between the host and its gut commensal microbiota.* Sci Transl Med, 2014. **6**(237): p. 237ra66.

40. Ju, C. and F. Tacke, *Hepatic macrophages in homeostasis and liver diseases: from pathogenesis to novel therapeutic strategies.* Cell Mol Immunol, 2016. **13**(3): p. 316-27.
41. Bilzer, M., F. Roggel, and A.L. Gerbes, *Role of Kupffer cells in host defense and liver disease.* Liver Int, 2006. **26**(10): p. 1175-86.
42. Strauss, O., et al., *The immunophenotype of antigen presenting cells of the mononuclear phagocyte system in normal human liver--a systematic review.* J Hepatol, 2015. **62**(2): p. 458-68.
43. Bigorgne, A.E. and I.N. Crispe, *TLRs in Hepatic Cellular Crosstalk.* Gastroenterology research and practice, 2010. **2010**: p. 618260.
44. Crispe, I.N., *Liver antigen-presenting cells.* J Hepatol, 2011. **54**(2): p. 357-65.
45. Crispe, I.N., *Immune tolerance in liver disease.* Hepatology, 2014. **60**(6): p. 2109-17.
46. Pallett, L.J., et al., *Metabolic regulation of hepatitis B immunopathology by myeloid-derived suppressor cells.* Nat Med, 2015. **21**(6): p. 591-600.
47. Grakoui, A. and I.N. Crispe, *Presentation of hepatocellular antigens.* Cell Mol Immunol, 2016. **13**(3): p. 293-300.
48. Galon, J., et al., *Towards the introduction of the 'Immunoscore' in the classification of malignant tumours.* J Pathol, 2014. **232**(2): p. 199-209.
49. Vivier, E., et al., *Functions of natural killer cells.* Nat Immunol, 2008. **9**(5): p. 503-10.
50. Bjorkstrom, N.K., H.G. Ljunggren, and J. Michaelsson, *Emerging insights into natural killer cells in human peripheral tissues.* Nat Rev Immunol, 2016. **16**(5): p. 310-20.
51. Caligiuri, M.A., *Human natural killer cells.* Blood, 2008. **112**(3): p. 461-9.
52. Mandal, A. and C. Viswanathan, *Natural killer cells: In health and disease.* Hematol Oncol Stem Cell Ther, 2015. **8**(2): p. 47-55.
53. Pallett, L.J., et al., *IL-2(high) tissue-resident T cells in the human liver: Sentinels for hepatotropic infection.* J Exp Med, 2017. **214**(6): p. 1567-1580.
54. Farhood, B., M. Najafi, and K. Mortezaee, *CD8(+) cytotoxic T lymphocytes in cancer immunotherapy: A review.* J Cell Physiol, 2019. **234**(6): p. 8509-8521.
55. Johnston, M.P. and S.I. Khakoo, *Immunotherapy for hepatocellular carcinoma: Current and future.* World journal of gastroenterology, 2019. **25**(24): p. 2977-2989.
56. Domogalla, M.P., et al., *Tolerance through Education: How Tolerogenic Dendritic Cells Shape Immunity.* Frontiers in Immunology, 2017. **8**(1764).
57. Li, F. and Z. Tian, *The liver works as a school to educate regulatory immune cells.* Cellular & molecular immunology, 2013. **10**(4): p. 292-302.
58. Tiberio, L., et al., *Chemokine and chemotactic signals in dendritic cell migration.* Cellular & molecular immunology, 2018. **15**(4): p. 346-352.
59. Chen, D.S. and I. Mellman, *Oncology meets immunology: the cancer-immunity cycle.* Immunity, 2013. **39**(1): p. 1-10.
60. Hato, T., et al., *Immune checkpoint blockade in hepatocellular carcinoma: current progress and future directions.* Hepatology, 2014. **60**(5): p. 1776-82.

61. Jochems, C. and J. Schlom, *Tumor-infiltrating immune cells and prognosis: the potential link between conventional cancer therapy and immunity.* Exp Biol Med (Maywood), 2011. **236**(5): p. 567-79.
62. Lee, G.R., *Phenotypic and Functional Properties of Tumor-Infiltrating Regulatory T Cells.* Mediators Inflamm, 2017. **2017**: p. 5458178.
63. Huang, F. and X.P. Geng, *Chemokines and hepatocellular carcinoma.* World J Gastroenterol, 2010. **16**(15): p. 1832-6.
64. Harlin, H., et al., *Chemokine expression in melanoma metastases associated with CD8+ T-cell recruitment.* Cancer Res, 2009. **69**(7): p. 3077-85.
65. Camus, M., et al., *Coordination of intratumoral immune reaction and human colorectal cancer recurrence.* Cancer Res, 2009. **69**(6): p. 2685-93.
66. Galon, J. and D. Bruni, *Approaches to treat immune hot, altered and cold tumours with combination immunotherapies.* Nat Rev Drug Discov, 2019. **18**(3): p. 197-218.
67. Nagarsheth, N., M.S. Wicha, and W. Zou, *Chemokines in the cancer microenvironment and their relevance in cancer immunotherapy.* Nat Rev Immunol, 2017. **17**(9): p. 559-572.
68. Haanen, J., *Converting Cold into Hot Tumors by Combining Immunotherapies.* Cell, 2017. **170**(6): p. 1055-1056.
69. Gnjatic, S., et al., *Identifying baseline immune-related biomarkers to predict clinical outcome of immunotherapy.* J Immunother Cancer, 2017. **5**: p. 44.
70. Aragon-Sanabria, V., G.B. Kim, and C. Dong, *From Cancer Immunoediting to New Strategies in Cancer Immunotherapy: The Roles of Immune Cells and Mechanics in Oncology.* Adv Exp Med Biol, 2018. **1092**: p. 113-138.
71. Dunn, G.P., L.J. Old, and R.D. Schreiber, *The three Es of cancer immunoediting.* Annu Rev Immunol, 2004. **22**: p. 329-60.
72. Quezada, S.A., et al., *Shifting the equilibrium in cancer immunoediting: from tumor tolerance to eradication.* Immunol Rev, 2011. **241**(1): p. 104-18.
73. Bazhin, A.V., A. Amedei, and S. Karakhanova, *Editorial: Immune Checkpoint Molecules and Cancer Immunotherapy.* Front Immunol, 2018. **9**: p. 2878.
74. Khong, H.T. and N.P. Restifo, *Natural selection of tumor variants in the generation of "tumor escape" phenotypes.* Nature immunology, 2002. **3**(11): p. 999-1005.
75. Restifo, N.P., et al., *Assumptions of the tumor 'escape' hypothesis.* Seminars in cancer biology, 2002. **12**(1): p. 81-86.
76. Makarova-Rusher, O.V., et al., *The yin and yang of evasion and immune activation in HCC.* J Hepatol, 2015. **62**(6): p. 1420-9.
77. Peggs, K.S., et al., *Blockade of CTLA-4 on both effector and regulatory T cell compartments contributes to the antitumor activity of anti-CTLA-4 antibodies.* J Exp Med, 2009. **206**(8): p. 1717-25.
78. Nguyen, L.T. and P.S. Ohashi, *Clinical blockade of PD1 and LAG3--potential mechanisms of action.* Nat Rev Immunol, 2015. **15**(1): p. 45-56.
79. Barber, D.L., et al., *Restoring function in exhausted CD8 T cells during chronic viral infection.* Nature, 2006. **439**(7077): p. 682-7.

80. Shi, F., et al., *PD-1 and PD-L1 upregulation promotes CD8(+) T-cell apoptosis and postoperative recurrence in hepatocellular carcinoma patients.* Int J Cancer, 2011. **128**(4): p. 887-96.
81. Gao, Q., et al., *Overexpression of PD-L1 significantly associates with tumor aggressiveness and postoperative recurrence in human hepatocellular carcinoma.* Clin Cancer Res, 2009. **15**(3): p. 971-9.
82. Erhardt, A., et al., *IL-10, regulatory T cells, and Kupffer cells mediate tolerance in concanavalin A-induced liver injury in mice.* Hepatology, 2007. **45**(2): p. 475-85.
83. Schon, H.T. and R. Weiskirchen, *Immunomodulatory effects of transforming growth factor-beta in the liver.* Hepatobiliary Surg Nutr, 2014. **3**(6): p. 386-406.
84. Kalathil, S., et al., *Higher frequencies of GARP(+)CTLA-4(+)Foxp3(+) T regulatory cells and myeloid-derived suppressor cells in hepatocellular carcinoma patients are associated with impaired T-cell functionality.* Cancer Res, 2013. **73**(8): p. 2435-44.
85. Shibue, T. and R.A. Weinberg, *EMT, CSCs, and drug resistance: the mechanistic link and clinical implications.* Nat Rev Clin Oncol, 2017. **14**(10): p. 611-629.
86. Radisky, D.C., *Epithelial-mesenchymal transition.* J Cell Sci, 2005. **118**(Pt 19): p. 4325-6.
87. Dongre, A. and R.A. Weinberg, *New insights into the mechanisms of epithelial-mesenchymal transition and implications for cancer.* Nat Rev Mol Cell Biol, 2019. **20**(2): p. 69-84.
88. Kalluri, R. and R.A. Weinberg, *The basics of epithelial-mesenchymal transition.* J Clin Invest, 2009. **119**(6): p. 1420-8.
89. Lamouille, S., J. Xu, and R. Derynck, *Molecular mechanisms of epithelial-mesenchymal transition.* Nat Rev Mol Cell Biol, 2014. **15**(3): p. 178-96.
90. Paoli, P., E. Giannoni, and P. Chiarugi, *Anoikis molecular pathways and its role in cancer progression.* Biochim Biophys Acta, 2013. **1833**(12): p. 3481-3498.
91. Pang, M.F., et al., *TGF-β1-induced EMT promotes targeted migration of breast cancer cells through the lymphatic system by the activation of CCR7/CCL21-mediated chemotaxis.* Oncogene, 2015. **35**: p. 748.
92. Ikenouchi, J., et al., *Regulation of tight junctions during the epithelium-mesenchyme transition: direct repression of the gene expression of claudins/occludin by Snail.* J Cell Sci, 2003. **116**(Pt 10): p. 1959-67.
93. Kidd, M.E., D.K. Shumaker, and K.M. Ridge, *The role of vimentin intermediate filaments in the progression of lung cancer.* Am J Respir Cell Mol Biol, 2014. **50**(1): p. 1-6.
94. Pani, G., et al., *Redox-based escape mechanism from death: the cancer lesson.* Antioxid Redox Signal, 2009. **11**(11): p. 2791-806.
95. Pinzani, M., *Epithelial-mesenchymal transition in chronic liver disease: fibrogenesis or escape from death?* J Hepatol, 2011. **55**(2): p. 459-65.
96. Siegel, R.L., K.D. Miller, and A. Jemal, *Cancer Statistics, 2017.* CA Cancer J Clin, 2017. **67**(1): p. 7-30.
97. Valderrama-Trevino, A.I., et al., *Hepatic Metastasis from Colorectal Cancer.* Euroasian J Hepatogastroenterol, 2017. **7**(2): p. 166-175.

98. Ai, D., et al., *Patterns of distant organ metastases in esophageal cancer: a population-based study.* J Thorac Dis, 2017. **9**(9): p. 3023-3030.
99. Houg, D.S. and M.F. Bijlsma, *The hepatic pre-metastatic niche in pancreatic ductal adenocarcinoma.* Mol Cancer, 2018. **17**(1): p. 95.
100. Steeg, P.S., *Tumor metastasis: mechanistic insights and clinical challenges.* Nat Med, 2006. **12**(8): p. 895-904.
101. Sceneay, J., M.J. Smyth, and A. Moller, *The pre-metastatic niche: finding common ground.* Cancer Metastasis Rev, 2013. **32**(3-4): p. 449-64.
102. Akhtar, M., et al., *Paget's "Seed and Soil" Theory of Cancer Metastasis: An Idea Whose Time has Come.* Adv Anat Pathol, 2019. **26**(1): p. 69-74.
103. Psaila, B. and D. Lyden, *The metastatic niche: adapting the foreign soil.* Nature reviews. Cancer, 2009. **9**(4): p. 285-293.
104. Peinado, H., et al., *Pre-metastatic niches: organ-specific homes for metastases.* Nature Reviews Cancer, 2017. **17**: p. 302.
105. Mehlen, P. and A. Puisieux, *Metastasis: a question of life or death.* Nature Reviews Cancer, 2006. **6**(6): p. 449-458.
106. Bosch, F.X., et al., *Epidemiology of hepatocellular carcinoma.* Clin Liver Dis, 2005. **9**(2): p. 191-211, v.
107. Marrero, J.A., et al., *Diagnosis, Staging, and Management of Hepatocellular Carcinoma: 2018 Practice Guidance by the American Association for the Study of Liver Diseases.* Hepatology, 2018. **68**(2): p. 723-750.
108. Majno, P.E., et al., *Primary liver resection and salvage transplantation or primary liver transplantation in patients with single, small hepatocellular carcinoma and preserved liver function: an outcome-oriented decision analysis.* Hepatology, 2000. **31**(4): p. 899-906.
109. Kudo, M., et al., *Lenvatinib versus sorafenib in first-line treatment of patients with unresectable hepatocellular carcinoma: a randomised phase 3 non-inferiority trial.* Lancet, 2018. **391**(10126): p. 1163-1173.
110. Bakouny, Z., et al., *Second-line Treatments of Advanced Hepatocellular Carcinoma: Systematic Review and Network Meta-Analysis of Randomized Controlled Trials.* J Clin Gastroenterol, 2019. **53**(4): p. 251-261.
111. Yau, T., et al., *Nivolumab in advanced hepatocellular carcinoma: Sorafenib-experienced Asian cohort analysis.* J Hepatol, 2019. **71**(3): p. 543-552.
112. Llovet, J.M., et al., *Molecular therapies and precision medicine for hepatocellular carcinoma.* Nat Rev Clin Oncol, 2018. **15**(10): p. 599-616.
113. Thillai, K., P. Ross, and D. Sarker, *Molecularly targeted therapy for advanced hepatocellular carcinoma - a drug development crisis?* World J Gastrointest Oncol, 2016. **8**(2): p. 173-85.
114. Wilhelm, S., et al., *Discovery and development of sorafenib: a multikinase inhibitor for treating cancer.* Nat Rev Drug Discov, 2006. **5**(10): p. 835-44.
115. Medavaram, S. and Y. Zhang, *Emerging therapies in advanced hepatocellular carcinoma.* Exp Hematol Oncol, 2018. **7**: p. 17.
116. Park, J.W., et al., *Sorafenib with or without concurrent transarterial chemoembolization in patients with advanced hepatocellular carcinoma: The phase III STAH trial.* J Hepatol, 2019. **70**(4): p. 684-691.

117. Zhu, Y.J., et al., *New knowledge of the mechanisms of sorafenib resistance in liver cancer.* Acta Pharmacol Sin, 2017. **38**(5): p. 614-622.
118. van Malenstein, H., et al., *Long-term exposure to sorafenib of liver cancer cells induces resistance with epithelial-to-mesenchymal transition, increased invasion and risk of rebound growth.* Cancer Lett, 2013. **329**(1): p. 74-83.
119. Garnelo, M., et al., *Interaction between tumour-infiltrating B cells and T cells controls the progression of hepatocellular carcinoma.* Gut, 2017. **66**(2): p. 342-351.
120. Kim, R., M. Emi, and K. Tanabe, *Cancer immunoediting from immune surveillance to immune escape.* Immunology, 2007. **121**(1): p. 1-14.
121. Redman, J.M., et al., *Mechanisms of action of therapeutic antibodies for cancer.* Mol Immunol, 2015. **67**(2 Pt A): p. 28-45.
122. Weiner, L.M., R. Surana, and S. Wang, *Monoclonal antibodies: versatile platforms for cancer immunotherapy.* Nat Rev Immunol, 2010. **10**(5): p. 317-27.
123. Darvin, P., et al., *Immune checkpoint inhibitors: recent progress and potential biomarkers.* Exp Mol Med, 2018. **50**(12): p. 165.
124. Simon, S. and N. Labarriere, *PD-1 expression on tumor-specific T cells: Friend or foe for immunotherapy?* Oncoimmunology, 2017. **7**(1): p. e1364828.
125. Vibhakar, R., et al., *Activation-induced expression of human programmed death-1 gene in T-lymphocytes.* Exp Cell Res, 1997. **232**(1): p. 25-8.
126. Ahmadzadeh, M., et al., *Tumor antigen-specific CD8 T cells infiltrating the tumor express high levels of PD-1 and are functionally impaired.* Blood, 2009. **114**(8): p. 1537-44.
127. Zou, W. and L. Chen, *Inhibitory B7-family molecules in the tumour microenvironment.* Nat Rev Immunol, 2008. **8**(6): p. 467-77.
128. Ribas, A. and J.D. Wolchok, *Cancer immunotherapy using checkpoint blockade.* Science, 2018. **359**(6382): p. 1350.
129. Larkin, J., et al., *Combined Nivolumab and Ipilimumab or Monotherapy in Untreated Melanoma.* The New England journal of medicine, 2015. **373**(1): p. 23-34.
130. Chabanon, R.M., et al., *Mutational Landscape and Sensitivity to Immune Checkpoint Blockers.* Clin Cancer Res, 2016. **22**(17): p. 4309-21.
131. Kim, J.M. and D.S. Chen, *Immune escape to PD-L1/PD-1 blockade: seven steps to success (or failure).* Ann Oncol, 2016. **27**(8): p. 1492-504.
132. Slaney, C.Y., et al., *CARs versus BiTEs: A Comparison between T Cell-Redirection Strategies for Cancer Treatment.* Cancer Discov, 2018. **8**(8): p. 924-934.
133. Dahlen, E., N. Veitonmaki, and P. Norlen, *Bispecific antibodies in cancer immunotherapy.* Ther Adv Vaccines Immunother, 2018. **6**(1): p. 3-17.
134. Kontermann, R.E. and U. Brinkmann, *Bispecific antibodies.* Drug Discov Today, 2015. **20**(7): p. 838-47.
135. Velasquez, M.P., C.L. Bonifant, and S. Gottschalk, *Redirecting T cells to hematological malignancies with bispecific antibodies.* Blood, 2018. **131**(1): p. 30-38.

136. Klinger, M., et al., *Harnessing T cells to fight cancer with BiTE(R) antibody constructs--past developments and future directions.* Immunol Rev, 2016. **270**(1): p. 193-208.
137. Goebeler, M.E., et al., *Bispecific T-Cell Engager (BiTE) Antibody Construct Blinatumomab for the Treatment of Patients With Relapsed/Refractory Non-Hodgkin Lymphoma: Final Results From a Phase I Study.* J Clin Oncol, 2016. **34**(10): p. 1104-11.
138. Alatrash, G., A.K. Crain, and J.J. Molldrem, *Chapter 7 Tumor-Associated Antigens*, in *Immune Biology of Allogeneic Hematopoietic Stem Cell Transplantation*. 2019. p. 107-125.
139. Martinez, M. and E.K. Moon, *CAR T Cells for Solid Tumors: New Strategies for Finding, Infiltrating, and Surviving in the Tumor Microenvironment.* Front Immunol, 2019. **10**: p. 128.
140. Morello, A., M. Sadelain, and P.S. Adusumilli, *Mesothelin-Targeted CARs: Driving T Cells to Solid Tumors.* Cancer Discov, 2016. **6**(2): p. 133-46.
141. Langhans, S.A., *Three-Dimensional in Vitro Cell Culture Models in Drug Discovery and Drug Repositioning.* Front Pharmacol, 2018. **9**: p. 6.
142. Breslin, S. and L. O'Driscoll, *Three-dimensional cell culture: the missing link in drug discovery.* Drug Discov Today, 2013. **18**(5-6): p. 240-9.
143. Bissell, M.J., et al., *The organizing principle: microenvironmental influences in the normal and malignant breast.* Differentiation, 2002. **70**(9-10): p. 537-46.
144. O'Brien, L.E., M.M. Zegers, and K.E. Mostov, *Opinion: Building epithelial architecture: insights from three-dimensional culture models.* Nat Rev Mol Cell Biol, 2002. **3**(7): p. 531-7.
145. Mazza, G., W. Al-Akkad, and K. Rombouts, *Engineering in vitro models of hepatofibrogenesis.* Adv Drug Deliv Rev, 2017. **121**: p. 147-157.
146. Kim, K., et al., *Preserved liver-specific functions of hepatocytes in 3D co-culture with endothelial cell sheets.* Biomaterials, 2012. **33**(5): p. 1406-13.
147. Gupta, G.P. and J. Massague, *Cancer metastasis: building a framework.* Cell, 2006. **127**(4): p. 679-95.
148. Mazza, G., et al., *Rapid production of human liver scaffolds for functional tissue engineering by high shear stress oscillation-decellularization.* Scientific Reports, 2017. **7**(1): p. 5534.
149. Herter, S., et al., *A novel three-dimensional heterotypic spheroid model for the assessment of the activity of cancer immunotherapy agents.* Cancer Immunol Immunother, 2017. **66**(1): p. 129-140.
150. Giannattasio, A., et al., *Cytotoxicity and infiltration of human NK cells in in vivo-like tumor spheroids.* BMC Cancer, 2015. **15**: p. 351.
151. Katt, M.E., et al., *In Vitro Tumor Models: Advantages, Disadvantages, Variables, and Selecting the Right Platform.* Front Bioeng Biotechnol, 2016. **4**: p. 12.
152. Dangles-Marie, V., et al., *A three-dimensional tumor cell defect in activating autologous CTLs is associated with inefficient antigen presentation correlated with heat shock protein-70 down-regulation.* Cancer Res, 2003. **63**(13): p. 3682-7.

153. Mestas, J. and C.C.W. Hughes, *Of Mice and Not Men: Differences between Mouse and Human Immunology.* The Journal of Immunology, 2004. **172**(5): p. 2731.
154. Nelson, B.H., *IL-2, Regulatory T Cells, and Tolerance.* The Journal of Immunology, 2004. **172**(7): p. 3983.
155. Björkström, N.K., H.-G. Ljunggren, and J. Michaëlsson, *Emerging insights into natural killer cells in human peripheral tissues.* Nature Reviews Immunology, 2016. **16**: p. 310.
156. Italiani, P. and D. Boraschi, *New Insights Into Tissue Macrophages: From Their Origin to the Development of Memory.* Immune network, 2015. **15**(4): p. 167-176.
157. Boyette, L.B., et al., *Phenotype, function, and differentiation potential of human monocyte subsets.* PLoS One, 2017. **12**(4): p. e0176460.
158. Coxon, A., et al., *A novel role for the beta 2 integrin CD11b/CD18 in neutrophil apoptosis: a homeostatic mechanism in inflammation.* Immunity, 1996. **5**(6): p. 653-66.
159. Ku, J.L. and J.G. Park, *Biology of SNU cell lines.* Cancer Res Treat, 2005. **37**(1): p. 1-19.
160. Jacquelot, N., et al., *Targeting Chemokines and Chemokine Receptors in Melanoma and Other Cancers.* Frontiers in Immunology, 2018. **9**(2480).
161. Prieto-Garcia, E., et al., *Epithelial-to-mesenchymal transition in tumor progression.* Med Oncol, 2017. **34**(7): p. 122.
162. Carloni, V., T.V. Luong, and K. Rombouts, *Hepatic stellate cells and extracellular matrix in hepatocellular carcinoma: more complicated than ever.* Liver Int, 2014. **34**(6): p. 834-43.
163. Bruix, J., M. Reig, and M. Sherman, *Evidence-Based Diagnosis, Staging, and Treatment of Patients With Hepatocellular Carcinoma.* Gastroenterology, 2016. **150**(4): p. 835-53.
164. Mittal, V., *Epithelial Mesenchymal Transition in Tumor Metastasis.* Annu Rev Pathol, 2018. **13**: p. 395-412.
165. Thiery, J.P., *Epithelial-mesenchymal transitions in tumour progression.* Nat Rev Cancer, 2002. **2**(6): p. 442-54.
166. Liu, C.Y., K.F. Chen, and P.J. Chen, *Treatment of Liver Cancer.* Cold Spring Harb Perspect Med, 2015. **5**(9): p. a021535.
167. Llovet, J.M., et al., *Sorafenib in advanced hepatocellular carcinoma.* N Engl J Med, 2008. **359**(4): p. 378-90.
168. Blanchet, B., et al., *Validation of an HPLC-UV method for sorafenib determination in human plasma and application to cancer patients in routine clinical practice.* J Pharm Biomed Anal, 2009. **49**(4): p. 1109-14.
169. Galon, J. and D. Bruni, *Approaches to treat immune hot, altered and cold tumours with combination immunotherapies.* Nature Reviews Drug Discovery, 2019. **18**(3): p. 197-218.
170. Fridman, W.H., et al., *The immune microenvironment of human tumors: general significance and clinical impact.* Cancer Microenviron, 2013. **6**(2): p. 117-22.

171. Chen, D.S. and I. Mellman, *Elements of cancer immunity and the cancer-immune set point.* Nature, 2017. **541**(7637): p. 321-330.
172. Bonaventura, P., et al., *Cold Tumors: A Therapeutic Challenge for Immunotherapy.* Front Immunol, 2019. **10**: p. 168.
173. van der Woude, L.L., et al., *Migrating into the Tumor: a Roadmap for T Cells.* Trends Cancer, 2017. **3**(11): p. 797-808.
174. Aktas, E., et al., *Relationship between CD107a expression and cytotoxic activity.* Cell Immunol, 2009. **254**(2): p. 149-54.
175. Chang, B., et al., *High number of PD-1 positive intratumoural lymphocytes predicts survival benefit of cytokine-induced killer cells for hepatocellular carcinoma patients.* Liver Int, 2018. **38**(8): p. 1449-1458.
176. Mocan, T., et al., *Programmed cell death protein-1 (PD-1)/programmed death-ligand-1 (PD-L1) axis in hepatocellular carcinoma: prognostic and therapeutic perspectives.* Clin Transl Oncol, 2019. **21**(6): p. 702-712.
177. Sia, D., et al., *Identification of an Immune-specific Class of Hepatocellular Carcinoma, Based on Molecular Features.* Gastroenterology, 2017. **153**(3): p. 812-826.
178. Chen, M.L., et al., *Sorafenib relieves cell-intrinsic and cell-extrinsic inhibitions of effector T cells in tumor microenvironment to augment antitumor immunity.* Int J Cancer, 2014. **134**(2): p. 319-31.
179. Liu, X. and S. Qin, *Immune Checkpoint Inhibitors in Hepatocellular Carcinoma: Opportunities and Challenges.* The oncologist, 2019. **24**(Suppl 1): p. S3-S10.
180. Bonaventura, P., et al., *Cold Tumors: A Therapeutic Challenge for Immunotherapy.* Frontiers in immunology, 2019. **10**: p. 168-168.
181. Bosch, F.X., et al., *Primary liver cancer: worldwide incidence and trends.* Gastroenterology, 2004. **127**(5 Suppl 1): p. S5-s16.
182. Ananthakrishnan, A., V. Gogineni, and K. Saeian, *Epidemiology of primary and secondary liver cancers.* Semin Intervent Radiol, 2006. **23**(1): p. 47-63.
183. Kobari, M., et al., *Establishment of six human pancreatic cancer cell lines and their sensitivities to anti-tumor drugs.* Tohoku J Exp Med, 1986. **150**(3): p. 231-48.
184. Sui, M., et al., *Establishment of specific cytotoxic T lymphocyte culture system and its inhibitory effect on ovarian cancer.* Oncology letters, 2016. **12**(5): p. 4087-4093.
185. Riazi Rad, F., et al., *Comparative analysis of CD4+ and CD8+ T cells in tumor tissues, lymph nodes and the peripheral blood from patients with breast cancer.* Iran Biomed J, 2015. **19**(1): p. 35-44.
186. Kasper, H.-U., et al., *Liver tumor infiltrating lymphocytes: comparison of hepatocellular and cholangiolar carcinoma.* World journal of gastroenterology, 2009. **15**(40): p. 5053-5057.
187. Riazi Rad, F., et al., *Comparative analysis of CD4+ and CD8+ T cells in tumor tissues, lymph nodes and the peripheral blood from patients with breast cancer.* Iranian biomedical journal, 2015. **19**(1): p. 35-44.
188. Ham, B., et al., *TNF Receptor-2 Facilitates an Immunosuppressive Microenvironment in the Liver to Promote the Colonization and Growth of Hepatic Metastases.* Cancer Res, 2015. **75**(24): p. 5235-47.

189. Ellerman, D., *Bispecific T-cell engagers: Towards understanding variables influencing the in vitro potency and tumor selectivity and their modulation to enhance their efficacy and safety.* Methods, 2019. **154**: p. 102-117.
190. Gohil, S.H., et al., *An ROR1 bi-specific T-cell engager provides effective targeting and cytotoxicity against a range of solid tumors.* Oncoimmunology, 2017. **6**(7): p. e1326437-e1326437.
191. Zhang, S., et al., *The onco-embryonic antigen ROR1 is expressed by a variety of human cancers.* Am J Pathol, 2012. **181**(6): p. 1903-10.
192. Makedonas, G., et al., *Rapid Up-Regulation and Granule-Independent Transport of Perforin to the Immunological Synapse Define a Novel Mechanism of Antigen-Specific CD8⁺ T Cell Cytotoxic Activity.* The Journal of Immunology, 2009. **182**(9): p. 5560.
193. Dean, M., T. Fojo, and S. Bates, *Tumour stem cells and drug resistance.* Nat Rev Cancer, 2005. **5**(4): p. 275-84.
194. Ventola, C.L., *Cancer Immunotherapy, Part 3: Challenges and Future Trends.* P & T : a peer-reviewed journal for formulary management, 2017. **42**(8): p. 514-521.
195. Huh, D., G.A. Hamilton, and D.E. Ingber, *From 3D cell culture to organs-on-chips.* Trends Cell Biol, 2011. **21**(12): p. 745-54.
196. Zanoni, M., et al., *3D tumor spheroid models for in vitro therapeutic screening: a systematic approach to enhance the biological relevance of data obtained.* Scientific Reports, 2016. **6**: p. 19103.
197. Levinger, I., Y. Ventura, and R. Vago, *Life is three dimensional-as in vitro cancer cultures should be.* Adv Cancer Res, 2014. **121**: p. 383-414.
198. Migliaccio, M., et al., *Mechanisms That Limit the In Vitro Proliferative Potential of Human CD8⁺ T Lymphocytes.* The Journal of Immunology, 2005. **174**(6): p. 3335.
199. Shin, C.S., et al., *Development of an in vitro 3D tumor model to study therapeutic efficiency of an anticancer drug.* Mol Pharm, 2013. **10**(6): p. 2167-75.
200. Fridman, W.H., et al., *The immune contexture in human tumours: impact on clinical outcome.* Nat Rev Cancer, 2012. **12**(4): p. 298-306.
201. Calderaro, J., et al., *Programmed death ligand 1 expression in hepatocellular carcinoma: Relationship With clinical and pathological features.* Hepatology, 2016. **64**(6): p. 2038-2046.
202. Liu, J., et al., *Targeting the PD-L1/DNMT1 axis in acquired resistance to sorafenib in human hepatocellular carcinoma.* Oncology reports, 2017. **38**(2): p. 899-907.
203. Wang, C., P. Kulkarni, and R. Salgia, *Combined Checkpoint Inhibition and Chemotherapy: New Era of 1(st)-Line Treatment for Non-Small-Cell Lung Cancer.* Mol Ther Oncolytics, 2019. **13**: p. 1-6.
204. Imamura, Y., et al., *Comparison of 2D- and 3D-culture models as drug-testing platforms in breast cancer.* Oncol Rep, 2015. **33**(4): p. 1837-43.
205. Köhnke, T., et al., *Increase of PD-L1 expressing B-precursor ALL cells in a patient resistant to the CD19/CD3-bispecific T cell engager antibody blinatumomab.* Journal of hematology & oncology, 2015. **8**: p. 111-111.